Technische Universität München
TUM School of Life Sciences

Structural and functional analysis of the D6 PROTEIN KINASE from *Arabidopsis thaliana*

Alina Graf

Vollständiger Abdruck der von der TUM School of Life Sciences der Technischen Universität München zur Erlangung einer

Doktorin der Naturwissenschaften (Dr. rer. nat.)

genehmigten Dissertation.

Vorsitz: Prof. Dr. Chris Carolin Schön

Prüfende der Dissertation:

1. Prof. Dr. Claus Schwechheimer
2. Prof. Dr. Kay H. Schneitz

Die Dissertation wurde am 09.07.2025 bei der Technischen Universität München eingereicht und durch die TUM School of Life Sciences am 02.09.2025 angenommen.

Abstract

The directed transport of the phytohormone auxin through polarly localized PIN-FORMED (PIN) auxin efflux carriers is fundamental for the spatio-temporal control of plant development. The *Arabidopsis thaliana* serine/threonine kinase D6 PROTEIN KINASE (D6PK) polarly localizes at the basal plasma membrane of many cells where it phosphorylates PINs and activates PIN-mediated auxin efflux. Its fast GNOM-dependent trafficking between the basal plasma membrane and the cytosol suggests that D6PK could act as a molecular switch for polar auxin transport.

D6PK is a member of the AGC1 subclade in the AGCVIII subfamily of protein kinases, which are characterized by a DFG to DFD motif exchange and the middle domain – an insertion preceding the activation segment (SXS) between the catalytic kinase subdomains VII and VIII. We previously identified the middle domain to be required and sufficient for plasma membrane association (Barbosa et al. 2016). However, we could not show how D6PK polarity is maintained, and we could not provide a mechanism for the rapid internalization from the plasma membrane. Here, I elucidate a multistep mechanism for membrane targeting and dissociation of D6PK, involving the previously described phosphoinositide recognition by a polybasic K/R-rich motif and integration into the plasma membrane through S-acylations in repeated CXX(X)P motifs. I further find that release from the plasma membrane and internalization is mediated by a phosphorylation-dependent electrostatic switch in serine residues preceding the polybasic K/R-rich motif. D6PK release from the plasma membrane is required to maintain polarity by restricting lateral diffusion, and directly or indirectly depends on the upstream kinase 3-PHOSPOINOSITIDE-DEPENDENT PROTEIN KINASE 1 (PDK1). The evolutionary conservation of the involved amino acid motifs in other AGC1 kinases as well as in D6PK from other species suggests that I have uncovered a mechanism for plasma membrane targeting and polarity regulation that may be conserved in other AGC1 kinases.

Zusammenfassung

Der gerichtete Transport des Pflanzenhormons Auxin durch polar lokalisierte PIN-FORMED (PIN) Auxin Efflux Transporter ist essenziell für die räumlich-zeitliche Kontrolle der Pflanzenentwicklung. Die *Arabidopsis thaliana* Serin/Threonin Kinase D6 PROTEIN KINASE (D6PK) lokalisiert polar an der basalen Plasmamembran vieler Zellen und phosphoryliert dort die PINs, um den PIN-gesteuerten Efflux Auxins aus der Zelle zu aktivieren. Der schnelle Verkehr der Kinase zwischen basaler Plasmamembran und Cytosol ist ein Hinweis, dass diese Kinase als molekularer Schalter für Auxintransport agieren könnte.

D6PK wird als AGC1-Kinase klassifiziert, die der Unterfamilie der AGCVIII-Kinasen angehört. Diese zeichnen sich aus durch einen Austausch des konservierten Motivs DFG zu DFD und die Mitteldomäne – eine Insertion vor dem Aktivierungssegment (SXS) zwischen den katalytischen Unterdomänen VII und VIII. Wir haben die Mitteldomäne zuvor als notwendig und ausreichend für die Membranassoziation beschrieben (Barbosa et al., 2016). Wie allerdings D6PK Polarität erhalten wird, wurde bisher nicht gezeigt und wir konnten auch keinen Mechanismus für die schnelle Dissoziation von der Plasmamembran beschreiben. Hier beschreibe ich einen mehrere Schritte umfassenden Mechanismus für Membranassoziation und -dissoziation von D6PK. Dieser umfasst die zuvor beschriebene Assoziation mit Phosphoinositolen durch ein polybasisches K/R-reiches Motiv und Verankerung in der Plasmamembran durch S-Acylierungen in wiederholten CXX(X)P Motiven. Anschließend wird die Dissoziation von der Plasmamembran durch eine Phosphorylierung an Serinen vor dem polybasischen K/R-reichen Motiv gesteuert, die eine Veränderung der elektrostatischen Ladung bewirkt. Die Dissoziation von der Plasmamembran wird benötigt, um die polare Lokalisierung zu erhalten, indem laterale Diffusion beschränkt wird, und ist, direkt oder indirekt, abhängig von der vorgelagerten 3-PHOSPHOINOSITIDE-DEPENDENT PROTEIN KINASE 1 (PDK1). Die evolutionäre Konservierung der beteiligten Aminosäuremotive in anderen AGC1-Kinasen sowie in D6PK-Orthologen aus anderen Spezies deutet darauf hin, dass ich einen Mechanismus für Plasmamembranassoziation und Polaritätskontrolle aufgedeckt habe, der in anderen AGC1-Proteinkinasen konserviert sein könnte.

Contents

List of Tables

List of Figures

Abbreviations

ARF	AUXIN RESPONSE FACTOR
AUX1	AUXIN RESISTANT 1
ADI3	AvrPto-DEPENDENT Pto-INTERACTING PROTEIN 3
ATP	Adenosine triphosphate
BFA	Brefeldin A
2-BP	2-Bromopalmitate
BRX	BREVIS RADIX
BSA	Bovine serum albumin
CAA	Chloroacetamide
CHX	Cycloheximide
Col-0	Columbia-0
Cy3	Cyanine 3
D6PK	D6 PROTEIN KINASE
DRMs	Detergent resistant membranes
DTT	Dithiothreitol
EDTA	Ethylenediaminetetraacetic acid
FRAP	Fluorescence recovery after photobleaching
GST	Glutathione S-transferase
GTP	Guanosine triphosphate
GDP	Guanosine diphosphate
HRP	Horseradish peroxidase
IAA	Indole-3 acetic acid
KIPK	KINESIN-LIKE CALMODULIN-BINDING PROTEIN INTERACTING PROTEIN KINASE
LAX1-3	LIKE AUX1-3
LOV domain	Light-oxygen-voltage-sensing domain
MES	2-(N-morpholino)ethanesulfonic acid
NEM	N-Ethylmaleimide
PAX	PROTEIN KINASE ASSOCIATED WITH BRX
PBS	Phosphate buffered saline
PCR	Polymerase chain reaction

PDK1	PHOSPHOINOSITIDE-DEPENDENT KINASE 1
PHOT	PHOTOTROPIN
PID	PINOID
PIF	PDK Interacting Fragment
PIN	PIN-FORMED Auxin Efflux Carrier
PIP5K	PHOSPHATIDYLINOSITOL-4-PHOSPHATE 5-KINASE
PMSF	Phenylmethanesulfonyl fluoride
PPT	Phosphinotricine
PTM	Posttranslational modification
qRT-PCR	Quantitative reverse transcription polymerase chain reaction
ROI	Region of interest
SDS-PAGE	Sodium dodecylsulfate-polyacrylamide gel electrophoresis
Stau	Staurosporine
Taq	*Thermus aquaticus*
TCEP	Tris(2-carboxyethyl)phosphine hydrochloride
T-DNA	Transfer DNA
TIR1/AFB	TRANSPORT INHIBITOR RESPONSE 1/ AUXIN-SIGNALING F-BOX
TMK1	TRANSMEMBRANE KINASE 1
Tris	Tris(hydroxymethyl)aminomethane
TUA	Tubulin alpha chain
UGPase	UDP-glucose pyrophosphorylase
YFP	YELLOW FLUORESCENT PROTEIN
MMTS	Methyl methanothiosulfonate

1 Introduction

1.1 D6 PROTEIN KINASE and its role for plant growth and development

Plants are sessile organisms. Hence, their survival requires them to perceive external signals and coordinate their development and growth closely with their environment throughout their entire lifecycle. These properties distinguish them from most other organisms. Scientists have been fascinated for centuries by the plants' ability to integrate external cues and adapt their growth and development accordingly.

Among these growth and developmental adaptations are the ability to grow towards light (phototropism), in response to the gravity stimulus (gravitropism) and the development of lateral roots. Extensive genetic and phenotypic analyses have enhanced the understanding of the mechanisms behind these and other adaptations through the identification of involved proteins and hormone pathways. Our laboratory contributed to this research and discovered a central role of the AGCVIII subfamily protein kinase D6 PROTEIN KINASE (D6PK) and its close homologues D6PK-LIKE1 (D6PKL1), D6PK-LIKE2 (D6PKL2), and D6PK-LIKE3 (D6PKL3) for plant growth and development in the model plant *Arabidopsis thaliana*. Their role for plant development was revealed by phenotypic analysis of T-DNA insertion loss-of-function mutant plants for the respective genes *D6PK*, *D6PKL1*, *D6PKL2,* and *D6PKL3*. They generated mutant combinations of these genes, analyzed the observed phenotypes and performed physiological assays. Additionally, they analyzed transgenic plants expressing YFP-D6PK fusion protein (Zourelidou et al., 2014; Willige et al., 2013; Zourelidou et al., 2009).

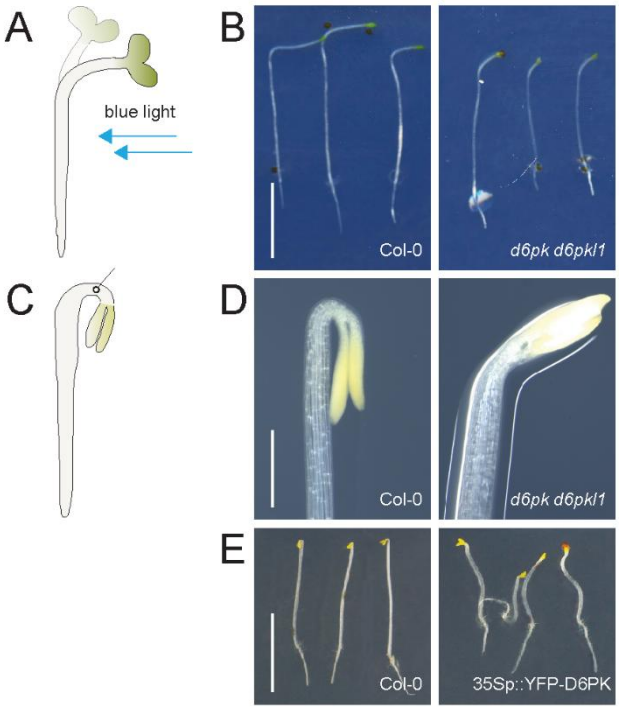

Figure 1. The role of D6PK for plant growth and development. **A.** Graphical representation of a dark grown Arabidopsis thaliana seedling bending towards a unilateral light source. **B.** *d6pk d6pkl1* mutant seedlings do not bend towards the light source anymore when illuminated from a unilateral light source. Scale bar = 0.5 cm **C.** Graphical representation of the apical hook structure in a dark grown seedling **D.** Dark grown *d6pk d6pkl1* seedlings are deficient in forming the apical hook structure. Scale bar = 0.5 mm **E.** Seedlings overexpressing YFP-D6PK show agravitropic and reduced growth. Scale bar = 0.5 cm.

The phenotypic analysis of complex mutants of *D6PK* revealed deficiencies in development and tropic growth compared to the wildtype *Arabidopsis thaliana* Columbia-0 (Col-0). The *d6pk d6pkl1 d6pkl2* triple mutants are deficient in lateral root formation at the seedling stage and may show fused or single cotyledons (Zourelidou et al., 2009). Dark grown *d6pk d6pkl1* double mutant and *d6pk d6pkl1 d6pkl2* triple mutant seedlings do not show phototropic hypocotyl bending towards a unilateral light source, and their hypocotyl does not respond to the gravity stimulus anymore, in contrast to wildtype Col-0 (Figure 1 A and B)(Willige et al., 2013). Additionally, they do not form an apical hook (Figure 1 C and D). Dark grown seedlings overexpressing YFP-D6PK under a constitutively active 35S CaMV promoter demonstrate impaired growth, as well as strong defects in hypocotyl tropisms and apical hook formation (Figure 1 E and F)(Barbosa et al., 2014; Zourelidou et al., 2009). Light grown seedlings overexpressing YFP-D6PK have fewer lateral roots, and adult plants stay smaller than wildtype plants (Zourelidou et al., 2009). In addition to these strong phenotypes, not many plants overexpressing D6PK were recovered in the past after repeated rounds of transformation, indicating that high levels of D6PK are lethal to the plant (Zourelidou et al., 2009). All the observed phenotypes support a central role of D6PK in directed plant growth.

Interestingly, the phytohormone auxin is at the center of many of the processes that are affected in the *d6pk d6pkl1* double mutant and the *d6pk d6pkl1 d6pkl2* triple mutant. Phototropic bending depends on the accumulation of auxin on the shaded side of the plant (Ding et al., 2011; Benková et al., 2003; Friml et al., 2002b). The curvature of the apical hook is achieved by growth inhibition at the inner side of the hook, requiring an asymmetric distribution of auxin (Vandenbussche et al., 2010; Žádníková et al., 2010). Furthermore, lateral root initiation requires the formation of a local auxin maximum, which is crucial for the emergence of the lateral root (Benková et al., 2003). In *d6pk d6pkl1 d6pkl2* triple mutants, the required auxin maxima are absent in the predicted sites of lateral root emergence (Zourelidou et al., 2009). Intriguingly, our group not only described striking phenotypes that suggest a role of D6PK in auxin biology, but they also found a distinctive polar localization of D6PK at the basal plasma membrane of cells (Zourelidou et al., 2009). This polar localization is particularly interesting, as auxin often takes part in directed processes that require a gradient of auxin in specific sites, achieved by the polar transport of auxin to those sites (Blilou et al., 2005; Benková et al., 2003). Taken together, these findings led to a strong motivation in our group to elucidate the mechanisms behind D6PK function for plant development and understand the significance of its polar localization for its role in auxin biology.

Studies on auxin biology date back to Darwin's studies on phototropism. Together with his son Francis, he conducted a series of experiments on several plant species to understand the basic principles of plants' growth towards a light source. They made an important observation – while the curvature takes place in the lower part of the shoot, light is sensed by the tip. The coverage of the tip rather than the site of bending led to an absence of phototropic bending, leading them to the postulation of a mobile substance responsible for the plants' ability to bend towards the light source (Darwin, 1880). Ultimately, this observation was the basis for the isolation and discovery of auxin that followed later (Holland et al., 2009; Kogl, 1931; Cholodny, 1928, 1927; Went, 1926).

Of the family of auxins, the molecule indole-3-acetic acid (IAA) is the most abundant auxin in plants (Zhao, 2010). Its biosynthesis mainly takes place in young leaves and the apexes of the shoot and root via tryptophane biosynthesis-dependent and -independent pathways (Normanly, 2010; Petersson et al., 2009; Ljung et al., 2005; Ljung et al., 2002). From its sites of synthesis, auxin is transported to its sites of action. The directionality of auxin

transport is established via AUX1/LAX influx facilitators and PIN-FORMED efflux facilitators (PINs) (Sauer et al., 2006; Wisniewska et al., 2006; Benková et al., 2003; Friml et al., 2003b; Friml et al., 2002b; Swarup et al., 2001; Gälweiler et al., 1998; Müller et al., 1998). At its sites of action, auxin is perceived and bound by TRANSPORT INHIBITOR RESISTANT 1/AUXIN F-BOX receptors (TIR1/AFB), which then bind their auxin/IAA coreceptors, causing their degradation in presence of auxin. In absence of auxin, these auxin/IAA coreceptors repress the activity of ARF transcription factors, leading to the auxin-dependent transcriptional response in the presence of auxin. The genes that are repressed or activated due to this transcriptional response cause the physiological effects of auxin in the plant (Mockaitis & Estelle, 2008; Dharmasiri et al., 2005; Kepinski & Leyser, 2005; Okushima et al., 2005; Tian et al., 2002). However, some auxin-dependent processes were suggested to occur independently of this transcriptional activity and had, even before discovery of the TIR1/AFB system, been explained by the acid-growth theory (Friml et al., 2022; Li et al., 2021; Takahashi et al., 2012; Moloney et al., 1981; Hager et al., 1971; Rayle & Cleland, 1970).

As auxin regulates many aspects of plant growth and development, plants deficient in auxin biosynthesis, transport, or signaling exhibit a range of phenotypes. Mutations in the PINs that are required for proper auxin distribution affect, amongst others, shoot differentiation, lateral root development, phototropism, and gravitropism (Benková et al., 2003; Friml et al., 2002b; Chen et al., 1998; Gälweiler et al., 1998; Luschnig et al., 1998; Müller et al., 1998). Our group could clearly link the phenotypes observed in complex mutants of *D6PK* to defects in PIN-dependent auxin transport (Zourelidou et al., 2014; Zourelidou et al., 2009). For example, lateral root formation was recovered by external application of auxin and, in line with this finding, the mutants were hypersensitive to the auxin transport inhibitor naphtylphtalamic acid (NPA) (Zourelidou et al., 2009). Additionally, the basipetal auxin transport rates of *d6pk d6pkl1* double and higher order mutants, and *pin* mutants are reduced compared to those of wildtype Col-0 in basipetal auxin transport assays with dark grown seedlings. In these assays radiolabeled IAA is applied to the cotyledon of a dark grown seedling, the basal segment of the hypocotyl is cut after several hours of incubation time, and the quantity of transported auxin is measured (Willige et al., 2013). Ultimately, our group also showed that D6PK directly phosphorylates PINs *in vitro*, and that PIN phosphorylation is reduced in *d6pk d6pkl1*

d6pkl2 mutants *in vivo*. This clearly indicated a direct role of D6PK in polar auxin transport through PIN phosphorylation (Zourelidou et al., 2014; Willige et al., 2013; Zourelidou et al., 2009).

The PINs show peculiar polar localizations in different tissues. The PIN localization in specific tissues correlates well with the observed auxin activity in these respective tissues, as shown in several studies (Figure 2 A)(Benková et al., 2003; Friml et al., 2003b; Gälweiler et al., 1998). Their specific polar localization in the main root led to the postulation and establishment of the reverse fountain model of polar auxin transport (Figure 2 A and B)(Blilou et al., 2005). According to the reverse fountain model, auxin is transported towards the root tip via basally localized PIN1, PIN3, and PIN7 in the vascular tissues in the stele, and basally localized PIN1 and PIN2 in the cortex (Blilou et al., 2005; Friml et al., 2002a; Müller et al., 1998). In the columella, a lateral redistribution of auxin takes place via PIN3, PIN4, and PIN7 (Friml et al., 2002a; Friml et al., 2002b). PIN2 transports auxin shootward in the epidermis, hence completing the reverse fountain model that ultimately leads to the typical auxin gradient in the root (Friml et al., 2003a; Müller et al., 1998). The formation of the auxin gradient and role of auxin distribution and action can be studied using reporter systems such as the auxin response element DR5 and the DII-based systems (Brunoud et al., 2012; Ulmasov et al., 1997). The proper establishment of auxin gradients was, with the help of these reporter systems and by careful phenotypic analysis, described to play a central role in many processes including embryogenesis, lateral root formation, tropic growth responses, or apical hook formation (Ding et al., 2011; Vandenbussche et al., 2010; Žádníková et al., 2010; Benková et al., 2003; Friml et al., 2003b; Friml et al., 2002b). Moreover, the central role of PINs in directing the auxin gradient in the main root can also be verified by computer models predicting auxin distribution based on PIN localization. These models show that analyzing PIN polar localization can be sufficient to properly predict auxin gradient formation in the main root (Van Berkel et al., 2013; Grieneisen et al., 2007). These models can be finetuned by including the differing PIN transport rates that were experimentally determined (Janacek et al., 2024).

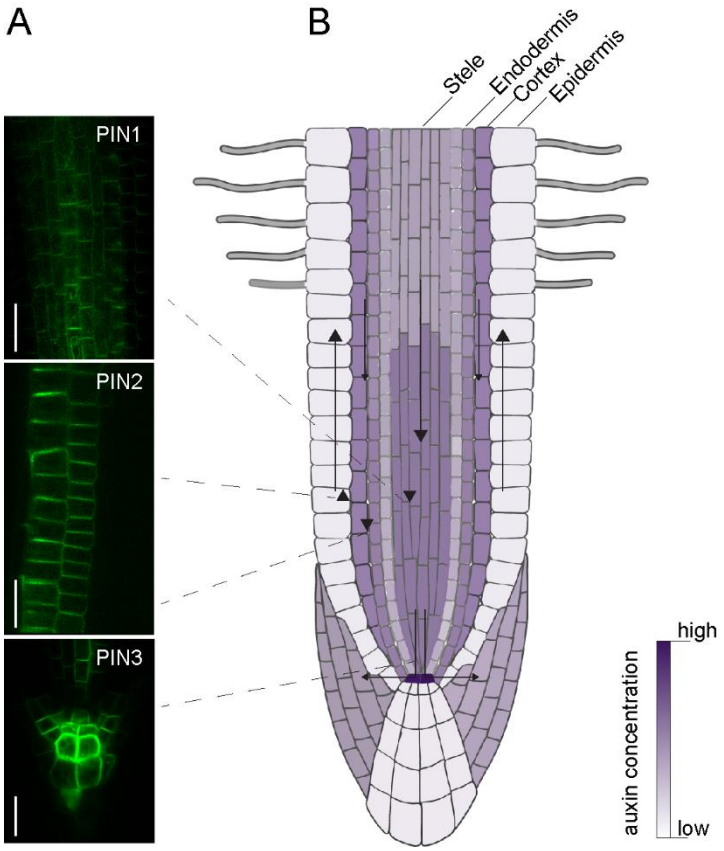

Figure 2. Auxin distribution and the role of polar auxin transport for plant development. **A.** PINs are polarly localized in many tissues. Representative polar localization of PIN1, PIN2, and PIN3 in the root is shown here (own confocal pictures). **B.** Auxin forms a gradient in the plant with local and global maxima and minima. Auxin distribution in the root is shown as an example (Petersson *et al.*, 2009b). The polar localization of PINs (A) correlates well with the observed gradient formation in the root (B). (Figure style and representation is adapted and modified from Petersson *et al.*, 2009b)

The PINs are transmembrane proteins, and a PIN monomer consists of ten transmembrane helices separated by a cytosolic loop in the middle (Ung et al., 2022). The cytosolic loop between the transmembrane domains in the long canonical PINs inhibits auxin transport, and phosphorylation by protein kinases, such as D6PK, is required to activate auxin efflux (Zourelidou et al., 2014). The dependence of PIN activity on a phosphorylating kinase was clearly shown in *Xenopus* oocyte efflux experiments. In these experiments, oocytes were injected with auxin, and the efflux from the cell, dependent on the expression of PIN and activating kinases, was measured directly (Fastner et al., 2017; Zourelidou et al., 2014). In these experiments it was also determined that the PINs differ significantly in their auxin transport rates which depend on the transmembrane domains and the cytosolic loop (Janacek et al., 2024). Structures of PINs have recently been published, and the transport mechanism for auxin elucidated, revealing that the PINs form homodimers with a well-defined auxin binding site (Su et al., 2022; Ung et al., 2022; Yang

et al., 2022). One intriguing outcome of the study is that the PINs have a low affinity for IAA, combined with a high conservation of the auxin binding pocket among the different PINs. This finding suggests that the observed differences in transport rates between the PINs are influenced by localization, abundance or activation of the PINs rather than differing auxin binding properties (Ung et al., 2022). Since, according to this finding, the catalytic activity of the kinases phosphorylating the PINs can be rate-limiting for their transport rate, studying the activating kinases in depth will lead to a more complete understanding of auxin transport in the plant.

Our lab got interested in D6PK due to the remarkable phenotypes observed in loss-of-function mutants associated with plant growth and development, along with its polar localization at the basal plasma membrane of cells. The PINs are auxin efflux carriers that require phosphorylation by kinases, such as D6PK, for activation. The importance of PIN polar localization for establishing the auxin gradient, which drives many aspects of plant development, has strengthened our group's commitment to further investigate D6PK regulation and polar localization at the basal plasma membrane and its role in PIN regulation. Besides D6PK, several other protein kinases have been implicated in auxin transport.

1.2 AGC kinases in polar auxin transport

Our lab demonstrated through multiple experiments that D6PK activity is required for the phosphorylation of the PINs and consequently activation of auxin efflux from the cell. Furthermore, the PINs can be phosphorylated and activated by other protein kinases, including PINOID (PID) or PROTEIN KINASE ASSOCIATED WITH BRX (PAX), which are essential for proper polar auxin transport in the plant. Loss-of-function mutants of these kinases differ in their phenotypes. Understanding commonalities and differences of these kinases, such as their cell biological behavior and regulation of their catalytic activity, may improve understanding of polar auxin transport (Marhava et al., 2018; Zourelidou et al., 2014; Michniewicz et al., 2007; Christensen et al., 2000; Bennett et al., 1995).

PID was the first AGCVIII protein kinase identified for its role in polar auxin transport, as evidenced by the pin-shaped inflorescence of *pid* mutants resembling the *pin1* phenotype (Christensen et al., 2000; Gälweiler et al., 1998; Bennett et al., 1995). PID is localized at the plasma membrane of cells without a distinct polarity, where it directly phosphorylates

and activates PIN auxin efflux carriers, both *in vitro* and *in vivo* (Zourelidou et al., 2014; Michniewicz et al., 2007). PIN polarity regulation requires phosphorylation by the protein kinase PID and subsequent dephosphorylation by protein phosphatases in the cytosolic loop (Michniewicz et al., 2007; Friml et al., 2004; Rashotte et al., 2001; Garbers et al., 1996). Although D6PK and PID both phosphorylate PINs and activate auxin transport, they act non-redundantly – they differ in their phenotypes, and promoter-swap experiments showed that they do not complement each other's phenotype (Zourelidou et al., 2014). Furthermore, PID is involved in PIN polarity control, while D6PK does not seem to play a role in this process (Zourelidou et al., 2014; Friml et al., 2004). Interestingly, they phosphorylate the same residues on the PINs with a different preference, indicating that additional factors must contribute to their physiological function beyond mere phosphorylation-site specificity (Weller et al., 2017).

Our lab, in collaboration with the Hardtke lab in Lausanne, elucidated the role of the D6PK-related protein kinase PAX in auxin transport. This kinase localizes polarly at the basal plasma membrane, resembling D6PK localization, and is strongly expressed in protophloem cells. In these cells, it interacts with the scaffold protein BREVIS RADIX (BRX) (Marhava et al., 2018). PAX regulates auxin transport in the protophloem by functioning as a molecular rheostat together with the scaffold protein BRX. PAX activates PIN-mediated auxin efflux, but PIN phosphorylation is dampened in the presence of BRX. Loss-of-function mutants of *pax* and *brx* show protophloem differentiation defects and a shorter primary root, supporting the importance of this molecular rheostat for plant development (Marhava et al., 2018).

D6PK and PAX are both polarly localized peripheral plasma membrane proteins. They are sensitive to the trafficking inhibitor Brefeldin A (BFA), as evidenced by their rapid internalization from the plasma membrane and accumulation in intracellular BFA compartments following BFA treatment (Marhava et al., 2018; Barbosa et al., 2014). PID, on the other hand, is not polarly localized and largely insensitive to BFA treatments (Barbosa et al., 2014; Kleine-Vehn et al., 2009). BFA inhibits the ARF-GEF GNOM which is implicated in exocytotic trafficking, and BFA was also characterized as an inhibitor of PIN secretion by inhibiting GNOM-dependent trafficking (Geldner et al., 2003). Treatments with BFA facilitate the examination of D6PK trafficking pathways. Using BFA treatments, we could show that D6PK cycles rapidly between cytosol and plasma

membrane and, upon inhibitor washout, is quickly and directly retargeted to the basal plasma membrane. The PINs also show GNOM-dependent trafficking. However, their recycling kinetics differ dramatically from those of D6PK, and therefore PIN and D6PK trafficking are independent of each other (Barbosa et al., 2014). The rapid cycling observed for D6PK indicated that D6PK localization is extremely responsive to external signals and that D6PK may potentially serve as a molecular switch for polar auxin transport (Barbosa et al., 2014).

D6PK, PAX, and PID can all be activated by the 3'-PHOSPHOINOSITIDE DEPENDENT PROTEIN KINASE 1 (PDK1) which is thus assumed to be a master regulator of these kinases (Tan et al., 2020; Xiao & Offringa, 2020; Zegzouti et al., 2006a). The *pdk1 pdk2* mutants exhibit significant developmental defects, including defects in protophloem differentiation typically observed for *pax* loss-of-function mutants, defects in phototropic hypocotyl bending and impaired lateral root formation, as reported for *d6pk d6pkl1 d6pkl2* (Tan et al., 2020; Xiao & Offringa, 2020). The respective phenotypes could be rescued by introduction of a phosphorylation-mimicking version of PAX or D6PK, where the phosphorylation in the activation segment, the PDK1 target site, was mimicked by an aspartate. This established the importance of PDK1-dependent activation for auxin transport (Tan et al., 2020; Xiao & Offringa, 2020).

Auxin transport and the associated kinases are crucial for plant growth and development, as evidenced by the broad range of phenotypes displayed by mutants of *PID*, *PAX* and *D6PK*. D6PK shows polar localization at the basal plasma membrane in many cells and functions non-redundantly with the AGCVIII kinase PID. Given D6PK's distinct biological function compared to PID and its intriguing cell biology, characterized by its polar localization, strong plasma membrane association and fast GNOM-dependent trafficking, my objective for this thesis was to enhance the understanding of D6PK polarity regulation and trafficking. Our group previously demonstrated that D6PK exocytosis is GNOM-dependent. Nevertheless, the mechanisms underlying its rapid internalization remained unclear (Barbosa et al., 2014). Comprehending the mechanism of D6PK trafficking and polar localization may yield a more profound molecular understanding of auxin gradient formation. This knowledge may be transferable to understand the localization and activity of related kinases. Therefore, I investigated D6PK on a biochemical and functional level

and analyzed the sequences of the AGCVIII subfamily, which includes D6PK, PID, and PAX to understand differences and commonalities of these kinases.

1.3 The AGCVIII subfamily of protein kinases

D6PK, PAX, PID, and PDK1 are AGC protein kinases. The Arabidopsis genome encodes 39 AGC kinases. 23 of them form the AGCVIII subfamily to which D6PK, PAX, and PID belong (Galván-Ampudia & Offringa, 2007; Bögre et al., 2003). This subfamily is further divided into the four clades AGC1 – AGC4, and genomic analysis suggests that they all derive from one ancestral kinase (Galván-Ampudia & Offringa, 2007; Hanks & Hunter, 1995). D6PK and PAX belong to the AGC1 clade, and PID, together with the kinases WAG1, WAG2, and PINOID-LIKE2 (PID2) forms the AGC3 clade of kinases (Figure 3)(Galván-Ampudia & Offringa, 2007). Among the four clades, the AGC4 clade is the evolutionary oldest clade. It contains the two blue light sensing kinases phototropin1 (phot1) and phototropin2 (phot2), which are the only AGCVIII kinases yet identified in unicellular green algae. The acquisition of further AGCVIII kinases may thus also mark the transition from water to land (Galván-Ampudia & Offringa, 2007). The AGCVIII subfamily is completed by the AGC2 clade, consisting of the four kinases UNICORN (UNC), UNICORN-LIKE (UNCL), OXI1, and AGC2.2 (Figure 3)(Galván-Ampudia & Offringa, 2007; Bögre et al., 2003).

AGC kinases are named after the well-studied cyclic AMP-dependent kinases (PKA), cGMP-dependent kinases (PKG), and the diacylglycerol-activated/phospholipid-dependent kinases (PKC) (Hanks & Hunter, 1995). Comparisons of the mammalian and the plant AGC kinases at the sequence level reveal a conserved catalytic core, resembling the mammalian kinases PKA, PKG, and PKC, thus classifying them as AGC kinases (Bögre et al., 2003; Hanks & Hunter, 1995). The Arabidopsis AGCVIII kinases are the closest relatives to the mammalian kinases PKA and PKC in flowering plants based on sequence similarity (Galván-Ampudia & Offringa, 2007). The catalytic core of AGC kinases can be divided into two catalytic domains. The catalytic subdomains I – VII include a lysine for binding the cofactor adenosine triphosphate (ATP), and end with the DFG motif required for Mg^{2+}-binding and positioning of ATP for transfer. The catalytic subdomains VIII – XI start with the activation segment, which is phosphorylated and required for the catalytic activity of the kinase (Pearce et al., 2010; Yang et al., 2002). The

phosphorylation in the activation segment causes a structural change which stabilizes ATP through a network of hydrogen bonds (Pearce et al., 2010; Komander et al., 2005; Yang et al., 2002). Many mammalian AGC kinases, as well as many Arabidopsis thaliana AGCVIII kinases, contain the PDK Interacting Fragment (PIF) in their C-terminus, which is required for interaction with their upstream kinase PDK1 leading to PDK1-dependent phosphorylation in the activation segment (Figure 4 A)(Zegzouti et al., 2006a; Biondi et al., 2000). The mechanistic activation through PDK1-dependent activation loop phosphorylation is conserved in the *Arabidopsis thaliana* AGCVIII kinases, as shown by various publications (Tan et al., 2020; Xiao & Offringa, 2020; Zegzouti et al., 2006a).

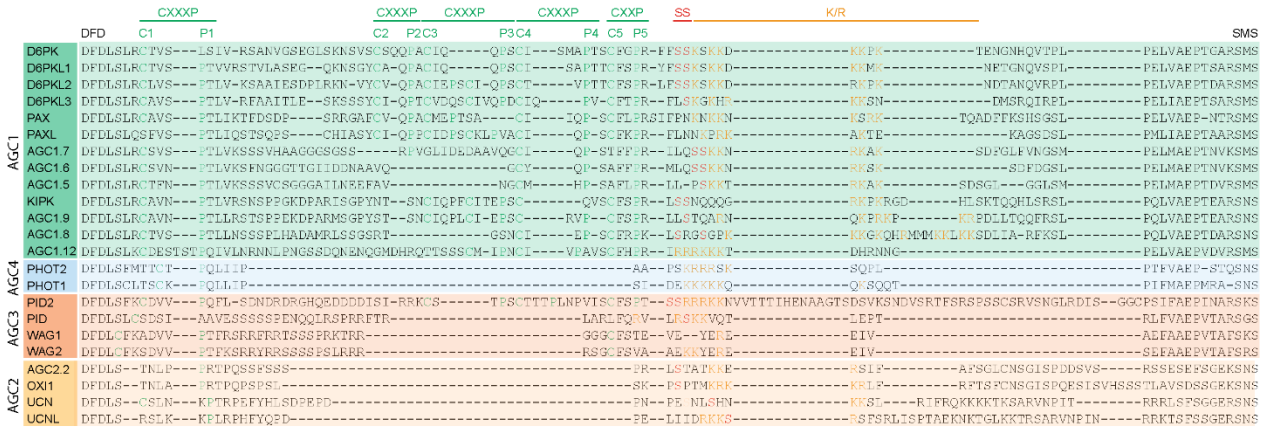

Figure 3. The AGCVIII subfamily of protein kinases. Muscle alignment of the middle domain sequences of Arabidopsis thaliana AGCVIII kinase middle domains. The different clades AGC1, AGC2, AGC3, and AGC4 kinases are highlighted in different colors. The CXX(X)P motifs, polybasic K/R-rich motif (K/R) and preceding serine residues are colored for better distinction. The conserved key residues of the kinase subdomains, DFD (VII) and SXS (VIII), are included and labeled for better comparison.

The closest relatives to the plant AGCVIII kinases, the mammalian kinases PKC and PKA, play central roles in mammalian cells. Especially atypical PKC is crucial in processes regulating cell polarity and polar growth therefore activity and localization are tightly controlled (Pearce et al., 2010; Joberty et al., 2000). Regulation of the PKC family with its twelve characterized isoforms typically takes place by recruitment to membranes and phosphorylation in two sites. These include the phosphorylation by PDK1 in the activation segment and phosphorylation by the mammalian target of rapamycin 2 kinase (mTOR2) in the hydrophobic motif (Facchinetti et al., 2008; Ikenoue et al., 2008; Le Good et al., 1998). Additionally, the release of a pseudosubstrate sequence is required to render PKC active, which is promoted by PKC interaction with diacylglycerol and calcium by the N-terminal C1 and C2 domains (House & Kemp, 1987). PKA forms a tetrameric complex

composed of two regulatory and two catalytic subunits prior to activation. The second messenger cAMP is required to bind to the regulatory subunits of the tetramer and release the catalytic subunits, which allows them to be phosphorylated in their activation segment and in turn phosphorylate their substrates (Taylor et al., 1990). It was found that localization of the inactive tetramer by A-kinase anchoring proteins (AKAPS) and levels of cAMP finetune PKA downstream signaling events, shaping the complexity of the regulation of the different PKA isoforms (Wong & Scott, 2004; Zaccolo & Pozzan, 2002). These findings all support the importance of subcellular localization and activity regulation for proper AGC kinase function and that their activity needs to be tightly regulated. This brings up the question of whether similar complex regulatory mechanisms may exist for the plant AGCVIII kinases, since many of them play central roles in plant development. The plant AGCVIII kinases, in contrast to the mammalian AGC kinases, are characterized by an exchange of the typical DFG motif to a DFD motif and a 36-90 amino acid insertion before the activation segment (SXS), which shows high sequence variability (Figure 3, Figure 4 and B)(Galván-Ampudia & Offringa, 2007). Of the 60 human mammalian AGC kinases, 42 possess functional domains other than the kinase core (Pearce et al., 2010). These domains can be involved in regulating kinase activity and localization by mediating membrane or substrate interaction, leading to the question of whether the plant-specific insertion could be such a functional domain for the plant AGCVIII kinases (Pearce et al., 2010).

Research on PID and D6PK showed that the plant-specific insertion preceding the activation segment is required for the plasma membrane localization of the AGCVIII kinases PID and D6PK (Barbosa et al., 2016; Zegzouti et al., 2006b). Our group demonstrated that the D6PK insertion is required and sufficient to target D6PK to the plasma membrane. Thus, it can be classified as a distinct functional domain outside of the kinase core, and we called it middle domain (Barbosa et al., 2016). The middle domain of many AGCVIII kinases contains a polybasic lysine/arginine (K/R)-rich motif, required for interaction with negatively charged phosphoinositides at the plasma membrane, as shown for PID and D6PK (Figure 3, Figure 4 A - C)(Barbosa et al., 2016; Simon et al., 2016; Zegzouti et al., 2006b). Substituting the lysines of the polybasic K/R-rich motif in the D6PK middle domain with alanines (D6PK_KA) results in loss of plasma membrane association and failure of D6PK_KA to bind to phosphoinositides in *in vitro* assays (Barbosa et al.,

2016). Furthermore, D6PK_KA is not able to complement the *d6pk d6pkl1* phototropism defect when expressed *in planta* under a *D6PK* promoter fragment, in line with a reduction of PIN phosphorylation in these plants, indicating that plasma membrane association mediated by the polybasic K/R-rich motif is required for D6PK biological function (Barbosa et al., 2016). Phosphoinositide binding in dependence on the polybasic K/R-rich motif was demonstrated for other AGC1 clade kinases, strongly suggesting that the polybasic K/R-rich motif in the middle domain is a conserved motif for phosphoinositide binding (Barbosa et al., 2016). Interestingly, the polybasic K/R-rich motif is also found in PID, indicating that the polybasic K/R-rich motif alone cannot explain the differences in localization and trafficking between PID and D6PK (Simon et al., 2016; Zegzouti et al., 2006b).

Multiple proteins that contain polybasic motifs for interactions with membranes have been identified. It was demonstrated that these polybasic motifs can mediate specificity for membranes enriched in specific lipids, believed to be obtained through differences in electrostatic potential (Heo et al., 2006; Papayannopoulos et al., 2005). Usually, the polybasic motifs found in peripheral membrane proteins are also enriched in hydrophobic amino acids to differentiate specificity for association with membranes from nuclear localization signals, which are also enriched in basic amino acids. According to these studies, surface charge together with hydrophobicity can act as a key determinant of protein localization (Heo et al., 2006). However, although the polybasic motifs in some peripheral membrane proteins are by themselves required and sufficient for membrane association, many peripheral membrane proteins use additional signals such as lipid modifications or unfolded sequences to increase avidity mediated by multiple components towards membranes, resulting in polar localization (Zhou et al., 2021; Meca et al., 2019; Ahearn et al., 2012; Rocks et al., 2005; McLaughlin & Aderem, 1995). In the case of the myristoylated alanine-rich C kinase substrate (MARCKS), the polybasic motif is required to target the protein to the membrane, but the protein also requires myristoylation and thus the combined action of the two for proper membrane localization (McLaughlin & Aderem, 1995). Another important signaling protein, the small GTPase KRAS, requires prenylation in addition to its polybasic motif for proper membrane localization, and it was shown that the prenyl anchor mediates polarity, expanding the specificity of the polybasic motif and allowing for more defined localizations (Zhou et al., 2021). Avidity generated by multivalent lipid interactions for membrane association is favored over single high-affinity

motifs to increase specificity of peripheral membrane proteins for certain membrane environments (Bigay & Antonny, 2012). These findings encouraged me to perform a more detailed analysis of the middle domain and D6PK polarity control beyond the previously identified polybasic K/R-rich motif.

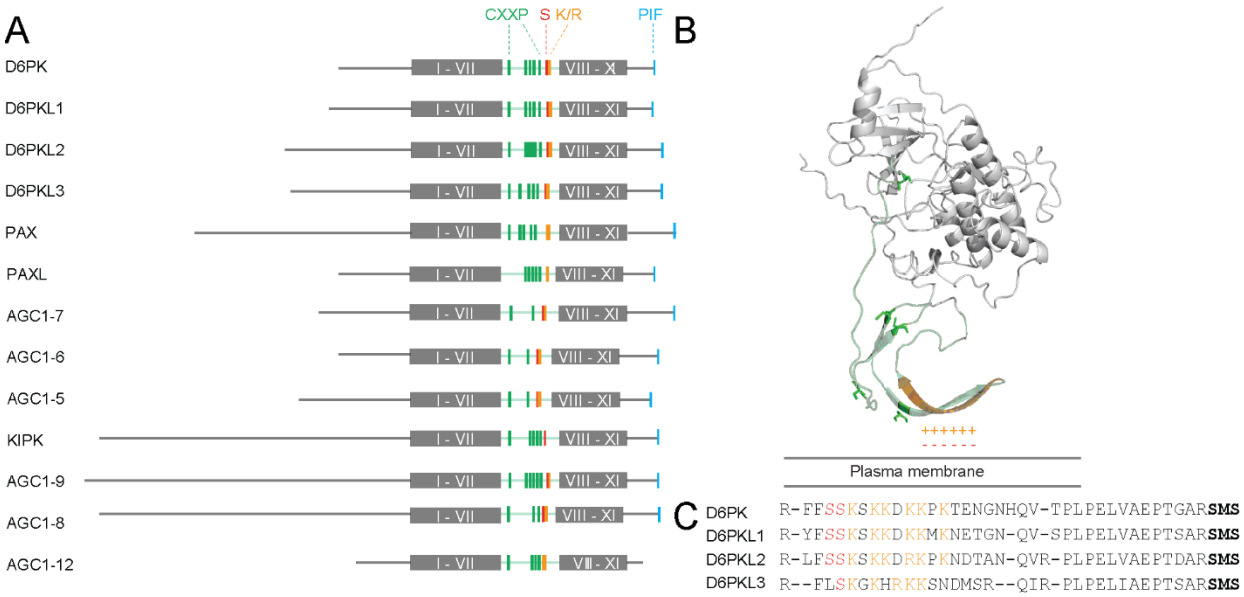

Figure 4. Regulatory elements of AGC kinases. Adapted from (Bassukas et al., 2022). **A.** Schematic representation of Arabidopsis thaliana AGC1 kinases. The conserved kinase domains are marked with black boxes, the middle domain localized between the conserved kinase domains is highlighted in light green, and the characterized polybasic K/R-rich motif (K/R) required for plasma membrane localization is marked in orange. The CXX(X)P repeats are marked in green. The C-terminal PIF motif required for interaction with the master regulator PDK1 is marked in light blue. **B.** The model structure of D6PK with the middle domain marked in red and the polybasic K/R-rich motif marked in orange, the cysteines of the CXX(X)P-repeats marked in green and the serines marked in red. **C**. Sequence alignment showing the polybasic K/R-rich motif of the D6PKs with the important amino acids marked in orange.

In addition to the polybasic K/R-rich motif, the middle domain features conserved repeats of a cysteine followed by a proline separated by two or three amino acids, which we named CXX(X)P motifs (Figure 3, Figure 4 A and B)(Bassukas et al., 2022). These repeated CXX(X)P motifs were first noted in the middle domain of KINESIN-LIKE CALMODULIN-BINDING PROTEIN INTERACTING PROTEIN KINASE (KIPK) but are conserved among the *Arabidopsis thaliana* AGC1 kinases and PID2 (Figure 3)(Bassukas et al., 2022; Day et al., 2000). The number of repeats and the sequence surrounding the motif differ between the members of the *Arabidopsis thaliana* AGC1 clade (Figure 3, Figure 4 A)(Bassukas et al., 2022). Cysteine is one of the least abundant of the 20 amino acids commonly found in proteins, although it frequently occurs in functionally significant sites of the protein and is one of the most conserved amino acids in proteins (Marino &

Gladyshev, 2010). This is probably attributable to their high reactivity. Cysteines are often found to contribute to a protein's structure, as they can form disulfide bonds with other cysteines (Marino & Gladyshev, 2010). Intriguingly, when modelling D6PK, we observed that the cysteines could be in spatial proximity to each other, possibly forming disulfide bonds (Figure 4 B). Cysteines can also form metal-ion clusters as in zinc fingers (Giles et al., 2003). The occurrence of the cysteines in repeats together with prolines is interesting since proline's nitrogen atom is covalently bound in its ring, restricting its backbone conformation and the conformation of preceding amino acid residues, consequently influencing protein structure (Williamson, 1994). Repeated cysteine-proline motifs are often found in proteins forming ligand complexes, such as iron-sulfur (Fe-S) clusters where the proline may be important to stabilize the structure of the active site (Sticht & Rösch, 1998). Therefore, the prolines in the CXX(X)P motifs could play critical roles for D6PK structure. The cysteines could also be sites of lipid modification such as S-acylation (Dunphy & Linder, 1998). Interestingly, lipid modifications such as S-acylations can occur in combination with polybasic motifs in peripheral and integral membrane proteins to promote localization in specific membrane environments (Ahearn et al., 2012; Tian et al., 2008). Due to the diverse roles cysteines can play for protein biochemistry, it is intriguing to speculate that the CXX(X)P motifs could contribute to the avidity of D6PK towards the plasma membrane. My goal for this thesis was to unravel whether the CXX(X)P motifs may play a mechanistic role for D6PK localization and function, by applying a structural and functional approach.

In addition to the polybasic K/R-rich motif and the repeated CXX(X)P motifs, D6PK contains serines in the middle domain preceding the polybasic K/R-rich motif (S310/S311). The serines preceding the polybasic K/R-rich motif are found in multiple but not all AGC1 kinases and in PID2 (Figure 3, Figure 4 A)(Bassukas et al., 2022). The serines S310/S311 could be phosphorylation sites, which, through their negative charge, would counteract the positive charge of the polybasic K/R-rich motif. Similar mechanisms have been described for several membrane-localized proteins (Gerganova et al., 2019; Bailey & Prehoda, 2015; McLaughlin & Aderem, 1995). For example, the aPKC substrates Lgl, Numb, and Mir possess phosphorylation sites located inside their polybasic motifs, resulting in charge neutralization and subsequent loss of plasma membrane association upon phosphorylation (Bailey & Prehoda, 2015; Dong et al., 2015; Smith et al., 2007).

Since we did not describe a mechanism for D6PK internalization previously, I wanted to understand whether phosphorylation of the serines S310/S311 could function as an electrostatic switch mechanism by counteracting the positive charge of the polybasic K/R-rich motif.

This study was motivated by the question of how D6PK polarity at the basal plasma membrane is established and maintained. I focused on studying the D6PK middle domain since we previously described the middle domain as required and sufficient for D6PK plasma membrane association. The middle domain is a plant-specific extension of the activation segment, which contains multiple interesting sequence motifs such as the polybasic K/R-rich motif, the CXX(X)P-repeats, and serines S310/S311 preceding the polybasic K/R-rich motif. Previous studies showed that the polybasic K/R-rich motif is required for D6PK localization at the basal plasma membrane. I wanted to find out whether the identified CXX(X)P motif and the serines S310/311 also contribute to the D6PK polar plasma membrane localization and its rapid trafficking by applying a structural and functional approach to study D6PK *in vitro* and *in vivo*.

1.4 Objective

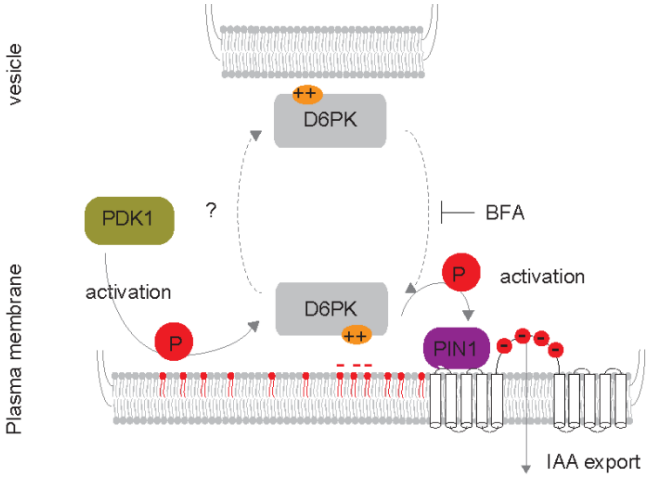

Figure 5. Model of D6PK membrane association and trafficking at the beginning of this project. D6PK strongly associates with membranes via its polybasic K/R-rich motif. Treatments with the trafficking inhibitor BFA lead to internalization of D6PK and association with internal membranes. The presence of the protein biosynthesis inhibitor CHX indicates that D6PK traffics rapidly between the plasma membrane and the cytosol. While D6PK is trafficked to the plasma membrane GNOM-dependently, the mechanism for its fast dissociation is yet to be described.

The present study aims to expand the previously established model of D6PK polar plasma membrane association with a focus on elucidating the mechanisms for its polar localization, strong plasma membrane anchoring, and fast cycling in greater detail. These aspects of D6PK localization cannot be entirely explained by plasma membrane targeting mediated through electrostatic interactions by the previously characterized polybasic K/R-rich motif. I therefore conducted a detailed analysis on the D6PK middle domain. I sought to examine whether there are additional features in the middle domain, such as the CXX(X)P motifs and the serines S310/S311, contributing to D6PK localization and trafficking. Insights acquired from this thesis may further enhance the comprehension of the cell biological behavior of other *Arabidopsis thaliana* AGC1 kinases. The knowledge gained through this thesis may lead to a more conclusive picture of plant development by providing an enhanced biochemical and cell biological understanding of the AGCVIII kinase subfamily.

1.5 List of publications

Parts of my thesis are published in the following publication:

Graf, A., Bassukas, A.E.L., Xiao, Y., Barbosa, I.C.R, Mergner, J., Grill, P., Michalke, B., Küster, B., Schwechheimer, C. “D6PK plasma membrane polarity requires a repeated CXX(X)P motif and PDK1-dependent phosphorylation.” *Nat. Plants* **10**, 300–314 (2024). https://doi.org/10.1038/s41477-023-01615-6

I contributed to this publication which is not part of this thesis:

Koh, S.W.H, Marhava, P., Rana, S., Graf, A., Moret, B., Bassukas, A.E.L., Zourelidou, M., Kolb, M., Hammes, U.Z., Schwechheimer, C., Hardtke, C.S. “Mapping and engineering of auxin-induced plasma membrane dissociation in BRX family proteins.” *The Plant Cell* **33**, 1945–1960 (2021). https://doi.org/10.1093/plcell/koab076

2 Materials and Methods

2.1 Material

2.1.1 Biological Material

Transgenic plants

All experiments were conducted in *Arabidopsis thaliana* wildtype Columbia-0 (Col-0) or previously published *d6pk01* (*d6pk d6pk-like1*), *d6pk012* (*d6pk d6pk-like1 d6pk-like2*) and *pdk1-14 pdk2-4* (*pdk1 pdk2*) mutants in the Col-0 background (Xiao & Offringa, 2020; Zourelidou et al., 2009). Transgenic lines expressing YFP-D6PK, YFP-D6PKΔMID with a middle domain deletion, or YFP-D6PK_MID with the middle domain alone from the 35S CaMV or under a *D6PK* promoter fragment in the *d6pk d6pkl1* mutant were previously described (Barbosa et al., 2016). The transgenic line expressing kinase-dead 35S::YFP-D6PK_KE was previously published (Barbosa et al., 2014). Transgenic lines expressing YFP-D6PK_SSAA and YFP-D6PK_SSDD under a *D6PK* promoter fragment were generated previously (Barbosa, 2015).

Bacterial strains

For plasmid propagation, *Escherichia coli* strains DH5α (fhuA2 Δ(argF-lacZ)U169 phoA glnV44 Φ80 Δ(lacZ)M15 gyrA96 recA1 relA1 endA1 this-1 hsdR17) were used, and for recombinant protein expression *Escherichia coli* Rosetta (DE3) (F^-ompT $hsdS_B(r_B^-\ m_B^-)$ gal dcm (DE3) pRARE (Cam^R)).

For plant transformation, the *Agrobacterium tumefaciens* strains PMP90 pSoup or RK were used depending on the required helper plasmid.

2.2.2 Nucleic acids

Plasmids

For protein expression in plants and protoplasts, the vector backbones pGreen, pExtag-YFP, pFAST-GFP and pUBN-Eos were used. The wildtype constructs pGreen-D6PKp::YFP-D6PK and pExtag-YFP-35Sp::YFP-D6PK were previously published, and mutagenesis in these constructs was performed as described.

Codon-optimized D6PK for expression in *Escherichia coli* was synthesized by Invitrogen GeneArt synthesis including a *BamH*I and *EcoR*I restriction site for subsequent cloning. For protein expression, the vector backbones PGEX6P-1, pET28B and pDest15 were used. A full list of plasmids is listed in the table.

Table 1. List of plasmids used for this study.

Name	Description	Reference
CAG01-pGreen-D6PK	pGreen-D6PKp::YFP:D6PK	This thesis
CAG02-pGreen-C1S	pGreen-D6PKp::YFP:D6PK_C1S	This thesis
CAG03-pGreen-C2S	pGreen-D6PKp::YFP:D6PK_C2S	This thesis
CAG04-pGreen-C3S	pGreen-D6PKp::YFP:D6PK_C3S	This thesis
CAG05-pGreen-C4S	pGreen-D6PKp::YFP:D6PK_C4S	This thesis
CAG06-pGreen-C5S	pGreen-D6PKp::YFP:D6PK_C5S	This thesis
CAG07-pGreen-C1-5S	pGreen-D6PKp::YFP:D6PK_C1-5S	This thesis
CAG08-pExtag-D6PK	pEXTAG-35Sp::YFP:D6PK	Melina Zourelidou (Zourelidou et al., 2009)
CAG09-pExtag-C1S	pEXTAG-35Sp::YFP:D6PK_C1S	This thesis
CAG10-pExtag-C2S	pEXTAG-35Sp::YFP:D6PK_C2S	This thesis
CAG11-pExtag-C3S	pEXTAG-35Sp::YFP:D6PK_C3S	This thesis
CAG12-pExtag-C4S	pEXTAG-35Sp::YFP:D6PK_C4S	This thesis
CAG13-pExtag-C5S	pEXTAG-35Sp::YFP:D6PK_C5S	This thesis
CAG14-pExtag-C1-5S	pEXTAG-35Sp::YFP:D6PK_C1-5S	This thesis
CAG15-pExtag-P2G	pEXTAG-35Sp::YFP:D6PK_P2G	This thesis
CAG16-pExtag-P3G	pEXTAG-35Sp::YFP:D6PK_P3G	This thesis
CAG17-pExtag-P4G	pEXTAG-35Sp::YFP:D6PK_P4G	This thesis
CAG18-pExtag-P5G	pEXTAG-35Sp::YFP:D6PK_P5G	This thesis
CAG19-pExtag-PAX	pEXTAG-35Sp::YFP:PAX	Lanassa Bassukas (Marhava et al., 2018)
CAG20-pExtag-PAX_C4S	pEXTAG-35Sp::YFP:PAX_C4S	This thesis
CAG21-pExtag-PAX_C5S	pEXTAG-35Sp::YFP:PAX_C5S	This thesis
CAG22-pExtag-KIPK	pEXTAG-35Sp::YFP:KIPK	Benjamin Weller, Yao Xiao (Xiao et al., 2025)
CAG23-pExtag-KIPK_C4S	pEXTAG-35Sp::YFP:KIPK_C4S	This thesis
CAG24-pExtag-KIPK_C5S	pEXTAG-35Sp::YFP:KIPK_C5S	This thesis
CAG25-pDest-D6PK	pDest15-T7p::GST-D6PK	Melina Zourelidou (Zourelidou et al., 2009)
CAG26-pDest-C1S	pDest15-T7p::GST-D6PK_C1S	This thesis
CAG27-pDest-C2S	pDest15-T7p::GST-D6PK_C2S	This thesis

CAG28-pDest-C3S	pDest15-T7p::GST-D6PK_C3S	This thesis
CAG29-pDest-C4S	pDest15-T7p::GST-D6PK_C4S	This thesis
CAG30-pDest-C5S	pDest15-T7p::GST-D6PK_C5S	This thesis
CAG31-pDest-C1-5S	pDest15-T7p::GST-D6PK_C1-5S	This thesis
CAG32-pDest-P2G	pDest15-T7p::GST-D6PK_P2G	This thesis
CAG33-pDest-P3G	pDest15-T7p::GST-D6PK_P3G	This thesis
CAG34-pDest-P4G	pDest15-T7p::GST-D6PK_P4G	This thesis
CAG35-pDest-P5G	pDest15-T7p::GST-D6PK_P5G	This thesis
CAG41-EOS-D6PK	pUBN-EOS-Dest-UBQp::EOS:D6PK	Inês Barbosa (Barbosa, 2015)
CAG42-EOS-D6PK_SSAA	pUBN-EOS-Dest-UBQp::EOS:D6PK_SSAA	Inês Barbosa (Barbosa, 2015)
CAG43-EOS-D6PK_SSDD	pUBN-EOS-Dest-UBQp::EOS:D6PK_SSDD	Inês Barbosa (Barbosa, 2015)
CPK21	pSEVA431_GST_CPK21full	Moritz Ruschhaupt (Ruschhaupt et al., 2019)
CPK21_vk	pSEVA431_GST_CPK21vk	Moritz Ruschhaupt (Ruschhaupt et al., 2019)
SAG03-pGreen-dSAN	pGreen-D6PKp::YFP-D6PK_dSAN	This thesis
SAG01-pET28b-D6PK	pET28b-His-SUMO-D6PK	This thesis

Primers

Table 2. Primers used for this study.

Primer	Name	Sequence
AG20	D6PK C1S	[Phos]TCCCTGAGATCTACTGTGAGC
AG21	D6PK C2S	[Phos]TCGGTTTCTTCTTCGCAACAACC
AG22	D6PK C3S	[Phos]ACAACCTGCATCTATCCAGCAAC
AG23	D6PK C4S	[Phos]AGCAACCATCTTCTATCTCAATGGC
AG24	D6PK C5S	[Phos]CTCCAACATCTTCTTCGGTCCTCG
AG46	D6PK P2G	[Phos]GCTCGCAACAAGGTGCATGCATC
AG47	D6PK P3G	[Phos]ATCCAGCAAGGATCTTGCATCTC
AG48	D6PK P4G	[Phos]CAATGGGCTGGAACATCTTGCTTCG
AG49	D6PK P5G	[Phos]TTGCTTCGGTGGTCGGTTCTTC
AG50	PAX C4S	[Phos]CCTACATCAGCTTCTATCATTCAACCC
AG51	PAX C5S	[Phos]CAACCCTCATCTTTCTTACCGCG
AG54	PAX sequencing	ATGGAATACTGTCCTGGAGG
AG52	KIPK C4S	[Phos]CGAACCATCTTCTCAGGTTTCGTG
AG53	KIPK C5S	[Phos]CAGGTTTCGTCTTTCAGCCCTAG
AG55	KIPK sequencing	CTCAGACAGAAGCAGCTAGGC
IB72	D6phosphomutantAA	[Phos]GGTCCTCGGTTCTTCGCAGCGAAATCCAAGAAAGACA

IB73	D6phosphomutantDD	[Phos]GGTCCTCGGTTCTTCGACGATAAATCCAAGAAAGAC
AG14	KD1 sequencing FW	GATCTGAAACCCGAGAACG
IB25	D6PK geno FW	TGATGGCTTCAAAAACTCCAGAAGGATC
IB26	D6PK geno RV	ACTCTGATCAGATCTTACAC
LBb1.3	LBb geno	ATTTTGCCGATTTCGGAAC
AG11	D6PK CDS FW	CTCCAGAAGGATC
AG12	D6PK CDS RV	GCCGATTTCGGAAC
AG78	D6PK qRT-primer FW	TTGCTTGTGAAGGAGCCACA
AG79	D6PK qRT-primer RV	TGCAGTGTCTTGATCACC
D87	Actin 2-8 FW	GGTAACATTGTGCTCAGTGGTGG
D86	Actin 2-8 RV	AACGACCTTAATCTTCATGCTGC

2.1.2 Chemicals

All chemicals were purchased from Roth Carl Roth (Karlsruhe, Germany) unless specified otherwise.

2.2 Methods

2.2.1 Sequence alignments

For protein alignments, protein sequences of AGC kinases from *Arabidopsis thaliana* and other plant species, as specified, were retrieved from PLAZA4.0 and aligned using the Muscle Alignment tool of the Geneious R11.1.3 software. To facilitate analysis, the alignments were manually adjusted for a refined alignment of the CXX(X)P motifs, the polybasic K/R-rich motif, and the serine residues preceding the polybasic K/R-rich motif.

2.2.2 Cloning procedures

Mutations in the D6PK, PAX, and KIPK sequences were introduced by mutagenesis PCR on vectors containing CDS sequences with the primers AG20-AG24, AG46-AG49, and AG50-AG53 listed in Table 2 using previously established protocols (Sawano & Miyawaki, 2000). In brief, plasmids containing the original CDS sequences were denatured, and up to five primers at a concentration of 0.14 µM each were annealed to the respective plasmids. Amplification was performed at 65°C with a rate of 30 sec/kB. Afterwards, the original plasmid was digested with the methylation-sensitive restriction enzyme *Dpn*I, and two more amplification cycles were performed subsequently. Half of the reaction was

transformed into DH5α cells. Single colonies were cultured, and plasmid extracted and purified using a NucleoSpin Plasmid Mini Kit (Machery-Nagel, Düren, Germany). Clones carrying the mutations were identified by sequencing and alignment in the Geneious R11.1.3 software (Biomatters, New Zealand).

For recombinant protein expression and biochemical in vitro studies, a codon-optimized sequence including *Bam*HI and *Xho*I restriction sites for subsequent cloning was synthesized by Invitrogen (Invitrogen, Waltham, MA). This clone was then digested with *Bam*HI and *Xho*I (Thermo Fisher Scientific, Waltham, MA) in 2x Tango buffer at 37°C for 1.5 h. The reaction was loaded on an 0.8% agarose gel, and the correctly sized band was cut and extracted from the gel using a gel and PCR purification kit (Macherey-Nagel, Düren, Germany).

2.2.3 Plant transformation and genotyping

Plants were transformed using the floral dip method. For transformation of pUBN, pGreen, or pFAST-based plasmids, the strain pMP90 RK was transformed using electroporation. Bacteria were plated and incubated for 2 days at 30°C. Single colonies were picked, confirmed by colony PCR, and incubated at 30°C. They were then transferred to a 500 mL culture and grown to an OD around 0.6. Agrobacteria were harvested by centrifugation (4000 *g*, 15 min) and resuspended in 300 mL floral dip solution (5% glucose, 0.05% Silwet L-77, 44 nM Benzylamino purine) (Clough & Bent, 1998). Flowers of plants at around three weeks of age were dipped in the solution and afterwards incubated overnight covered in a plastic bag. Plants were sprayed and cleaned with water the next day and transferred to continuous light growth conditions. Seeds were harvested after three more weeks of growth, and selection was either carried out with the pFAST red fluorescence system or using BASTA selection on plates filled with ½ Murashige & Skoog medium containing 15 µg/mL phosphinotricine (PPT) (Clough & Bent, 1998).

Genotyping for the genetic background was performed using the primers IB25 and IB26 to amplify the wildtype sequence and LBb1.3 and IB26 to genotype for the T-DNA insertion and amplification with Taq polymerase. PCR product was loaded on a 1 % agarose gel to confirm homozygous genetic background. The transgene was amplified using primers AG11 and AG12 with Phusion polymerase. The PCR product was purified using a gel and PCR purification kit (Macherey Nagel, Düren, Germany) and subsequently sent for

sequencing with primer AG14. Plants carrying the transgene with the proper mutation were identified after alignment using the Geneious R11.1.3 software (Biomatters, New Zealand).

2.2.4 Protoplast transformation

Protoplast transformation was conducted on an *Arabidopsis thaliana* root cell culture as described previously (Katsiarimpa et al., 2011). In brief, cells were harvested by centrifugation and repeatedly washed in Sol1 (0.4 M Mannitol , 5 mM EGTA), and afterwards digested with cellulase (Serva, Heidelberg, Germany) and Macerozyme (Serva, Heidelberg, Germany) in Sol1 for 2 hours at room temperature (RT) in the dark. Protoplasts were afterwards filtered using a 100 µM pore diameter nylon mesh and repeatedly washed in SolA (0.4 M Mannitol, 70 mM $CaCl_2$, 5 mM MES pH 5.7). In the end, protoplasts were transferred to MMM (0.4 M Mannitol, 15 mM $MgCl_2$, 5 mM MES pH 5.7). Protoplasts were mixed with 30 µg plasmid DNA and transformed by titrating a poly-ethylenglycol (PEG) solution (0.4 M Mannitol, 100 mM $Ca(NO_3)_2$, 4% PEG6000) and subsequently washed using Dilution Sol (0.4 M Mannitol, 125 mM $CaCl_2$, 50 mM KCl, 50 mM Glucose, 15 mM MES pH 5.7). Finally, protoplasts were transferred to 0.4 M Mannitol enriched with MS salts and vitamins (Sigma, St. Louis, MO) and incubated for at least 14 hours in the dark at room temperature. Afterwards, the transformed protoplasts were imaged for cellular protein distribution using an Olympus FV1000 microscope with high-sensitivity Gallium Arsenide Phosphide (GaAsP) detectors using identical acquisition settings between samples (Olympus, Hamburg, Germany). Remaining protoplasts were afterwards harvested by centrifugation and resuspended in 50 µL 2x Laemmli (65.8 mM Tris-HCl, pH 6.8, 2.1% SDS, 26.3% (w/v) glycerol, 0.01% bromophenol blue). 10 µL were then loaded on a gel for further analysis using SDS-PAGE and immunoblotting.

2.2.5 Physiological experiments

For the investigation of phototropic hypocotyl bending responses, three-days-old seedlings were grown in the dark on ½ Murashige & Skoog medium. Etiolated seedling hypocotyls were straightened under a safe-green light and then exposed to a unilateral light stimulus of 4.9 µmol m^{-2} s^{-1} in a FloraLED chamber for four hours (CLF Plant Climatics, Wertingen, Germany). The bending angle was calculated from scanned seedling images using the angle measurement tool of Fiji (NIH ImageJ) and displayed on

rose diagrams using the Origin software (OriginLab Corporation, Northampton, MA, USA) (Schindelin et al., 2012). For examination of apical hook formation, three-days-old etiolated seedlings were imaged with an Olympus BX61 light microscope (Olympus, Hamburg, Germany).

2.2.6 *In vivo* auxin transport assays

Auxin transport assays in hypocotyls of etiolated seedlings were carried out as previously described with slight modifications (Willige et al., 2013). Briefly, ^{3}H-IAA (25 Ci mmol^{-1}; ARC, St. Louis, MO) was brought to a final concentration of 400 nM in 5 mM MES (pH 5.5), 1% glycerol. Four-days-old dark grown seedlings were placed with their cotyledon and apical part of the hypocotyl onto 6 mm Parafilm (Beemis Company, Neenah, WI) on ½MS plates. 0.5 µl ^{3}H-IAA solution was applied to the cotyledons of each seedling. Seedlings were then incubated vertically in the dark for four or six hours as indicated. Subsequently, the lower part of the hypocotyl was cut. For scintillation counting, five seedlings were grouped into one scintillation vial containing 2 ml Ultima Gold liquid scintillation cocktail and counted in a Tri-Carb 4910TR Liquid Scintillation counter (Perkin Elmer, Rodgau, Germany).

2.2.7 Microscopy

Transgenic plants expressing YFP-tagged fusion proteins were investigated for cellular protein distribution using an Olympus FV1000 microscope (Olympus, Hamburg, Germany) with high sensitivity Gallium Arsenide Phosphide (GaAsP) detectors, applying identical acquisition settings between samples. Treatments were generally performed in liquid MS medium with the concentration and time indicated in the respective descriptions. Seedlings were then mounted on the carrier in the liquid medium containing the treatment, and imaging was carried out as described.

For fluorescent recovery after photobleaching (FRAP) experiments, five-days-old seedlings were analyzed on a Leica SP8 (Leica Microsystems, Wetzlar, Germany) using the FRAP function by bleaching a 4 µm x 1 µm window at the basal plasma membrane of root epidermal cells with a 514 nm Argon laser, using the same acquisition settings between samples. Fluorescence recovery was quantified from 200 or 500 frames after photobleaching with 0.233 seconds per frame. Recovery was compared to five frames taken before bleaching. For image alignment and quantification, the 3D drift correction

tool and the measure tool of Fiji were used (Schindelin et al., 2012). The resulting measurements were analyzed using the easyFRAP Matlab package (Koulouras et al., 2018).

2.2.8 Histological methods

To assess D6PK S310/SS311 *in vivo*, the antibody anti-S310p/S311p was used which was produced in rabbits against the chemically synthesized peptide (H-CPRFF-phosphoS-phosphoS-KSKKDK-NH2) and validated for binding using an ELISA (Eurogentec, Liege, Belgium). To assess PIN1 S1 phosphorylation a previously established anti-PIN1-S1p antibody was used (Weller et al., 2017). For immunostaining, five-days-old light grown seedlings were treated with 10 µM BFA or a corresponding mock solution for 30 min, and fixed for 1 hr at room temperature under vacuum in 4% (v/v) paraformaldehyde in PBS pH 7.4. Cell walls were partially digested for 30 min at 37 °C with 2% (w/v) Driselase (Sigma, Taufkirchen, Germany). Plasma membranes were permeabilized for 1 hr at room temperature with 3% (v/v) Nonidet P-40 (AppliChem, Darmstadt, Germany) in 10% (v/v) DMSO/PBS. The samples were blocked for 1 h at room temperature with 4% (w/v) BSA in PBS before anti-aS310p/S311p (1:100), diluted in blocking solution, was added for 4 hours at 37°C. Following washes with 0.1% Triton X-100 (AppliChem, Darmstadt, Germany) in PBS, the primary antibody was detected with a Cy3-conjugated anti-rabbit antibody (1:600; Dianova, Hamburg, Germany) after 4 hours incubation at 37°C. The immunostained roots were washed again and afterwards were examined in an Olympus FV1000 confocal laser scanning microscope (Olympus, Hamburg, Germany).

2.2.9 Image quantification and statistical methods

To determine relative plasma membrane localization and polar distribution of proteins in the cell, confocal microscopy images were analyzed using the Fiji software (Schindelin et al., 2012). To determine the relative plasma membrane localization of proteins, a ROI at the basal plasma membrane was drawn and then the same ROI was moved upwards into the cytosol. The average intensity was measured in both ROIs, and a ratio of the plasma membrane towards the total fraction was formed. For each quantification, five to six epidermis cells from three seedlings were measured for each genotype. These data points were plotted and compared using one-way-ANOVA. For polarity index determination,

profile plots were generated passing through the lateral sides of the cell and the basal plasma membrane. The average signal was subtracted from the maximum signal of each plot, allowing me to locate enrichments of signal, and a ratio was formed of basal to the total basal and lateral signal. Again, five to six epidermis cells from three seedlings were used for each genotype, and data points were plotted and compared using one-way-ANOVA.

2.2.10 Immunoblot analysis

For immunoblot analysis of plant protein extracts, YFP-D6PK or its variants were analyzed by SDS-PAGE using 40 µg total protein and. If specified, subcellular fractionation were carried out through 1 hr ultracentrifugation at 100,000 *g*. SDS-PAGE were blotted and probed with anti-GFP (aGFP; 1:3000, lab stock), anti-Tubulin A (aTUA; 1:2000, Agrisera, Vännäs, Sweden), anti-H-ATPase (aAHA, 1:1000, Agrisera, Vännäs, Sweden) or anti-UDP glucose pyrophosphorylase (aUGP; 1:1500, Agrisera, Vännäs, Sweden) primary antibodies and an anti-rabbit horse radish peroxidase-conjugated secondary antibody (1:1000; Invitrogen, Waltham, MA). Chemiluminescence was detected with a Fujifilm LAS 4000 mini (Fuji, Japan) and quantified using the measure and profile functions of the Fiji (ImageJ) software (Schindelin et al., 2012).

2.2.11 Quantitative reverse transcription PCR

RNA for qRT-PCR was extracted using a NucleoSpin RNA Plant kit (Macherey-Nagel, Düren, Germany). 1 µg RNA was reverse transcribed using an oligo(dT) primer and M-MuLV reverse transcriptase (Thermo Fisher Scientific, Waltham, MA). D6PK transcript levels were determined with the primers AG78 and AG79 from 3.125 ng cDNA using Takyon™ No ROX SYBR 2X MasterMix blue dTTP (Eurogentec, Liege, Belgium) in a CFX384 Real-Time System Cycler (Bio-Rad, Hercules, MA). Amplification was performed using a four-step protocol (step 1, 50°C for 3:00 min; step 2, 95°C for 3:00 min; step 3, 95°C for 0:15 min; step 4, 60°C for 0:40 min) with 41 repeats of steps 3 and 4 and a final melt curve step from 65°C to 95°C for 0:05 min at 0.5°C increments. For comparison of gene expression, the results were normalized to *ACTIN2* and *ACTIN8*, which were amplified using the primers D86 and D87.

2.2.12 Recombinant protein expression and purification

Recombinant GST-D6PK or His-SUMO-D6PK were obtained after transformation of Escherichia coli strain Rosetta DE3 (Novagen, Madison, WI) and induction with 0.5 mM IPTG once the density of the LB24-grown culture had reached an OD_{600} of 0.9. After induction, cultures were grown at 18°C for 14-18 hours and harvested by centrifugation (Beckmann-Coulter, Brea, CA) (5000 *g*, 10 min, 4°C). Cells were disrupted by sonication in buffer E (50 mM Na-Phos pH 7.4, 150 mM NaCl, 1 mM DTT, 0.5 % Triton-X-100, 5% Glycerol, Lysozyme, PMSF, PiC). For kinase assays, proteins were purified on 2 mL spin columns using 50 µL of Glutathione Agarose 4B beads (Macherey-Nagel, Düren, Germany) per 200 mL of culture grown as described above. Beads were washed with five times 1 mL buffer A (50 mM Tris-HCl pH 7.5, 100 mM NaCl, 1 mM PMSF) and protein was eluted with 100 µL buffer B (20 mM reduced glutathione (Sigma, St. Louis, MO), 50 mM Tris-HCl pH 7.5, 100 mM NaCl). For storage glycerol was added to 10%.

For structural studies and metal binding, GST-D6PK was purified on an ÄKTA purifier (GE Healthcare, Chicago, IL) using a 1 mL GSTrap FF column (GE Healthcare, Chicago, IL), washed with 15 CV buffer A, and eluted with buffer B. For further structural studies, His-SUMO-D6PK was expressed as described above, and cells were disrupted by sonication in buffer E + 5 mM imidazole and then purified on a 5 mL Co^{2+} TALON crude column (GE Healthcare, Chicago, IL) on an ÄKTA purifier (GE Healthcare, Chicago, IL) by washing with 20 CV buffer A-His 100 mM Na-Phos pH 7.4, 150 mM NaCl, 5 mM Imidazole, 1 mM DTT and eluted using on column cleavage with 1U SUMO protease (Thermo Fisher Scientific, Waltham, MA) and subsequent washing with buffer A. The eluted protein was dialyzed against IEx buffer (50 mM HEPES pH 8.0, 20 mM NaCl, 1 mM DTT) and purified on a HiTrap SP HP cation exchange column (GE Healthcare, Chicago, IL) with a gradient of 20-500 mM NaCl.

2.2.13 Thermofluor measurements

Thermofluor assays to optimize purification and test for protein stability were conducted as described previously (Boivin et al., 2013; Phillips & De La Peña, 2011). In brief, a protein-SYPRO Orange master solution was prepared with a final concentration of 10 µM protein (around 1.5 mg/mL for D6PK) mixed with 25x SYPRO Orange (Invitrogen, Waltham, MA) in protein buffer (20 mM Tris-HCl pH 7.5, 50 mM NaCl). For stability

screens 20 µL of this mix was pipetted into a 96-well PCR-plate and sealed with transparent microplate sealing foil. For buffer screens 16 µL of this mixture was pipetted to a plate containing 4 µL 5x stock solution of the desired buffer and plates were sealed. Melt curves were analyzed on a Bio-Rad CFX96 (Bio-Rad Laboratories, Hercules, MA) with the FRET filter from 25 to 65°C in 30 sec 1°C increments.

2.2.14 Analytical gel filtration chromatography

To determine molecular weight of purified D6PK and link the specific peak with spectral properties, purified protein was loaded on a TSKgel G2000SWXL (Tosoh Bioscience) column and eluted with Gefi buffer (50 mM HEPES pH 7.5, 300 mM NaCl, 1 mM DTT) at 0.5 ml/min and pressure of 28 bar on a LC-10Ai (Shimadzu). Intensity was monitored at a wavelength of 280 nm to monitor elution of protein and additionally screened for spectral properties.

2.2.15 Lipid binding assays

To test for lipid binding properties of AGC kinases, lipid binding assays were performed on commercially available PIP-strips (Echelon Biosciences, Salt Lake City, UT, United States) containing 15 lipids and a blank control according to manufacturer specifications. Membranes were blocked at 4°C overnight with blocking buffer (4% BSA in TBS 0.1% Tween). Afterwards, recombinantly expressed and purified proteins were diluted in blocking buffer (4% BSA in TBS 0.1% Tween) to a concentration of 0.5 µg/mL and incubated with the membrane for 1 h at room temperature. Membranes were washed three times with washing buffer (TBS 0.1% Tween) and then incubated with anti-GST antibody (aGST; 1:2000, GE Healthcare, Chicago, IL, United States) for 1 h at room temperature. The washing procedure was repeated, and the membrane was incubated with anti-goat peroxidase conjugate secondary antibody in blocking buffer (1:8000). After washing three times, chemiluminescence was detected with a Fujifilm LAS 4000 mini (Fuji, Japan) and quantified using the measure and profile functions of the Fiji (ImageJ) software.

2.2.16 *In vitro* phosphorylation assays

In vitro phosphorylation experiments were carried out using approximately 0.5 µg purified recombinant GST-tagged kinases in combination with purified recombinant GST-tagged

substrate proteins (0.5 – 1 µg). The recombinant proteins were incubated for 30 minutes in phosphorylation buffer (50 mM Tris-HCl pH 7.5, 100 mM NaCl, 10 mM $MgCl_2$, 1x Complete Protease Inhibitor Cocktail – Roche, Basel, Switzerland) supplemented with 5 µCi [g-32P]ATP (Hartmann Analytic, Braunschweig, Germany). The reaction was stopped by adding 1x Laemmli buffer and boiling the mix at 95°C for 5 min. The reactions were separated on a 10% SDS polyacrylamide gel (SDS-PAGE) and analyzed using autoradiography after drying the SDS-PAGE.

2.2.17 Mass spectrometry

All experiments requiring mass spectrometric analysis were performed by Julia Mergner from the Chair of Proteomics and Bioanalytics and Bavarian Center for Biomolecular Mass Spectrometry (TUM, Weihenstephan, Germany). In brief, immunoprecipitated proteins were run on a short gel, and in-gel trypsin digestion was performed according to standard procedures (Shevchenko et al., 2006). The tryptic peptides were eluted and dried in a vacuum concentrator and dissolved in 0.1% (v/v) formic acid in HPLC grade water prior to liquid chromatography-mass spectrometry (LC-MS) analysis. LC-MS/MS analysis was performed on Orbitrap mass spectrometer systems (Thermo Fisher Scientific, Waltham, MA) coupled on-line to a Dionex 3000 HPLC (Thermo Fisher Scientific, Waltham, MA) with a 75 µm × 2 cm trap column (Reprosil Pur ODS-3.5 µm particles (Dr. Maisch HPLC GmbH, Ammerbuch, Germany)) and a 75 µm × 40 cm analytical column (3 µm particles C18 Reprosil Gold 120 (Dr. Maisch HPLC GmbH, Ammerbuch, Germany). Results from mass-spectrometric analysis are deposited in the ProteomeXChange server via the PRIDE database (PRIDE ID: PXD037885).

2.2.18 Analysis of metal binding

To assess whether D6PK can bind metals, recombinant GST-GNC, GST-PIN1 HL, GST-D6PK, GST-D6PKΔMID, GST-D6PK_MID, GST-CPK21, and GST-CPK21 (short) were expressed and purified as described above. Proteins from three independent purifications were pooled, and three technical replicate measurements were performed with 1 mL of the pooled samples at a concentration of 1 mg ml^{-1} in 20 mM Tris HCl, pH 7.5; 50 mM NaCl. Element determination was performed by Peter Grill and Bernhard Michalke at the Helmholtz Zentrum in Munich. For element determination, the samples were diluted to 3 ml with milli-Q water. Measurements of the elements Ca^{2+} (spectral element line 183.801

nm), Fe^{2+} (259.941 nm), Mg^{2+} (279.079 nm), and Zn^{2+} (213.856 nm) were performed with inductively coupled plasma atomic emission spectrometry (ICP-AES) using an Optima 7300 DV (Perkin Elmer, Waltham, MA). Calculation of results was carried out by Peter Grill and Bernhard Michalke on a computerized lab data management system, relating the sample measurements to calibration curves, blank determinations, and control standards.

2.2.19 Analysis of disulfide bond formation

Disulfide bond analysis was performed as previously described with modifications (Pérez et al., 2010). Two reactions of 1 mg of total protein extract were prepared in 50 mM HEPES pH 7.5, 150 mM NaCl, 0.5% Triton-X-100, 0.2% SDS, 1 mM PMSF, 1 mM EDTA, 1x Protease Inhibitor Cocktail (Sigma, Taufkirchen, Germany). One reaction included 20 mM TCEP to selectively reduce disulfide bonds. Free cysteines were blocked using 100 mM NEM (N-ethylmaleimide) for 4 hours, and afterwards the reaction was stopped by incubating with 20 mM DTT for 30 min. Protein was diluted 1:5 and immunoprecipitated using GFP-Trap magnetic agarose (Chromotek, Planegg, Germany). Mass spectrometric analyses to assess disulfide bond formation were performed as described before.

2.2.20 Analysis of S-acylation

The acyl biotin exchange assay was performed as previously with total protein isolated from transgenic lines overexpressing YFP-D6PK (Hemsley, 2013). Frozen seedling material was ground to a fine powder in liquid nitrogen, resuspended in extraction buffer (1x PBS pH 7.4, 1x Complete Protease Inhibitor Cocktail (Sigma, Taufkirchen, Germany), 1 mM EDTA) and transferred to a potter tube. The sample was pottered for 1 min, and final concentrations of 1% Triton-X-100 and 25 mM NEM were added. The extract was incubated on a wheel at 4°C for 15 min to solubilize proteins and insoluble material was removed via centrifugation (5000 xg, 15 min). The protein concentration was determined using a Bradford assay. Protein concentrations were adjusted to 1 mg/mL using extraction buffer and 1 mL was used as input for the assay. Blocking of free cysteines was performed overnight in the dark at 4°C on a wheel and was followed by hydroxylamine treatment leading to the hydrolysation of S-acylations. For the negative control, the hydroxylamine treatment was substituted with 50 mM Tris pH 7.4. Subsequently, the extract was labelled with sulfhydryl-reactive biotin-HPDP, which reacts with the thiol groups of unmodified cysteines. The modified proteins were enriched on streptavidin beads, loaded on a SDS-PAGE and subjected to immunoblot analysis with aGFP. Tubulin A (TUA), a palmitoylation

substrate previously identified *in planta*, served as a positive control (Hemsley et al., 2008).

To assess dynamic S-acylation of YFP-D6PK, an acyl resin-assisted capture assay was performed after seedlings were treated with mock or BFA, and after ultracentrifugation of 1 mg total protein extract at 100,000 *g* protein as previously described (Forrester et al., 2011). After blocking free cysteines with 0.1% methyl methanothiosulfonate (MMTS) and hydrolysis of S-acylations with hydroxylamine, free thiols could directly be captured on thiopropyl Sepharose and eluted using 50 mM DTT. Immunoblot analysis was carried out as described before.

2.2.21 Determination of D6PK *in vitro* phosphorylation sites

Mass spectrometric analyses to assess D6PK *in vitro* phosphorylation sites were performed in collaboration with the Küster chair. Purified proteins were phosphorylated using 5 mM ATP and 5 mM $MgCl_2$ for 30 min at 28°C. The reaction was stopped by adding 1x Laemmli buffer, loaded on a 10% Acrylamide Tris-Glycine PAGE, and separated for 45 min. The gel was stained using Coomassie Brilliant Blue (CBB) and destained. The band corresponding to D6PK was excised from the gel and used for further mass spectrometric analysis. In-gel trypsin digestion and mass spectrometric analysis was performed as described before.

3 Results

3.1 Analysis of AGC1 kinase middle domains

3.1.1 AGC1 kinase middle domains contain conserved features

My project was motivated by further investigating the mechanisms behind the polar localization of D6PK. Since our group previously described the middle domain of D6PK to be required and sufficient for D6PK plasma membrane association, I decided to further examine the role of the middle domain for polar plasma membrane association (Barbosa et al., 2016). The middle domain is a conserved feature of all AGCVIII kinases – distinguishing this kinase subfamily from other *Arabidopsis thaliana* AGC kinases. However, among all AGCVIII kinases, the middle domain sequence is most extended in the AGC1 kinases and contains a previously described polybasic K/R-rich motif and repeated CXX(X)P motifs, apart from which the sequence varies highly between the different kinases. By making alignments and comparing middle domain sequences of all the Arabidopsis thaliana AGC1 kinases but also orthologues from other species, I wanted to find out which CXX(X)P repeats are conserved and may thus be central to kinase function *in vivo*. Additionally, I looked at the serines preceding the polybasic K/R-rich motif and whether they also occur in other AGC1 kinases.

Using an alignment of all AGC1 middle domain sequences, I analyzed the pattern of previously identified CXX(X)P repeats, that was first noted in KIPK and is present in all AGC1 kinases and PID2, and I investigated the serines preceding the polybasic K/R-rich motif (Bassukas et al., 2022; Day et al., 2000). The conserved signature of the CXX(X)P motifs includes a cysteine interspaced by two or three amino acids and followed by a proline. The number of repeats ranges from six in D6PKL3 and D6PKL2 to two in AGC1.5, AGC1.6 and AGC1.7 (Figure 3, Figure 4 A). The number of repeats and the sequence surrounding the motif are not conserved among all members of the AGC1 clade. Most strongly conserved in position and sequence identity are the cysteines of the CXX(X)P1 and CXX(X)P5 motif. The CXX(X)P1-motif in D6PK misses the proline which disagrees with the motif signature. However, the cysteine in the sequence alignment with the other D6PKs can be identified as C1 (Figure 3). Among the AGC3 kinases, only PID2 possesses four CXX(X)P motifs, resembling an AGC1 kinase rather than an AGC3 kinase based on this criterion (Figure 3).

Interestingly, the cysteine of the first CXX(X)P motif located closely to the Mg^{2+}-binding DFD motif is also present in AGC4 and AGC3 kinases interspaced with one amino acid between cysteine and proline (CXP). As phot1 and phot2 in the AGC4 clade, represent the evolutionary oldest AGC1 kinases, this could suggest that the other CXX(X)P motifs are a duplication of this CXP1 motif found in the phots (Galván-Ampudia & Offringa, 2007). Thus, it could represent the evolutionary origin of these repeats found in the middle domain.

In D6PK and many other AGC1 kinases the middle domains contain a high number of serines. Most strikingly, in all the D6PKs, the CXX(X)P5 motif and the polybasic K/R-rich motif are separated by serines. In D6PK these serines corresponded to S310 and S311 (Figure 3). To understand whether the identified and described CXX(X)P motifs and serines are functionally relevant, I carried out experiments throughout this thesis to understand their role for protein localization and activity.

3.1.2 AGC1 middle domain motifs are evolutionary conserved

To ascertain whether the repeated CXX(X)P motifs are a unique feature of Arabidopsis thaliana AGCVIII kinases or are also found in other species, I searched the Plaza database for AGCVIII orthologues from other species and aligned them with the AGCVIII kinases from *Arabidopsis thaliana*. I constructed a phylogenetic tree to identify orthologues of specific kinases. In my subsequent analysis, I included D6PKs, AGC1.5, AGC1.6 and AGC1.7 from *Arabidopsis thaliana* along with their corresponding orthologues from other species. Sequences from *Zea maize* (Zm), *Oryza sativa* (Os), *Solanum lycopersicum* (Solyc), *Medicago truncatula* (Medtr) and *Gingko biloba* (GIB) were selected due to their well-annotated genomes and representation of monocots, dicots, and gymnosperms. An alignment of the middle domain sequences revealed that the previously characterized polybasic K/R-rich motif and the CXX(X)P motif are found in all the AGC1 kinases across all the examined species (Figure 6 A). I noted the conservation of the CXX(X)P motifs in number and position among kinase orthologues from different species. D6PK, D6PKL1 and their closest orthologue from *Oryza sativa* possess five CXX(X)P repeats, while D6PKL2, D6PKL3 and their respective orthologues have six repeats (Figure 6 B). Intriguingly, *Arabidopsis thaliana* AGC1.5, AGC1.6 and AGC1.7 only contain two CXX(X)P motifs in their middle domain, and this property is conserved in their orthologues from *Oryza sativa*, *Medicago truncatula* and *Solanum*

lycopersicum (Figure 6 C). The conserved number and position of the CXX(X)P motifs may indicate its functional significance.

Additionally, I noted that the polybasic K/R-rich motifs of D6PKs from all species analyzed are preceded or flanked by serine residues. Interestingly, the number of serines correlates with the length of the polybasic K/R-rich motifs as some D6PKL2 orthologues from *Oryza sativa* and *Zea maize* depicted a higher number of the basic amino acids lysine or arginine as well as an increased number of serines (Figure 6 B). Among AGC1.5, AGC1.6, AGC1.7 and their orthologues the presence of serine residues preceding the polybasic K/R-rich motif is highly variable. Not all the analyzed kinases contain these serine residues, and some contain other amino acid residues, such as tyrosine or threonine, preceding the polybasic K/R-rich motif that may potentially be phosphorylated (Figure 6 C). I concluded that the CXX(X)P repeats are conserved in their quantity and relative position between AGC1 kinase orthologues from different plant species, while the presence of serine residues shows higher variation. Among all the kinases the CXX(X)P1, the CXX(X)P4, and the CXX(X)P5 motifs are the most conserved of all the motifs suggesting functional significance.

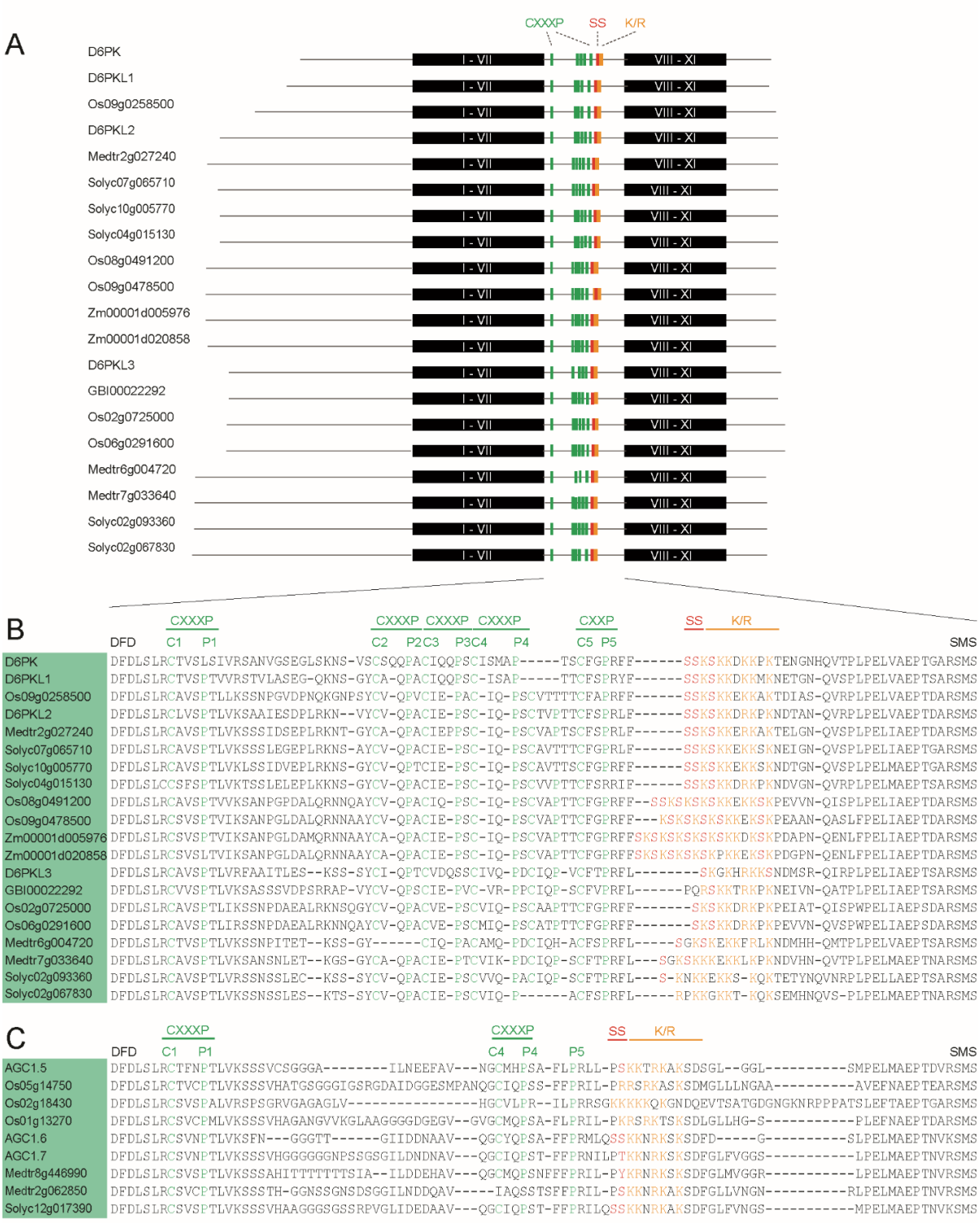

Figure 6. CXX(X)P motif repeats are conserved among vascular plants and the number of repeats is conserved among orthologues. A. – B. Schematic representation of D6PK orthologues from rice *Oryza sativa* (Os.), *Medicago truncatula* (Medtr.), *Solanum lycopersicum* (Solyc.), *Gingko biloba* (GB) (A) and muscle alignment of their middle domains (B). **C.** Muscle alignment of middle domains of *Arabidopsis thaliana* AGC1.5 – AGC1.7 orthologues from *Oryza sativa*, *Medicago truncatula* and *Solanum lycopersicum*. CXX(X)P motifs, the polybasic K/R-rich motif (K/R) and adjacent serine residues are colored for better distinction. The conserved key residues of the kinase subdomains – DFD (VII) and SXS (VIII) - are included and labeled for better comparison.

3.1.3 AGC kinases from other species also bind to PIPs indicating a conserved role of the K/R- motif

One additional question is whether the function and biochemical characteristics of AGCVIII are evolutionary conserved. One aspect that was interesting for me and my work was whether the function of the middle domain is conserved, and the polybasic K/R-rich motif found in the evolutionary first AGC1 kinases from *Marchantia polymorpha* can also bind to phosphoinositides, suggesting that they may localize at the plasma membrane like D6PK and show similar cell biological features.

In a joint effort with B.Sc. students and different members of the laboratory, we cloned AGC1 kinases from *Marchantia polymorpha*. Me and my student later expressed and purified the AGC1 kinase orthologues from *Marchantia polymorpha* Mapoly0030s0017 (Mp17), Mapoly0008s0088 (Mp88) and Mapoly0060s0068 (Mp68) to test their behavior in lipid binding assays. Interestingly, six repeated CXX(X)P motifs are already found in the middle domain of Mp17, the closest *Marchantia polymorpha* orthologue to D6PK, supporting that the motif and its function is evolutionary conserved. All *Marchantia polymorpha* kinases possess a polybasic K/R-rich motif in their middle domains although less pronounced in Mp88 (Figure 7 A). We performed lipid-protein interaction assays using membranes spotted with different phospholipids (PIP-strips) to examine their phosphoinositide binding properties *in vitro* and whether their binding profile differs in dependence of the composition of the polybasic K/R-rich motif as previously described for other AGC1 kinases from *Arabidopsis thaliana* (Barbosa et al., 2016). All three kinases were able to bind to the phospholipids on the PIP-strips. However, they differed in their affinity to the different phosphoinositides and other lipids present on the membrane. Mp17 showed a pattern very similar to that of D6PK with a strong affinity for PtdIns(3)P and some binding to phophatidic acid, while a different pattern could be observed for Mp88 and Mp68. Mp68 showed strong binding to phosphatidic acid and PtdIns(3,5)P2 and less affinity to other phophoinositides. Mp88 showed an overall strong binding to phophoinositides with less pronounced preference for a specific phosphoinositide (Figure 7 B). Additionally, we calculated the BH-score for the tested kinases. The BH-score predicts interaction of proteins with negatively charged phospholipids based on the occurrence of basic and hydrophobic amino acids (Bailey & Prehoda, 2015; Brzeska et al., 2010). All three kinases passed the threshold of 0.6 and thus were predicted to interact

with phospholipids based on this score. However, only for two of them, Mp17 and Mp68, this interaction was predicted to be dependent on the middle domain polybasic K/R-rich motif (Figure 7 C).

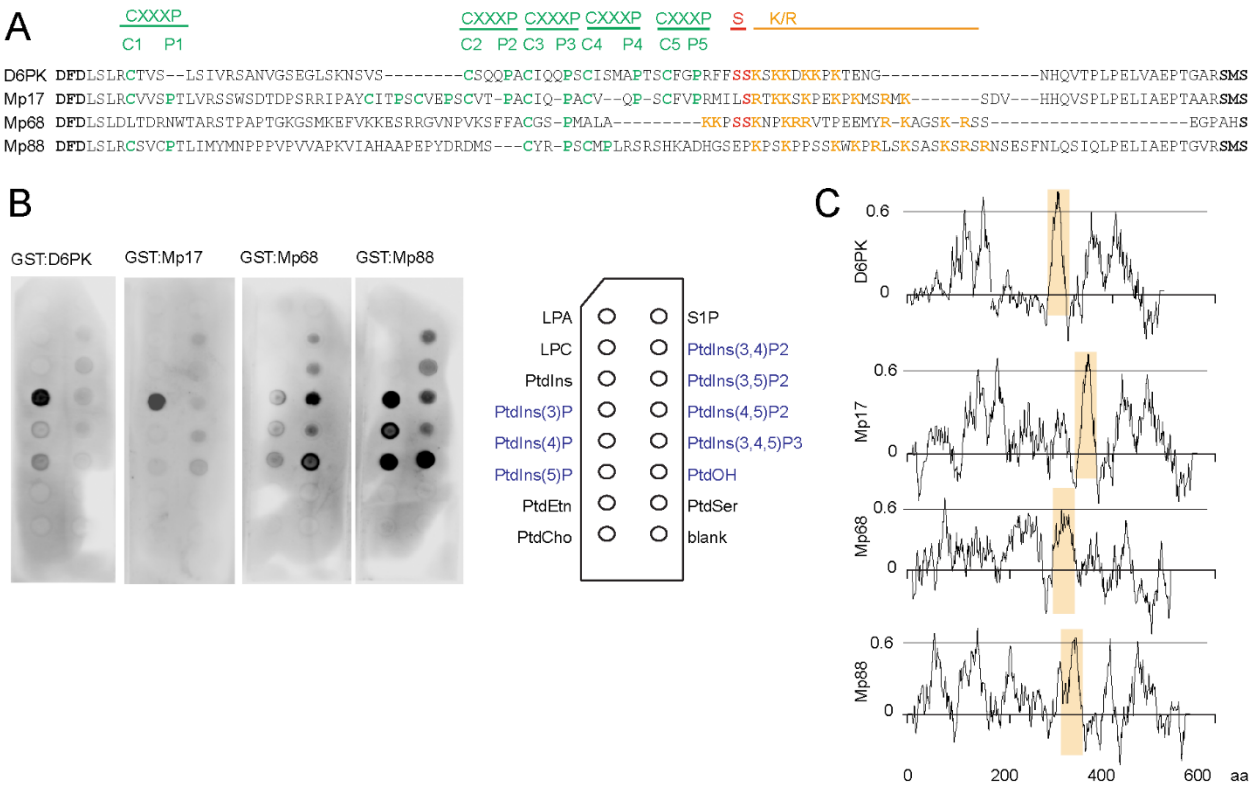

Figure 7. ***Marchantia polymorpha*** **AGC1 kinases contain conserved middle domain motifs and bind phosphoinositides** ***in vitro***. **A**. Alignment of the middle domains of three Marchantia polymorpha AGC kinases with the D6PK middle domain. The CXX(X)P motifs, serines and K/R-rich motif are marked. **B.** PIP-strips with the recombinantly expressed GST-D6PK, GST-Mp17, GST-Mp68 and GST-Mp88 kinases detected by an aGST antibody. **C.** BH-score of basic and hydrophobic kinases with the residues belonging to the middle domain polybasic K/R-rich motif marked. Note that only Mp17 and D6PK show clear peaks in this position.

We concluded that the resemblance of the lipid binding profile of the Marchantia polymorpha AGC1 orthologues to D6PK examined on the PIP-strips correlated with the similarity of their polybasic K/R-rich motif compared to D6PK. This finding supported the hypothesis that the composition of the polybasic K/R-rich motifs plays a central role in mediating PIP-binding affinity and may account for differences in kinase localization in the cell. The role of other middle domain motifs, such as the CXX(X)P motif or the serine residues preceding the polybasic K/R-rich motif, that could contribute to differences in binding pattern between the *Marchantia polymorpha* kinases would require further investigation.

3.2 Functional analysis of middle domain CXX(X)P motifs and their biochemical and cell biological role

3.2.1 Structural characterization of D6PK

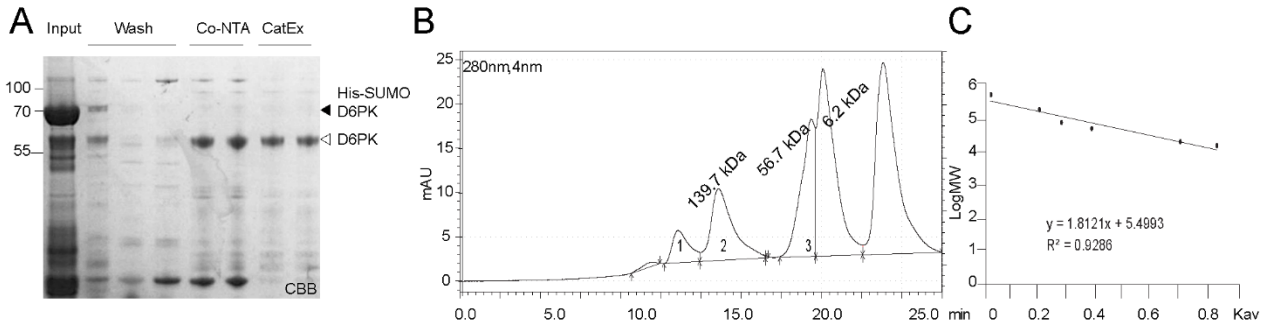

Figure 8. Purification and analytical gel filtration chromatography of D6PK. A. Coomassie Brilliant Blue stained gels of the His-SUMO-D6PK purification procedure including input and the eluates from metal affinity purification (Co-NTA) and cation exchange chromatography (CatEx). **B.** Analytical size exclusion chromatography (SEC) of purified D6PK with the applied calibration curve shown in (C).

In the first part of my thesis, I conducted a detailed analysis of the AGCVIII kinase middle domain sequences and described the conserved CXX(X)P motifs. Cysteines can have a crucial role for protein structure due to their reactivity, and prolines can play an important role due to their backbone properties (Marino & Gladyshev, 2010; Williamson, 1994). I wanted to elucidate the role of the D6PK middle domain, particularly the significance of the CXX(X)P motifs, by obtaining a structural resolution of the D6PK middle domain using crystallization or NMR techniques. To do so, I established a purification strategy together with my lab colleague Franziska Anzenberger. Our objective was to purify D6PK to a level sufficient for further structural characterization. We purified His-SUMO-D6PK on a Co^{2+} TALON column, eluted D6PK by cleaving the His-SUMO tag on the column and subsequently performed cation exchange chromatography on the eluted D6PK (Figure 8 A). The successful purification process was verified using mass spectrometry. D6PK was further analyzed on an analytical gel filtration chromatography. The potential D6PK elution peak was observed at an estimated molecular weight of 56.7 kDa (Figure 8 B and C). D6PK has a molecular weight of 54.8 kDa. Consequently, this peak could indicate monomeric D6PK. The first peak at a higher molecular weight corresponded to a molecular weight of 139.7 kDa. However, this is inconsistent with the size of dimeric D6PK. I concluded that D6PK is a monomeric and globular protein since it was soluble

when expressed from *E.coli* and the predominant elution peak from the gel filtration column corresponded to its anticipated molecular weight.

Unfortunately, further structural characterization was not successful. Due to the unsuccessful structural characterization of D6PK, I decided to functionally analyze the D6PK middle domain. I wanted to answer whether the CXX(X)P motifs can help to explain the strong plasma membrane association of D6PK, its polar localization, and its fast cycling. I established fluorescent recovery after photobleaching (FRAP) experiments to study D6PK kinetics and trafficking in the cell. Moreover, I introduced mutations in the CXX(X)P motifs to study their significance for protein localization in the cell and, ultimately, protein function *in vivo,* assessed using phototropism assays and auxin transport assays.

3.2.2 D6PK is a fast-cycling protein, and its recovery at the basal plasma membrane is likely independent of diffusion

We previously characterized D6PK to associate with the plasma membrane and exhibit transmembrane protein properties due to its strong attachment to the plasma membrane, but lacking obvious transmembrane domains (Barbosa et al., 2016). However, we also showed that although D6PK strongly associates with membranes, D6PK traffics rapidly from and to the plasma membrane in a GNOM-dependent manner as evidenced in BFA treatments in the presence of CHX (Barbosa et al., 2014). To further answer how this strong membrane association can be reconciled with the fast cycling of D6PK, I conducted solubilization studies with D6PK to investigate its association with the plasma membrane and established FRAP experiments. FRAP experiments allow calculating D6PK kinetics and the estimation of the mobile fraction of D6PK in the cell by bleaching a region of interest (ROI) at the basal plasma membrane and monitoring the recovery of the YFP-signal in the bleached area.

To understand the strength of D6PK association with the plasma membrane, I performed solubilization experiments on protein isolated from seedlings expressing YFP-D6PK under the 35S CaMV promoter. I treated the protein extract with different chemicals and ultracentrifuged the extract to distinguish between the membrane associated and the soluble fraction of D6PK after each treatment. After each ultracentrifugation step, samples from both the soluble and the membrane fraction were collected for immunoblot analysis. I found that D6PK was only solubilized by the application of 1% Triton-X-100, with a minor

quantity detected in the detergent-insoluble fraction. D6PK mostly remained associated with membranes when fractionated in the presence of 100 mM sodium carbonate or 1 M sodium chloride (Figure 9 A). Sodium carbonate or sodium chloride would interfere with purely hydrophobic or ionic interactions such as electrostatic interactions mediated by the polybasic motif (Fujiki et al., 1982). Following the solubilization of YFP-D6PK with 1% Triton-X-100, residual YFP signal was detected in the membrane fraction. H^+-ATPase, serving as a reference for a transmembrane protein, was completely solubilized following the application of 1% Triton-X-100, whereas UGPase, acting as a control for the soluble fraction, was entirely solubilized after the first extraction step (Figure 9 A). As ionic strength was not sufficient to solubilize D6PK, I concluded that additional mechanisms to the polybasic motif may exist that strongly anchor D6PK to membranes.

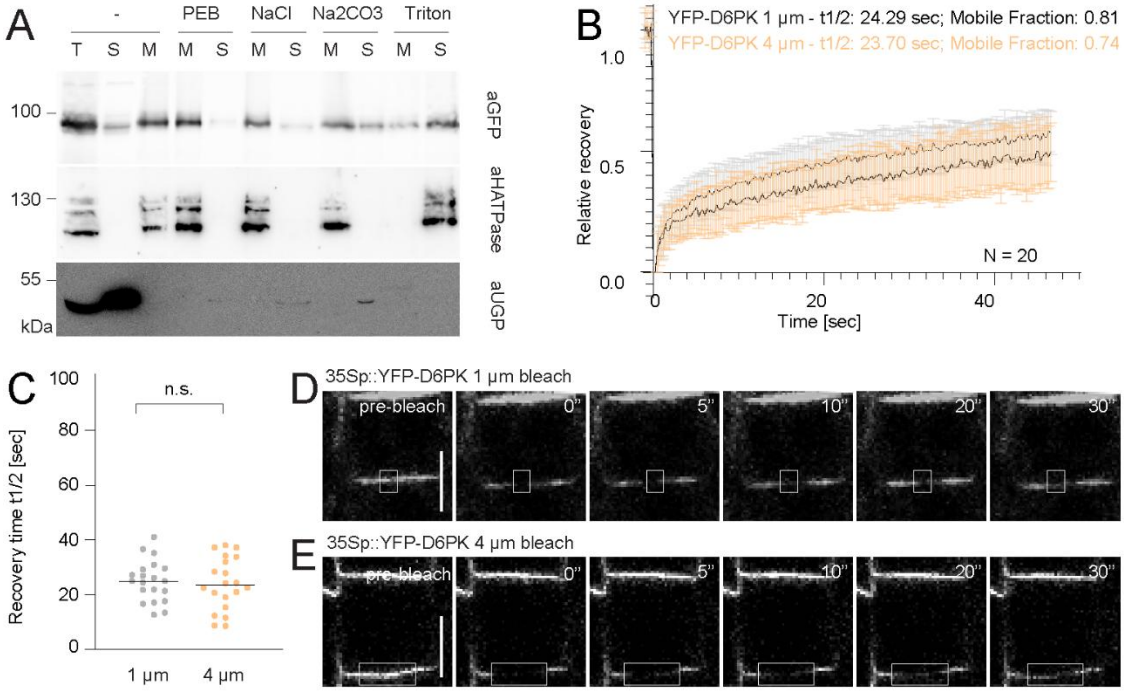

Figure 9. FRAP experiments reveal YFP-D6PK dynamics. **A**. Immunoblot of solubilization experiments of protein extracted from six-days-old Arabidopsis thaliana seedlings overexpressing YFP-D6PK under the 35S-promoter. aGFP recognizes the YFP-tag, aH-ATPase recognizes the transmembrane proton-ATPase and serves as a control for the membrane fraction, aUGPase is a marker for the soluble fraction. **B**. and **C**. Results of FRAP experiments comparing recovery time and mobile fraction of YFP-D6PK bleached in 1 µm or 4 µm ROIs. Shown are normalized recovery curves (B) and individual half-recovery times (C). Statistically significant differences were determined using a Student's t-test (n.s., not significant, *, $p<0.05$). **D**. **and E.** Representative confocal microscopy images of the recovery of 35Sp::YFP-D6PK in a 1 µm ROI (D) or a 4 µm ROI (E) at the basal plasma membrane in the timeframe as indicated in the images.

From the immunoblots I could see that D6PK is a membrane associated protein that exists in two states: membrane-bound and a smaller soluble fraction. FRAP experiments are

appropriate for elucidating the dynamics of D6PK in relation to the plasma membrane, as they facilitate the examination of lateral diffusion within the membrane and the exchange of protein between the cytoplasm and the membrane (Goehring et al., 2010). I bleached 4 µm wide ROIs of YFP-D6PK at the basal plasma membrane of epidermis cells of seedlings expressing YFP-D6PK and followed the recovery at the basal plasma membrane for 200 frames after photobleaching. FRAP data is usually fitted as an exponential curve influenced by the association and dissociation rate of a protein. YFP-D6PK recovery at the basal plasma membrane could be modeled with a double-exponential curve, indicating that two fractions of YFP-D6PK exist with independent association and dissociation kinetics (Figure 9 B). I hypothesized that these two fractions describe a combined recovery depending on lateral diffusion and reversible membrane association.

To further elucidate the characteristics of this double-exponential recovery and the cellular dynamics of D6PK, I conducted FRAP experiments and evaluated the recovery in small 1 µm and wider 4 µm ROIs to understand the contribution of lateral diffusion to recovery. Notably, the recovery time in the 1 µm and 4 µm ROIs did not show a significant difference, suggesting that lateral diffusion does not strongly influence D6PK kinetics, since in this case I would expect a faster recovery in the smaller ROI (Figure 9 B and C). However, I could observe an initial faster recovery in the recovery curve, possibly indicating a fast initial recovery driven by lateral diffusion (Figure 9 B). I concluded that FRAP experiments can effectively assess D6PK kinetics *in vivo*. I used them throughout my project to examine D6PK kinetics and to elucidate the influence of middle domain CXX(X)P motifs and serines on D6PK intracellular kinetics.

3.2.3 Cysteine residues in the CXX(X)P motifs are required for D6PK plasma membrane association and biological function

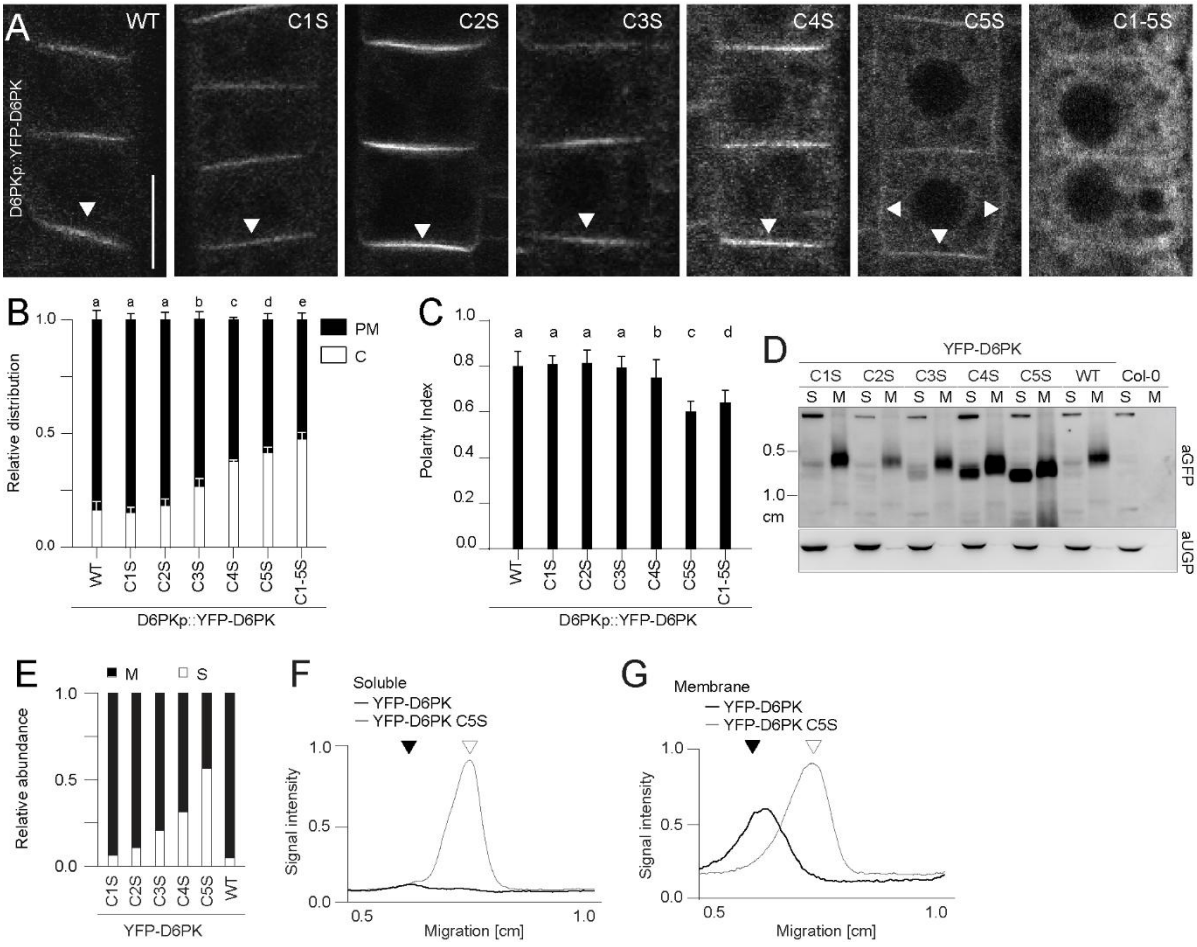

Figure 10. Cysteine residues in the CXX(X)P motifs are required for D6PK plasma membrane association. **A.** Representative confocal microscopy images of root epidermal cells of stably transformed six-days-old *Arabidopsis thaliana* seedlings (A) expressing the wildtype YFP-D6PK or mutant variants with individual cysteines mutated to serines (C1S – C5S) or all five cysteines substituted with serines (C1-5S) under a *D6PK* promoter fragment. Scale bar = 20 µM (A) **B.** and **C.** Bar charts with mean and standard deviation of YFP-D6PK cellular cytosolic (C) to plasma membrane (PM) distribution (B) and plasma membrane polar distribution (C) as determined from confocal microscopy images of n > 15 cells as shown in (A) from at least three seedlings. The statistically significant difference between groups was determined by one-way ANOVA (B, $F(6,63) = 184.8$, $p<0.0001$; C, $F(6,98) = 97.08$, $p>0.001$). Different letters indicate a statistically significant difference. **D.** Immunoblot of protein extracted from six-days-old seedlings expressing the wildtype YFP-D6PK under it's a *D6PK* promoter fragment or mutants with individual cysteines mutated to serines (C1S – C5S) after ultracentrifugation and subcellular fractionation into soluble (S) and membrane (M) fraction (D). anti-GFP (aGFP) recognizes the YFP-tag; anti-UGPase (aUGP) is a marker for the soluble fraction and efficient subcellular fractionation. **E.** Bar chart with relative soluble (S) and membrane fraction (M) from the immunoblot in (D). **F.** and **G.** migration profile for wildtype YFP-D6PK and mutant variant YFP-D6PK_C5S soluble (F) and membrane fraction (G) plotted from the immunoblot (D). X-axis marks the migration in the gel used for measurement as indicated in (D).

Since the structural analysis of D6PK was not successful, I changed the approach to conduct a functional analysis by mutagenizing the identified repeated CXX(X)P motifs and

examining the cell biological behavior of the generated D6PK variants. I mutagenized individual cysteines (C1S – C5S) or the complete set of cysteines (C1-5S) to the sterically similar serines and expressed these variants under a *D6PK* promoter fragment in the *d6pk d6pkl1* mutant background. In confocal microscopy images of root epidermal cells of six-days-old seedlings, I noted a progressive increase in D6PK cytosolic abundance upon substitution of the cysteines of the CXX(X)P motifs with serines. Interestingly, the quantity of cytosolic D6PK correlated with the proximity of the mutagenized cysteine to the previously identified polybasic K/R-rich motif. The cellular distribution of YFP-D6PK_C1S, YFP-D6PK_C2S and YFP-D6PK_C3S resembled the cellular distribution observed for the wildtype YFP-D6PK protein. YFP-D6PK_C4S and YFP-D6PK_C5S were more internalized than wildtype YFP-D6PK, while YFP-D6PK_C1-5S showed an even stronger intracellular accumulation, accommodated by a reduced plasma membrane polarity (Figure 10 A – C). To test whether the internalized protein was still able to associate with internal membranes, I extracted protein in absence of detergent and enriched membrane fractions using an ultracentrifugation step (1h, 100000 xg). In agreement with the cellular distribution, I could observe a relative increase of D6PK cysteine mutants in the soluble fraction the closer the mutagenized cysteine was located to the polybasic K/R-rich motif, indicating that the mutagenized cysteines promoted not only plasma membrane association, but affected the solubility of D6PK in general (Figure 10 D – E). Additionally, I noticed a faster migration of the YFP-D6PK_C4S and the YFP-D6PK_C5S mutants in the SDS gel when compared to the migration behavior of the wildtype YFP-D6PK protein which could indicate a modification on the mutagenized cysteines or a structural feature influencing gel migration (Figure 10 D, F, G).

I examined whether the CXX(X)P motifs were relevant for D6PK function *in vivo* by assessing whether the cysteine mutants could complement the *d6pk d6pkl1* impairment in phototropic bending. I grew seedlings expressing the YFP-D6PK variants under a *D6PK* promoter fragment in the dark for 2.5 days, exposed them to unilateral blue light for four hours, and measured the bending angle of the hypocotyl. Wildtype YFP-D6PK as well as the variants YFP-D6PK_C1S, YFP-D6PK_C2S and YFP-D6PK_C3S rescued the d*6pk d6pkl1* phototropism defect, while YFP-D6PK_C4S and YFP-D6PK_C5S were partially, and YFP-D6PK_C1-5S fully impaired to compensate for the phototropism defect (Figure 11 A and B). This effect correlated well with their reduced abundance at the basal plasma

membrane and the reduced polarity as described for YFP-D6PK_C5S and YFP-D6PK_C1-5S (Figure 10 A-C). To determine whether this impaired ability to rescue was a result of the loss of plasma membrane association or of a reduced kinase activity, I recombinantly expressed the proteins as GST-fusions in *E.coli* and tested their phosphorylation activity towards the PIN1 cytosolic loop. Repeatedly, neither the auto- nor the transphosphorylation activity of the mutants was affected beyond normal experiment-to-experiment variation, suggesting that the reduced plasma membrane association rather than impaired catalytic activity was the reason for the observed physiological effects (Figure 11 C).

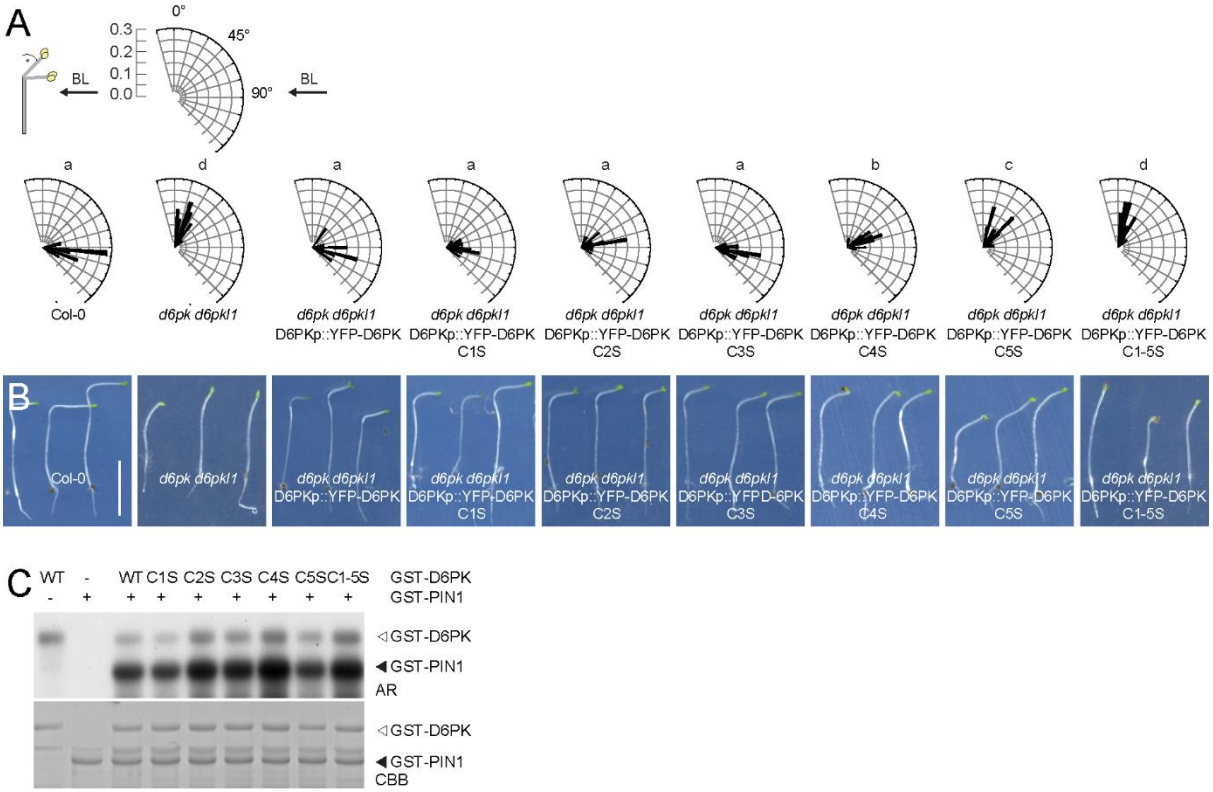

Figure 11. CXX(X)P motif cysteine mutations impair D6PK-mediated phototropic hypocotyl bending but not D6PK catalytic activity. A. Rose diagrams with frequency distribution in 5° intervals of hypocotyl beding angles of three-days-old dark grown seedlings of the genetic backgrounds as specified after 4 hour exposure to unilateral blue light (BL). The arrow indicated the direction of the blue light exposure. The statistically significant difference between groups was validated using a One-way ANOVA ($F(8,550) = 211.8$, $p<0.0001$) and means were compared using a Tukey's test **B**. Photographs of three representative seedlings from the experiment validated in (A). Scale bar = 0.5 cm. C. Autoradiography and Coomassie Brilliant Blue-stained gel from in vitro kinase assay experiment with recombinantly expressed and purified wildtype GST-D6PK or mutant variants as specified and the hydrophilic loop fragment of PIN1 (GST-PIN1) as phosphorylation substrate.

I could show that the cysteine of the C5XX(X)P motif and the C4XX(X)P motif are required for the plasma membrane association of YFP-D6PK. Since I observed an increase in cytosolic signal, as well as a higher abundance of YFP-D6PK in the soluble sample after

subcellular fractionation, I concluded that the cysteines of the CXX(X)P4 and the CXX(X)P5 motif and possibly the other CXX(X)P motifs may contribute to anchor D6PK to the plasma membrane. YFP-D6PK-C4S, YFP-D6PK_C5S and YFP-D6PK_C1-5S were not able to fully complement the phototropism defect of *d6pk d6pkl1* double mutants, whereas the phosphorylation activity of GST-D6PK_C4S, GST-D6PK_C5S and GST-D6PK_C1-5S towards the PIN1 cytosolic loop did not differ from wildtype GST-D6PK *in vitro* (Figure 11 A - C). This indicated that the failure of the mutagenized D6PK variants to complement the impairment in phototropic bending was a direct consequence of the loss of protein associated with the basal plasma membrane and that the CXX(X)P motifs are important for YFP-D6PK function *in vivo*. Interestingly, I did not observe a different migration behavior of the recombinantly expressed CXX(X)P-mutant variants compared to wildtype GST-D6PK on the SDS-PAGE as previously observed for the YFP-D6PK variants extracted from seedlings (Figure 10 D – G, Figure 11 C). I concluded that the observed migration shift was plant specific, indicating a modification that only occurred *in planta* or a structural difference.

3.2.4 Cysteine but not proline residues contribute to D6PK plasma membrane association

The cysteines in the identified repeated CXX(X)P motifs are typically succeeded by a proline, which can have a central role for protein structure (Williamson, 1994). I questioned whether the mutagenesis of prolines would similarly influence YFP-D6PK cellular distribution. I also wanted to validate that the loss of plasma membrane association, observed for YFP-D6PK_C4S, YFP-D6PK_C5S and YFP-D6PK_C1-5S, is not an artefact caused by the introduction of an additional serine in the middle domain in proximity to the polybasic K/R-motif, since a serine could serve as a phosphorylation site, leading to a stronger negative charge. To evaluate this, I generated constructs where I replaced the cysteine of the CXX(X)P motif with alanine and constructs where I substituted the proline of the CXX(X)P motif with glycine. I expressed these YFP-D6PK variants in protoplasts and analyzed their localization.

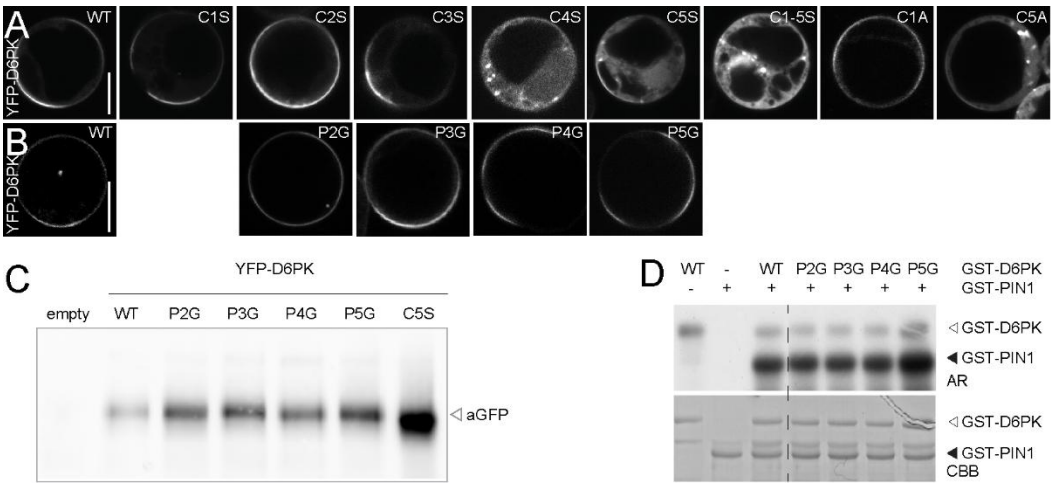

Figure 12. CXX(X)P cysteine but not proline residues are required for YFP-D6PK plasma membrane association. A. and **B.** Representative confocal microscopy images of transiently transformed protoplasts overexpressing wildtype YFP-D6PK from the 35S CaMV-promoter or its mutant variants with individual cysteines (C) mutated to serines (C1S – C5S, C1-5S) or mutated to alanines (C1A, C5A) (A) or prolines substituted with glycines (P2G – P5G) (B). Scale bar = 10 µm. **C.** Immunoblot of protein extracted from transiently transformed protoplasts as shown in A and B expressing the specified constructs. **D**. Autoradiography and CBB-stained gel from *in vitro* kinase assay experiment with recombinantly expressed and purified wildtype GST-D6PK or mutant variants as specified and the hydrophilic loop fragment of PIN1 (GST-PIN1) as phosphorylation substrate.

The mutant construct YFP-D6PK_C5A showed the same subcellular localization as observed for YFP-D6PK_C5S expressed in protoplasts, while the mutant variant YFP-D6PK_C1A behaved like the mutant variant YFP-D6PK_C1S and thus showed the same distribution as the wildtype YFP-D6PK protein in these experiments (Figure 12 A). None of the proline to glycine variants showed obvious defects in cellular distribution when compared to the wildtype YFP-D6PK protein nor significant differences in migration on a SDS-PAGE gel as observed for YFP-D6PK_C5S (Figure 12 B and C). To find out whether the proline plays a role for the activity of the kinase, I tested the phosphorylation activity of recombinant GST-D6PK protein towards the PIN1 cytosolic loop. The catalytic activity of GST-D6PK was not affected by the mutagenized proline in *in vitro* kinase assays beyond normal variation (Figure 12 D).

I observed the same effect on YFP-D6PK localization replacing the cysteine of the CXX(X)P motif with alanine as when the cysteine was substituted with a serine, therefore I concluded that it is the loss of the cysteine rather than the gain of a serine that is responsible for the decreased plasma membrane association observed for YFP-D6PK_C5S. I could also show that mutagenizing the proline does not affect YFP-D6PK cellular distribution, indicating that only the cysteine within the CXX(X)P motif is required

for the plasma membrane association. I thus focused on elucidating the function of the cysteines for D6PK localization in subsequent experiments.

3.2.5 The CXX(X)P motifs do not play a role in D6PK GNOM-dependent trafficking

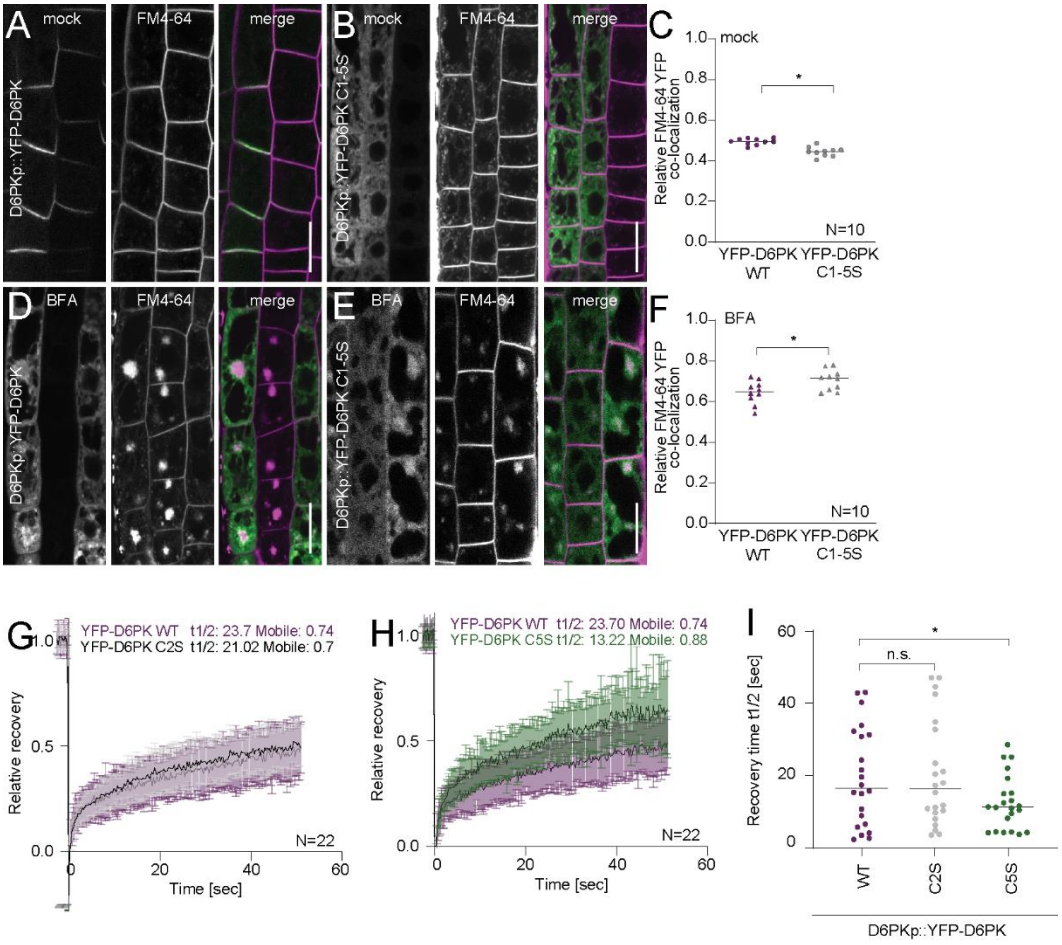

Figure 13. CXX(X)P mutations affect cellular dynamics but not trafficking of YFP-D6PK. A, B, D and **E.** Representative confocal microscopy images of root epidermal cells of five-days-old seedlings after mock (A,B) or 10 µM BFA (D,E) treatment including one hour 50 µM Cycloheximide pre-treatment and using a FM4-64 co-staining to mark the plasma membrane. Scale bars = 20 µm. **C.** and **F.** Mean and individual values of Pearson's correlation at the plasma membrane and in the cytosol of YFP and FM4-64 signal after mock (C) and BFA (F) treatment. **G – I.** Results of FRAP experiments comparing recovery time and mobility at the basal plasma membrane of wildtype YFP-D6PK and the mutant variants YFP-D6PK_C2S and YFP-D6PK_C5S. Shown are the normalized recovery curves (G,H) and the individual half-recovery times t1/2 (I). Statistically significant differences to the behavior of the wildtype YFP-D6PK in (C, F, I) were determined using a Student's t-test (n.s., not significant, *, $p<0.05$).

YFP-D6PK rapidly traffics to and from the plasma membrane, dependent on the guanine nucleotide exchange factor GNOM, which can be inhibited by treatment with BFA (Barbosa et al., 2014). I analyzed whether the increase in cytosolic abundance observed for the CXX(X)P-mutants could be due to an impairment in their trafficking. Therefore, I performed treatments with 10 µM BFA on five-days-old seedlings expressing the wildtype

YFP-D6PK protein or the mutant variant YFP-D6PK_C1-5S, which previously showed the most pronounced internalization relative to wildtype YFP-D6PK. To confirm that I am observing recycling protein rather than newly synthesized YFP-D6PK protein, I included a pretreatment with the protein synthesis inhibitor cycloheximide (CHX). As anticipated, wildtype YFP-D6PK rapidly internalized after BFA treatment and accumulated in BFA compartments as verified with the membrane dye FM4-64 (Figure 13 A-C). The mostly cytosolic YFP-D6PK_C1-5S remained susceptible to treatments with 10 µM BFA and showed accumulation in BFA compartments as confirmed by the membrane marker FM4-64. I quantified and analyzed the co-localization of YFP-D6PK and FM4-64 in BFA compartments using a Pearson's correlation coefficient for co-localization with FM4-64 before and after BFA treatment (Figure 13 D-F). I concluded that the reduced plasma membrane signal and increased cytosolic abundance of YFP-D6PK_C1-5S was not caused by a defect in secretion and that it was still subject to intracellular protein trafficking.

To understand better which role the CXX(X)P-motifs play for plasma membrane anchoring and protein dynamics, I performed FRAP experiments with the YFP-D6PK wildtype, YFP-D6PK_C2S and the YFP-D6PK_C5S protein. As previously demonstrated, YFP-D6PK_C2S showed a distribution at the basal plasma membrane comparable to wildtype YFP-D6PK. YFP-C5S showed a significant increase in cytosolic abundance but still retained some plasma membrane signal, allowing for analysis using FRAP experiments (Figure 10 A - C). The FRAP experiments revealed that YFP-D6PK_C2S did not exhibit a significantly different recovery time at the basal plasma membrane when compared to wildtype YFP-D6PK. YFP-D6PK_C5S exhibited a faster recovery and an increased mobile fraction in the FRAP experiments, most likely due to the increased amount of soluble protein, and thus an enhanced exchange of cytosolic protein with the plasma membrane. These results supported that the CXX(X)P5 motif is required for D6PK plasma membrane association and its kinetics towards or within the basal plasma membrane.

3.2.6 Cysteine residues in the CXX(X)P motifs are not redox sensitive

My experiments indicated a crucial function of the CXX(X)P motifs for D6PK plasma membrane association. Consequently, I wanted to elucidate the mechanistic contribution of the CXX(X)P motifs for D6PK plasma membrane association. Given that cysteines are reactive amino acids and can undergo many modifications to influence the properties of a

protein, I examined the CXX(X)P-motifs for some of the most common cysteine modifications.

I investigated the ability of the cysteines in the CXX(X)P motifs to engage in intra- or intermolecular disulfide bond formation, applying a dual labeling approach and mass spectrometric analysis with recombinant protein and plant protein enriched by immunoprecipitation (IP). For this purpose, protein was extracted under denaturing conditions in presence or absence of the reducing agent Tris(2-carboxyethyl)phosphine hydrochloride (TCEP). Free cysteines were blocked using N-ethylmaleimide (NEM). Subsequently, the samples were loaded on a short gel and subjected to full reduction with Dithiothreitol (DTT) to release cysteines engaged in disulfide bonds followed by blocking of cysteines with chloroacetamide (CAA) for subsequent mass spectrometric analysis. The analysis identified D6PK cysteines C183 and C189, but none of the five CXX(X)P motif cysteines as sensitive to the redox conditions reflected in a differential labeling in the non-reduced compared to the fully reduced sample (Figure 14 A). Most of the other cysteines were identified as insensitive to the conditions, which was reflected in comparable NEM-labeling efficiencies in reduced and non-reduced samples. Some cysteines were observed to show an overall low labeling efficiency. Interestingly, the labeling efficiency of the CXX(X)P-motif cysteines was very low when compared to the labeling efficiency of other cysteines in the completely reduced control. I reasoned that this may be caused by inefficient denaturation of proteins leading to structural constraints that may hinder the efficient penetration of the modifying agent, or from the presence of alternative cysteine modifications that may block labeling with NEM. This is possible since the usage of TCEP is highly selective for disulfide bond identification and may not lead to the hydrolysis of other potential cysteine-modifications which could be the case for DTT (Ji et al., 2013). I concluded that the CXX(X)P-motif cysteines do not engage in disulfide bonds as I could not observe a difference in NEM-labeling between the protein extracted in reducing and non-reducing conditions for these cysteines.

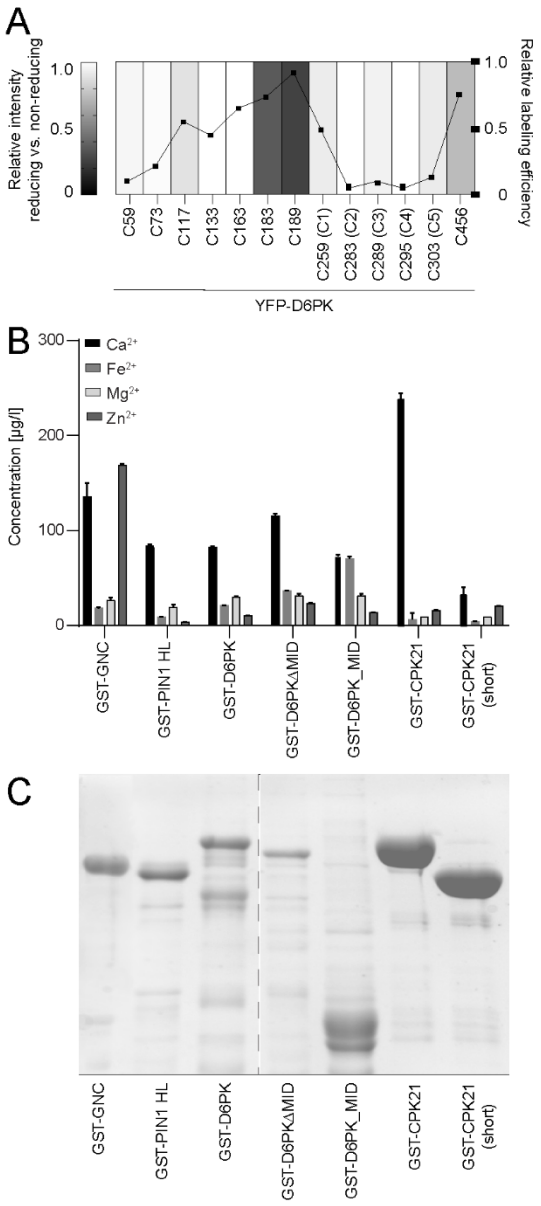

Figure 14. The D6PK middle domain does not engage in disulfide bond formation or cation complexation. A. Result from a mass-spectrometry based analysis for disulfide bond formation showing reducing to non-reducing properties of the individual cysteines as specified (grey scale on the left – darker grey indicates a stronger difference). And the relative NEM-labeling efficiency of the respective cysteine with the scale indicated on the right (data point above the indicated cysteine). **B**. Bar chart displaying the results of ionometric analyses of recombinantly expressed and purified GST-tagged proteins as specified. The measured elements are differentiated in grey scale. **C.** Image of Coomassie Brilliant Blue-stained gel with purified recombinant proteins used for the ionometric analysis in (B). GST-GNC (GATA, NITRATE-INDUCIBLE, CARBON-METABOLISM-INVOLVED) is a GST-fusion of a Zn^{2+}finger transcription factor, (Richter et al., 2010); GST-CPK21 is the GST-fusion of a calcium-binding protein kinase (Geiger et al., 2011) and they serve as positive controls for Zn^{2+} and Ca^{2+} respectively; GST-CPK21 (short) is a truncated version of CPK21, missing the Ca^{2+}-binding domain and serves as negative control for calcium-binding; GST-PIN1 HL is a GST-fusion with the hydrophilic loop of PIN1 (Zourelidou et al., 2009), that does not contain any cysteines and serves as another negative control; GST-D6PKΔMID is the GST-fusion of the middle domain deletion variant of D6PK and GST-D6PK_MID is a GST-fusion of the D6PK middle domain (Barbosa et al., 2016). The dotted line marks splicing of the gel to remove irrelevant sample lanes.

3.2.7 The CXX(X)P motifs are not involved in metal ion complexation

CXX(X)P repeats are common in metal binding proteins, such as zinc fingers or Fe-S-clusters (Giles et al., 2003). I assessed the ability of D6PK to bind metals using ionometric analyses. I purified recombinantly expressed GST-D6PK, GST-D6PKΔMID, GST-D6PK_MID, GST-PIN1 HL, GST-GNC, GST-CPK21 and GST-CPK21 vk (Figure 14 C). GST-GNC is a GATA transcription factor containing a Zn^{2+}-finger and thus serving as a positive control (Richter et al., 2010; Bi et al., 2005). GST-CPK21 is a Ca^{2+}-binding kinase and can be expressed with its Ca^{2+}-binding domain deleted (vk), thus serving as positive and negative control for protein Ca^{2+} binding (Geiger et al., 2011). GST-PIN1 HL is another

control as the PIN1 hydrophilic loop does not contain any cysteines or any recognizable metal binding motifs. Although cation binding was measured by the ionometric analyses in the samples containing GST-D6PK, this binding was unaffected by deletion of the middle domain and GST-D6PK and GST-D6PKΔMID exhibited the same binding profile (Figure 14 B). I consequently ruled out that the middle domain engages in binding to the cations tested. I can confirm that the analysis is suitable to test protein-metal interactions as I could observe Zn^{2+}-binding for the GATA transcription factor GST-GNC and strong Ca^{2+}-binding for GST-CPK21 but not for GST-CPK21 vk (Figure 14 B).

3.2.8 YFP-D6PK is an S-acylated protein

Cysteine S-acylation is a reversible post-translational modification, attaching a lipid moiety, most commonly palmitate, to a protein, hence enhancing its hydrophobicity (Dunphy & Linder, 1998; Paige et al., 1993). S-acylation can be indirectly assessed by blocking free cysteines followed by the specific hydrolysis of S-acyl groups with hydroxylamine and a subsequent differential labeling or enrichment of the free cysteines (Drisdel & Green, 2004). I hypothesized that D6PK could be S-acylated in the middle domain, serving as an anchor for plasma membrane association, which therefore would result in the observed loss of membrane association in YFP-D6PK_C4S, YFP-D6PK_C5S and YFP-D6PK_C1-5S. To test this hypothesis, I used an acetyl biotin exchange (ABE) assay, allowing for enrichment of potentially S-acylated proteins through the attachment of biotin to the free cysteines after hydrolysis with hydroxylamine. To ensure sufficient labeling efficiency, a negative control without hydroxylamine-mediated hydrolyzation of S-acylation sites was included.

When visualized on an immunoblot, this analysis provided a clear indication for an S-acylation of YFP-D6PK. I could still detect S-acylation in YFP-D6PKΔMID and YFP-D6PK C1-5S, although the fraction of S-acylated protein may be reduced, suggesting that the middle domain was not the site of S-acylation in YFP-D6PK (Figure 15 A). To test whether the middle domain itself was also S-acylated, I conducted another ABE assay with the YFP-D6PK_MID fragment alone, which demonstrated that S-acylation also occurred in the middle domain (Figure 15 B).

To evaluate the effect of S-acylation for protein cellular distribution of YFP-D6PK, I treated six-days-old seedlings with increasing concentrations of the competitive S-acylation

inhibitor 2-bromopalmitate (2-BP). I observed a dosage-dependent change of cellular localization of YFP-D6PK. Treatments with 10 µM 2-BP resulted a reduced polarity but maintained plasma membrane localization, whereas treatments with 50 µM or 100 µM 2-BP led to an increased cytosolic abundance of D6PK (Figure 15 C – E). Next, I wanted to examine whether the treatments affected the membrane association of YFP-D6PK. I extracted protein from six-days-old seedlings after 2-BP treatments without detergents and separated the insoluble membrane fraction from the soluble fractions by ultracentrifugation (100 000 *g*, 1h). The fractions were analyzed on an immunoblot. In comparison to the mock treated control, the 2-BP treatments led to an increased abundance of YFP-D6PK in the soluble fraction, an increased quantity of total protein and faster migration on the SDS-PAGE (Figure 15 F – H). To elucidate the kinetics of S-acylation for YFP-D6PK, I treated seedlings with 2-BP for two hours and carried out an acyl resin-assisted capture assay (Acyl-RAC) – a modification of the previously described ABE assay (Tewari et al., 2020). The treatment with 100 µM 2-bromoplamitate resulted in a complete loss of YFP-D6PK S-acylation (Figure 15 I). I did not observe a significant loss of S-acylation in treatments with 10 µM 2-BP and only a slight loss when seedlings were treated with 50 µM 2-BP, which was in line with the observed effects of 2-BP treatment on YFP-D6PK intracellular localization. Although 2-BP can affect many cellular processes, the effects of 2-BP treatments on D6PK localization and migration on the SDS-PAGE resembled the behavior observed for the cysteine-mutated YFP-D6PK.

In the previous experiments, I ruled out that the middle domain CXX(X)P motifs are involved in disulfide bond formation or metal ion complexation. When I tested for potential lipid modifications in the CXX(X)P motifs, I identified D6PK to be S-acylated and treatments with the S-acylation inhibitor 2-BP showed comparable effects on YFP-D6PK localization as previously observed for YFP-D6PK_C4S, YFP-D6PK_C5S and YFP-D6PK_C1-5S. I concluded that D6PK is S-acylated inside its middle domain, contributing to its strong membrane association.

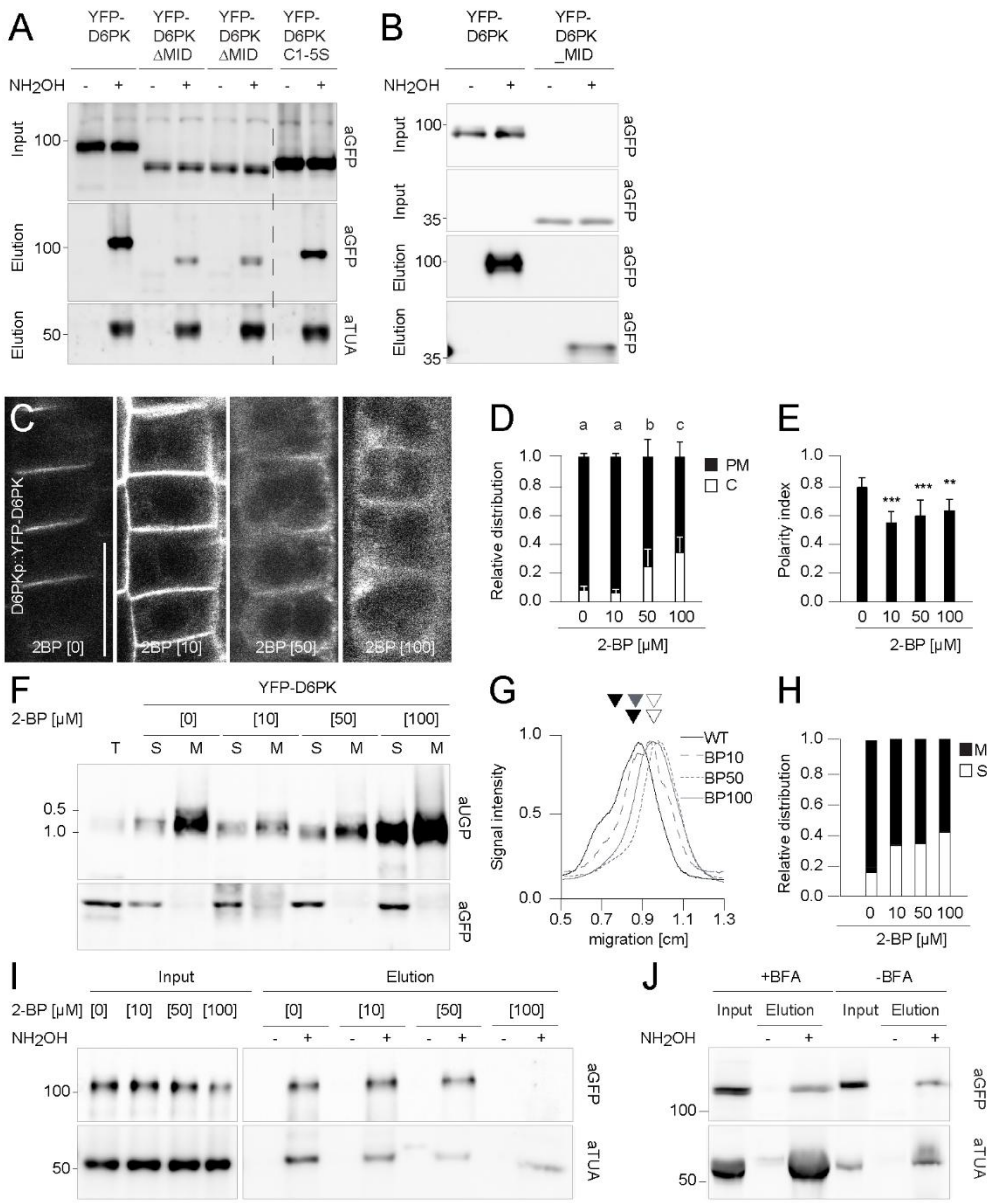

Figure 15. D6PK is S-acylated in- and outside of the middle domain independently of its plasma membrane association status. **A, B, I** and **J**. Immunoblots of isolated protein from transgenic plants overexpressing wildtype YFP-D6PK or specified variants after acetyl-biotin exchange (A, B) or acyl resin-assisted capture (I, J). Shown are input and elution with hydroxylamine (NH_2OH) serving as a control for selectivity for S-acylation. Anti-GREEN FLUORESCENT PROTEIN (aGFP) recognizes the YFP-tag; anti-tubulin A (aTUA) is a positive control for the assay. **C.** Representative confocal microscopy images of root epidermis cells of six-days-old *Arabidopsis thaliana* seedlings expressing wildtype YFP-D6PK after 2 h treatments with the S-acylation inhibitor 2-BP. **D** and **E.** Bar graphs with the mean and standard deviation for the cellular cytosolic (C) to plasma membrane (PM) distribution (D) and polarity (E) quantified from >15 cells from at least three seedling from confocal microscopy images as in (C). The statistically significant difference between groups in (D) was determined by one-way ANOVA ($F(3,68) = 117.1$) and means were compared using a Tukey's test. Different letters indicate a statistically significant difference. In (E), polarity indices were compared to that of the mock-treated control using a Student's t-test: **, $p < 0.01$; *** < 0.001. **F.** Immunoblot of protein extracts from transgenic plants expressing wildtype YFP-D6PK treated with 2-BP as specified after ultracentrifugation into soluble (S) and membrane (M) fraction. Anti-UDP-glucose-pyrophosphorylase (aUGP) is a marker for the soluble fraction. **G**. Migration profile of the membrane fraction in the immunoblot (F), arrow heads indicate signal maxima. **H.** Graph displaying the relative distribution of soluble and membrane fraction quantified from the immunoblot shown in (F).

3.2.9 YFP-D6PK S-acylation is a largely non-dynamic modification

Protein S-acylation is a reversible lipid modification that can dynamically influence protein localization depending on its S-acylation status, as demonstrated for the GTPase Ras (Rocks et al., 2005). A reversible S-acylation in D6PK could possibly facilitate internalization of D6PK from the plasma membrane, owing to its reversible characteristics, thereby mediating D6PK membrane anchoring and potentially influencing its trafficking and polar localization, as proposed for other proteins (Abrami et al., 2021; Ashery et al., 2006; Rocks et al., 2005). If S-acylation governed D6PK internalization and possibly a selective association with internal membranes or the plasma membrane, I anticipated a differential S-acylation between membrane associated and internalized protein. Consequently, I tested whether internalized YFP-D6PK after BFA treatment had a different S-acylation pattern compared to the untreated plasma membrane-bound protein. I found no apparent differences of D6PK S-acylation depending on its subcellular localization (Figure 15 J). I concluded that although S-acylation is required for proper plasma membrane association and may serve as a membrane anchor, YFP-D6PK internalization occurred independently of its S-acylation status since YFP-D6PK remained S-acylated to approximately the same extent in internalized samples after BFA treatment when compared to the membrane fraction as observed in S-acylation assays. I concluded that the S-acylation status of D6PK is not driving its internalization and cycling to and from the basal plasma membrane, indicating the presence of another mechanism for D6PK internalization.

3.2.10 S-acylation dynamics are comparable between YFP-D6PK_MID and wildtype YFP-D6PK

I found out that D6PK is S-acylated in the middle domain. Since we had previously observed the middle domain YFP-D6PK_MID expressed *in planta* to be sufficient to mediate polar plasma membrane association, I wanted to understand whether the middle domain S-acylation dynamics differ from those described for wildtype YFP-D6PK. Therefore, I tested the response of YFP-D6PK_MID to different concentrations of 2-BP treatments by treating six-days-old seedlings expressing YFP-D6PK_MID with 10 µM, 50 µM or 100 µM 2-BP. I could observe increased internalization and loss of plasma membrane association in treatments with 100 µM 2-BP (Figure 16 A and B). The

quantification of its polar localization could not be conducted due to low signal intensities in the confocal microscopy images with the lines expressing YFP-D6PK_MID. I concluded that the middle domain is sensitive to treatments with 2-BP, in line with the observations made for wildtype YFP-D6PK.

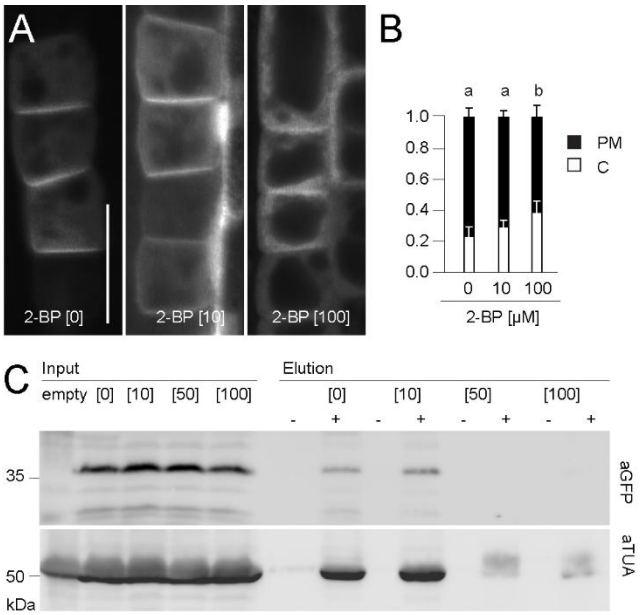

Figure 16. The D6PK middle domain alone is sufficient to show S-acylation dynamics after 2-BP treatments comparable to *wildtype YFP-D6PK*. A. Representative confocal microscopy images of root epidermal cells from six-days-old stably transformed Arabidopsis thaliana seedlings expressing YFP-D6PK_MID after treatment with the S-acylation inhibitor 2-BP. Scale bar = 20 µm. **B.** Graph displaying the mean and standard distribution of cellular distribution of n>15 cells quantified from confocal microscopy images as displayed in (A) from at least three seedlings. The statistically significant difference between groups in (B) was determined by one-way ANOVA ($F(2, 42) = 22.54$, $p < 0.001$). Different letters indicate a statistically significant difference. **C.** Immunoblot of input and eluted protein after an acyl resin assisted capture assay from extracts of six-days-old transgenic plants expressing YFP-D6PK_MID after 2h 2-BP treatments as described.

I additionally examined the dynamics of YFP-D6PK_MID S-acylation in response to the different concentrations of 2-BP treatments as performed previously for wildtype YFP-D6PK. Consistent with my data on wildtype YFP-D6PK, I observed a complete loss of S-acylation after treatment with 100 µM 2-BP (Figure 16 C). I also noted a complete loss of S-acylation after treatment with 50 µM 2-BP, indicating a stronger sensitivity to 2-BP treatments of YFP-D6PK_MID when compared to that of wildtype YFP-D6PK. However, these differences could also be due to experimental variations and the overall reduced protein quantity of YFP-D6PK_MID when compared to wildtype YFP-D6PK. I concluded that the observations made for the S-acylation dynamics of wildtype YFP-D6PK mostly reflected the S-acylation dynamics of the middle domain.

3.2.11 2-BP treatments do not lead to a difference in protein stability but increased *YFP-D6PK* transcript abundance

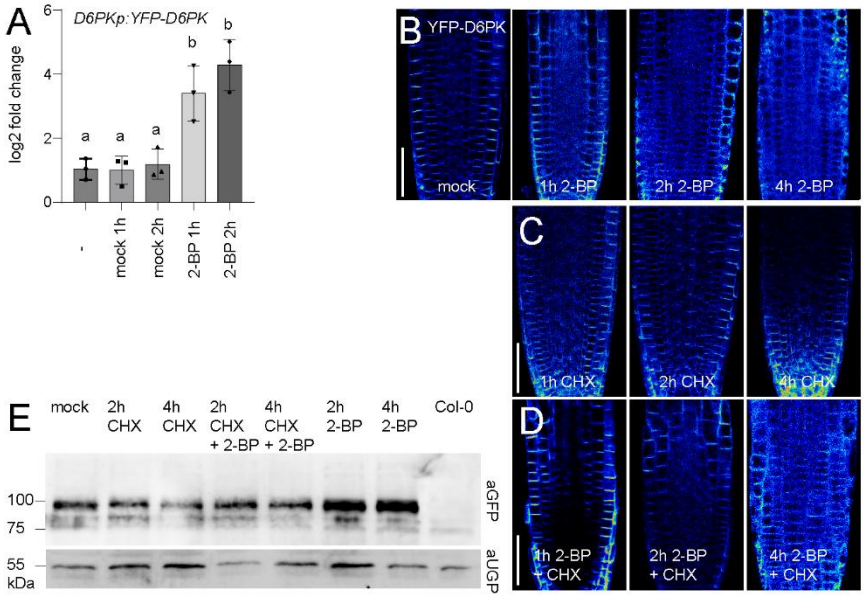

Figure 17. 2-BP treatments lead to increased *YFP-D6PK* transcript abundance. **A.** Results from qRT PCR examining *D6PK* transcript level in six-days-old seedlings treated with mock or 2-BP as indicated. The quantification was performed with three biological replicates. Expression levels (A) were compared using a One-way ANOVA ($F(4, 10) = 18.85$, $p = 0.0001$.) Different letters indicate a statistically significant difference. **B. – D.** Representative confocal microscopy images of five-days-old seedlings expressing YFP-D6PK under a *D6PK* promoter fragment in the *d6pk d6pkl1* double mutant background after treatments with mock or cycloheximide (CHX) (A), 2-BP (B) or 2-BP and CHX (C) for the times indicated. **E**. Immunoblot of extracted protein from seedlings treated as in B.-D. Anti-GREEN FLUORESCENT PROTEIN (aGFP) recognizes the YFP-tag**.** Anti-UGPase serves as a loading control.

I consistently noted a substantial increase in YFP-D6PK quantity after prolonged 2-BP treatments in confocal microscopy images and on immunoblots (Figure 15 C and F). I investigated whether this increase may be attributable to an enhanced YFP-D6PK *de novo* synthesis or to an increased YFP-D6PK protein stability. I hypothesized that the increase in YFP-D6PK abundance after the 2-BP treatments may result from a transcriptional upregulation of *YFP-D6PK* in plants treated with 100 µM 2-BP. I performed qRT-PCRs to test this hypothesis. After two hours of 2-BP treatment, I observed an approximately fourfold increase of *YFP-D6PK* transcript when compared to a corresponding mock treatment (Figure 17 A). To ascertain if 2-BP treatments additionally affected protein stability, potentially by prolonging YFP-D6PK half-life and indicating that S-acylations alter protein degradation rates, I performed 2-BP treatments together with the protein synthesis inhibitor CHX. These experiments allowed me to trace whether changes in D6PK abundance were due to protein synthesis or a change in protein stability.

If 2-BP also influenced YFP-D6PK degradation rate, I expected an increased YFP-D6PK abundance in treatments with CHX and 2-BP compared to treatments with only CHX. In line with previous experiments and the qRT-PCR, treatments with 2-BP led to an increase in protein abundance compared to the mock treatment (Figure 17 B and E). I did not find any detectable changes in D6PK abundance between seedlings treated with CHX and 2-BP or those treated only with CHX compared to the mock treatment, suggesting that D6PK did not undergo strong degradation in the time course of the treatment and that *de novo* synthesis was required for the increased YFP-D6PK abundance in the 2-BP treatments (Figure 17 C-E).

This finding suggested that the increase in YFP-D6PK abundance, repeatedly observed in the 2-BP treatments, is likely caused by a transcriptional upregulation and thus enhanced *de novo* synthesis, potentially as a compensatory feedback response to the reduced plasma membrane localization, rather than an increased YFP-D6PK protein stability due to a reduced degradation rate. These experiments additionally demonstrated that YFP-D6PK exhibits relative stability within the cell, as a decline in YFP-D6PK abundance was only noted after 4 hours of CHX treatment.

3.2.12 CXX(X)P motifs are required for plasma membrane association in other AGC1 kinases

The presence of repeated CXX(X)P motifs is conserved in *Arabidopsis thaliana* AGC1 kinases and in AGC1 kinases from other plant species (Figure 3, Figure 6). However, the AGC1 kinases differ in the number of CXX(X)P repeats found in their middle domains. The CXX(X)P5 repeat is conserved in many AGC1 kinases. To test whether the cysteines of the CXX(X)P4 and CXX(X)P5 motifs, which were most prominently required for D6PK plasma membrane association, are also required for plasma membrane association of other AGC1 kinases, I substituted these cysteines with serines in the AGC1 kinases PAX and KIPK. I subsequently analyzed PAX and KIPK localizations by transiently overexpressing them under the 35S CaMV promoter in protoplasts. Wildtype YFP-PAX strongly associated with the plasma membrane in protoplasts as demonstrated before, while the mutant variants YFP-PAX_C4S and YFP-PAX_C5S displayed an enhanced internalization when compared to the wildtype YFP-PAX protein (Figure 18 A and B)(Marhava et al., 2018). I did not detect a robust plasma membrane association for YFP-

KIPK when expressed in protoplasts, nevertheless I noted a total absence of plasma membrane association in YFP-KIPK_C4S and YFP-KIPK_C5S (Figure 18 C and D). I conducted ABE assays to determine whether YFP-PAX and YFP-KIPK might undergo S-acylation *in vivo*, as previously demonstrated for YFP-D6PK. I isolated protein from six-days-old seedlings expressing YFP-D6PK, YFP-PAX or YFP-KIPK under the 35S CaMV promoter and performed ABE assays as previously outlined. YFP-D6PK, YFP-PAX and YFP-KIPK were all found to be S-acylated (Figure 18 E). However, it is important to note that YFP-KIPK did not show the predicted migration behavior in the SDS-PAGE and was detected at a lower size than expected on the immunoblot (Figure 18 E).

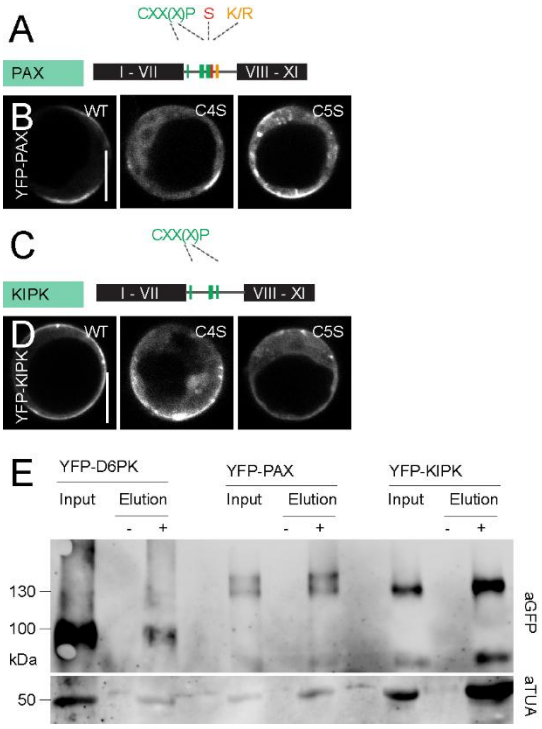

Figure 18. CXX(X)P motifs are conserved in their function in the AGC1 kinases PAX and KIPK. **A.** and **B.** Schematic representation of kinase domains and middle domain of PAX (A) and KIPK (B) from *Arabidopsis thaliana* with the repeated CXX(X)P motifs, polybasic K/R-rich motif (K/R) and adjacent serines highlighted. **C.** and **D.** Representative confocal microscopy images of transiently transformed protoplasts overexpressing wildtype YFP-PAX (C) and YFP-KIPK (D) from the 35S CaMV promoter or their mutant variants with individual cysteines mutated to serines (C4S, C5S). Scale bar = 10 µm. **E.** Immunoblot of input and eluted protein after acetyl biotin exchange assay from protein extracts of six-days-old stably transformed transgenic plants overexpressing YFP-D6PK, YFP-PAX or YFP-KIPK as specified. Anti-GREEN FLUORESCENT PROTEIN (aGFP) recognizes the YFP-tag; anti-tubulin A (aTUA) recognizes the S-acylated tubulin A protein.

These experiments indicated that the function of the cysteines of the CXX(X)P motif for plasma membrane association may be preserved across the AGC1 kinase clade and that YFP-PAX and YFP-KIPK are also S-acylated *in vivo* resembling YFP-D6PK. In the case of KIPK this is noteworthy since it does not contain a polybasic K/R-rich motif in the middle domain and since wildtype YFP-KIPK showed a less pronounced plasma membrane association compared to YFP-D6PK and YFP-PAX when expressed in protoplasts, suggesting that its membrane association may be mechanistically different from that of YFP-D6PK (Figure 18 A - D)(Bassukas et al., 2022).

In the second part of my project, I described the role of the CXX(X)P motifs for plasma membrane anchoring. I found that the CXX(X)P motifs and S-acylation are required to anchor YFP-D6PK to the basal plasma membrane and that this mechanism may be conserved in other AGC1 kinases. Another goal of my project was to improve the model for D6PK trafficking since we did not describe a mechanism for D6PK internalization previously. Although S-acylations have been described to be reversible modifications and may therefore influence protein localization, I showed that for YFP-D6PK S-acylation status remained the same when treated with the trafficking inhibitor BFA, indicating that S-acylations are not involved in its trafficking. Therefore, I decided to analyze the role of phosphorylations with focus on the serines S310/S311 preceding the polybasic K/R-rich motif for D6PK localization and trafficking.

3.3 Functional analysis of the serines S310/S311 and their biochemical and cell biological role

3.3.1 D6PK phosphorylation and dephosphorylation are required for proper localization and trafficking

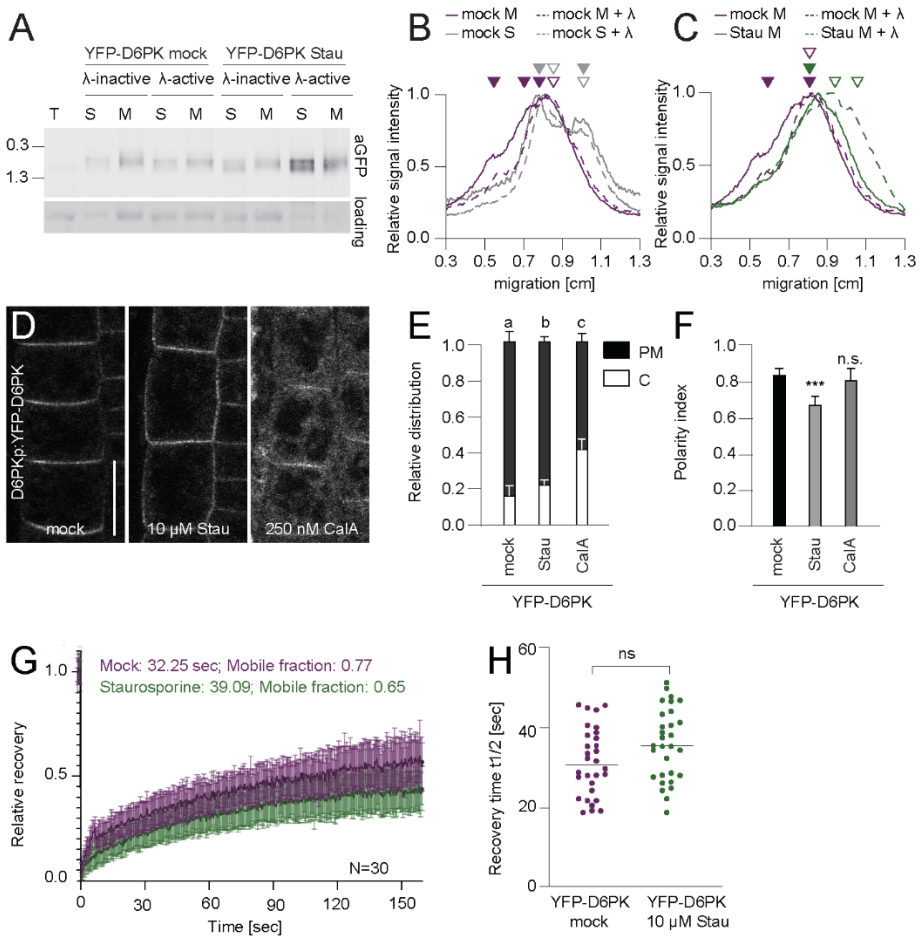

Figure 19. D6PK is differentially phosphorylated in the soluble and membrane fraction and YFP-D6PK phosphorylation-status affects cellular distribution. **A**. Immunoblot of protein extracts from transgenic plants expressing wildtype YFP-D6PK after treatments as specified and subcellular fractionation. **B** and **C.** Migration profiles of the immunoblot shown in (A) to compare migration of soluble and membrane protein (B) and migration of membrane fractions after the specified treatments (C). **D.** Representative confocal microscopy images of root epidermis cells of stably transformed six-days-old Arabidopsis thaliana seedlings expressing wildtype YFP-D6PK after 2 hour treatments as specified. Scale bar = 20 µm. **E**. and **F.** Bar graphs with mean and standard deviation of cellular distribution (E) and polarity index (F) of n > 15 cells from at least three seedlings from confocal microscopy images as shown in (D). The statistically significant difference between groups in (E) was determined by one-way ANOVA ($F(2, 42) = 69.29$, $p < 0.001$) and means were compared using a Tukey's test. Different letters indicate a statistically significant difference. In (E), polarity indices were compared to that of the mock-treated control using a Student's t-test: n.s., not significant, *** < 0.001. **G.** and **H.** Results from FRAP experiments performed with epidermal cells of five days old seedlings expressing wildtype YFP-D6PK after treatments as specified. Shown are normalized recovery curves (G) and mean and individual recovery times t1/2 (H) at the basal plasma membrane for wildtype YFP-D6PK and mutant YFP-D6PK_SSAA. Recovery times were compared using a Student's t-test: n.s., not significant.

In my previous experiments I showed that CXX(X)P motifs are required for D6PK plasma membrane association and that D6PK contains S-acylations, enhancing its anchoring to the membrane. However, I also demonstrated that the CXX(X)P motifs are not involved in D6PK trafficking, and the mechanism by which D6PK is internalized from the plasma membrane remained to be elucidated. To investigate the hypothesis that phosphorylation at the serines S310/S311 may serve as an electrostatic switch, counteracting the positive charge of the polybasic K/R-rich motif and therefore facilitating D6PK internalization, I examined the role of phosphorylation for D6PK cell biology and function. Previous research by Inês Barbosa in our group indicated that D6PK, fractionated into soluble and membrane-associated protein, exhibited different phosphorylation pattern as evidenced by different SDS-PAGE migration behavior following subcellular fractionation. We hypothesized that these phosphorylations could influence D6PK localization. I decided to follow up on her experiments to understand the role of the differential phosphorylation status of D6PK in membrane and soluble fraction.

I confirmed her finding by isolating protein from six-days-old seedlings after two hours of treatment with mock or with 10 µM Staurosporine (Stau), an inhibitor of Ser/Thr kinases, followed by subcellular fractionation. An aliquot of each extract was treated with λ-phosphatase to verify whether potential differences in migration were caused by phosphorylation. I observed a phosphorylation smear in the membrane fraction of the mock treated sample, which migrated more slowly than the protein in the soluble fraction. This smear was largely eliminated when the protein extract underwent dephosphorylation by λ-phosphatase treatment, resulting in a more pronounced overlap of the membrane signal peak with the main signal peak of the soluble fraction (Figure 19 A and B). I also noted a migration shift in the soluble fraction following λ-phosphatase treatments, although it was less pronounced than in the membrane fraction, indicating that YFP-D6PK was phosphorylated in both the soluble and membrane fraction but to a different level (Figure 19 A and B). The Staurosporine-treated samples exhibited a migration pattern on the SDS-PAGE comparable to that of mock-treated YFP-D6PK dephosphorylated by λ-phosphatase treatment (Figure 19 A and C). The λ-phosphatase treatment showed less effect on the migration behavior of Staurosporine-treated YFP-D6PK than on mock-treated YFP-D6PK (Figure 19 A and C).

Having noted that YFP-D6PK phosphorylations differ between the soluble and membrane fraction, I wanted to understand the effect of the phosphorylations on YFP-D6PK cellular distribution. To assess the impact of phosphorylation on YFP-D6PK cellular distribution, I imaged root epidermal cells of six-days-old seedlings expressing YFP-D6PK under a *D6PK* promoter fragment after two-hour treatments with Staurosporine or the phosphatase inhibitor Calinculin A. Notably, altering the intracellular phosphorylation-status of YFP-D6PK with Staurosporine affected its cellular distribution and led to a less pronounced polar localization and an enhanced YFP-D6PK abundance at the lateral plasma membrane of cells compared to the mock-treated YFP-D6PK (Figure 19 D - F). Treatments with the phosphatase inhibitor Calinculin A resulted in an increased cytosolic signal compared to mock-treated YFP-D6PK (Figure 19 D - F).

To ascertain the impact of YFP-D6PK phosphorylation status for its cellular dynamics, I performed FRAP experiments following a two-hour treatment of seedlings expressing YFP-D6PK in liquid medium with mock or 10 µM Staurosporine. I observed a slower recovery and a decreased mobility of YFP-D6PK at the basal plasma membrane for the Staurosporine-treated seedlings when compared to the mock control. When I evaluated the calculated recovery times, however, this difference was not statistically significant (Figure 19 G and H).

I concluded that YFP-D6PK is phosphorylated in soluble and membrane fraction. Its phosphorylation was at least partially inhibited by treatments with Staurosporine as shown in λ-phosphatase treatments. Furthermore, YFP-D6PK phosphorylation status affected its cellular distribution. Inhibiting the phosphorylation with Staurosporine led to a less pronounced polarity at the basal plasma membrane, and inhibiting its dephosphorylation with Calinculin A led to an increase in cytosolic signal. These results suggested that dynamic phosphorylations and dephosphorylations may control YFP-D6PK cellular distribution.

3.3.2 D6PK S310 and S311 are required for proper localization, trafficking, and function

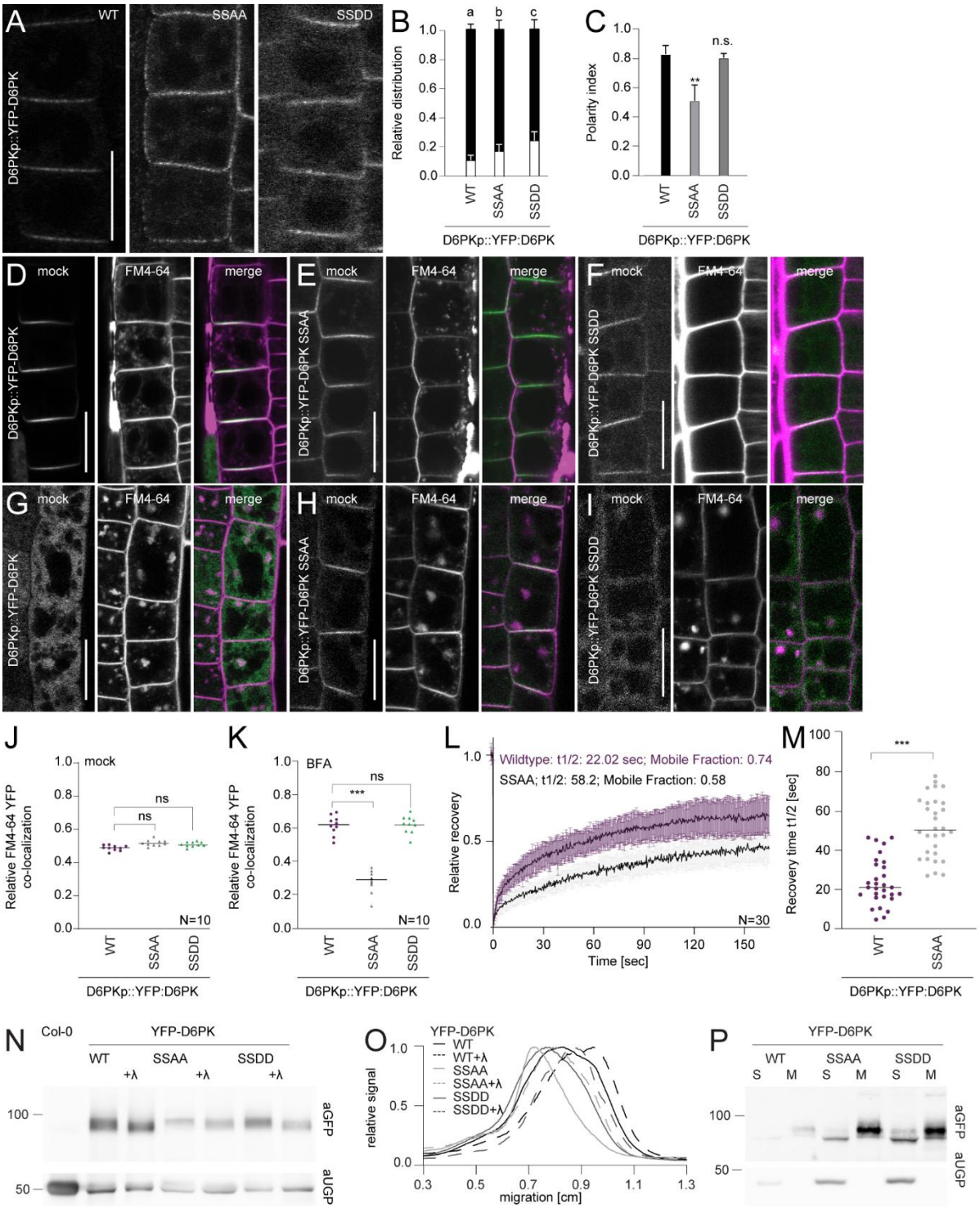

Figure 20. D6PK S310/S311 are phosphorylation targets preceding the polybasic K/R-rich motif and are required for YFP-D6PK trafficking and polarity maintenance.A. Representative confocal microscopy images of root epidermal cells from six-days-old *Arabidopsis thaliana* seedlings expressing wildtype YFP-D6PK and mutant variants YFP-D6PK_SSAA and YFP-D6PK_SSDD in *d6pk*

d6pkl1. Scale bar = 20 µm. **B**. and **C.** Bar graphs with mean and standard deviation of cellular distribution (B) and polarity index (C) quantified in n > 15 cells from at least three seedlings from confocal microscopy images as shown in (A). The statistically significant difference between groups was determined by one-way ANOVA (B, C), and means were compared using a Tukey's test (B, $F(2, 36) = 56.43$, $P < 0.0001$; C, $F(2, 36) = 24.63$, $P < 0.0001$). Different letters indicate a statistically significant difference. **D. – I.** Representative confocal microscopy images of root epidermal cells of five-days-old seedlings of the specified genetic backgrounds after mock (D, E, F) or 10 µM BFA (G, H, I) treatment and a 1 hour 50 µM Cycloheximide pre-treatment using a FM4-64 co-staining to mark the plasma membrane. Scale bars = 20 µm. **J.** and **K.** graphs with mean and individual values of YFP-D6PK and FM4-64 co-localization from 10 cells from confocal microscopy images as shown in (D) – (I) after mock (J) and BFA (K) treatment. Co-localization values were compared to the wildtype using a Student's t-test: n.s., not significant; ***, $p < 0.001$. **L.** and **M.** Results from FRAP experiments performed with epidermal cells of five-days-old seedlings expressing the transgenes as specified. Shown are normalized recovery curves (L) and mean and individual recovery times t1/2 (M) at the basal plasma membrane for wildtype YFP-D6PK and mutant YFP-D6PK_SSAA. Recovery times were compared using a Student's t-test (J, K, M): n.s., not significant; ***, $p < 0.001$. **N.** Immunoblot of total protein extracts from six-days-old *Arabidopsis thaliana* seedlings expressing the transgenes as specified. Part of the extract was treated with λ-phosphatase as specified. aGFP recognizes the YFP-tag; aUGP serves as a loading control. O. Migration profile from the immunoblot shown in (N). Arrow heads indicate signal peaks P. Immunoblot of protein extracts from six-days-old *Arabidopsis thaliana* seedlings expressing the transgenes specified after subcellular fractionation into soluble (S) and membrane (M) fraction.

After having established that phosphorylation status may determine D6PK localization, I further examined which phosphorylation sites may be responsible for controlling D6PK localization. We hypothesized in our lab that the serines S310/S311 preceding the polybasic K/R-rich motif function as an electrostatic switch to drive YFP-D6PK plasma membrane association and dissociation (Bassukas et al., 2022). To test this, I used the phosphorylation-impaired variant YFP-D6PK_SSAA and the phosphorylation-mimicking variant YFP-D6PK_SSDD, previously established in the lab, and examined their cellular distribution (Barbosa, 2015).

When expressed in root epidermis cells under a *D6PK* promoter fragment, the phosphorylation-mutant YFP-D6PK_SSAA showed increased localization at the lateral plasma membrane and thus a less pronounced polarity at the basal plasma membrane compared to wildtype YFP-D6PK. The phosphorylation-mimicking YFP-D6PK showed enhanced internalization compared to wildtype YFP-D6PK (Figure 20 A - C). Consequently, YFP-D6PK_SSAA subcellular localization notably mirrored the effects of the kinase inhibitor Staurosporine on YFP-D6PK localization, while the enhanced internalization of YFP-D6PK_SSDD resembled the effect of the phosphatase inhibitor Calinculin A on YFP-D6PK localization (Figure 20 A-C, Figure 19 D-F).

To evaluate differences in intracellular trafficking of YFP-D6PK_SSAA and YFP-D6PK_SSDD in comparison to wildtype YFP-D6PK, I performed treatments with BFA. YFP-D6PK_SSAA exhibited reduced sensitivity to the trafficking inhibitor BFA, but YFP-

D6PK_SSDD showed no difference in sensitivity when compared to wildtype YFP-D6PK (Figure 20 D - K). Pre-treatments with the protein biosynthesis inhibitor CHX were included to ensure that only recycled protein was examined. I hypothesized that YFP-D6PK_SSAA was not effectively internalized during the BFA treatments due to the absence of S310/S311 phosphorylation, functioning as an electrostatic switch, resulting in a longer residence time at the plasma membrane. I argued that, if this hypothesis was true, YFP-D6PK_SSAA would likely also show an altered mobility within and towards the plasma membrane, which might be assessed with FRAP experiments. Following bleaching a ROI at the basal plasma membrane in FRAP experiments, YFP-D6PK_SSAA recovered more slowly and less efficiently at the basal plasma membrane compared to wildtype YFP-D6PK. I observed a decrease in the half recovery time t(1/2) and a reduction in the mobile fraction (Figure 20 L and M). These data may suggest a reduction in the internalized pool resulting from an impaired release of protein from the plasma membrane, supporting that phosphorylation is required for D6PK internalization.

To elucidate the impact of the mutations on YFP-D6PK subcellular localization, I isolated protein from transgenic lines expressing YFP-D6PK, YFP-D6PK_SSAA and YFP-D6PK_SSDD. An aliquot of each extract was treated with λ-phosphatase and analyzed on an immunoblot. I could observe a migration shift for all proteins after treatment with λ-phosphatase, indicating that YFP-D6PK as well as YFP-D6PK_SSAA and YFP-D6PK_SSDD were phosphorylated *in vivo*. Notably, the untreated YFP-D6PK_SSAA migrated more slowly than YFP-D6PK and YFP-D6PK_SSDD and even following λ-phosphatase treatment, YFP-D6PK_SSAA did not migrate as fast as YFP-D6PK or YFP-D6PK_SSDD (Figure 2o N). This observation led me to conclude that the migration shift observed for YFP-D6PK_SSAA compared to YFP-D6PK and YFP-D6PK_SSDD was not induced by differences in phosphorylation. I additionally evaluated whether YFP-D6PK_SSAA or YFP-D6PK_SSDD show a similar ratio of soluble to membrane protein as wildtype YFP-D6PK. An increased solubility and thus reduced membrane association could explain the increased internalization of YFP-D6PK_SSDD. I extracted protein and performed an ultracentrifugation step to separate soluble and membrane fraction. Although YFP-D6PK_SSAA and YFP-D6PK_SSDD were both more soluble than the wildtype YFP-D6PK, these differences were minor (Figure 10 D, E). I concluded that the observed increased internalization in YFP-D6PK_SSDD was not due to a loss of

membrane association and an increase in soluble protein but may rather be caused by an increased association with internal membranes when compared to wildtype YFP-D6PK.

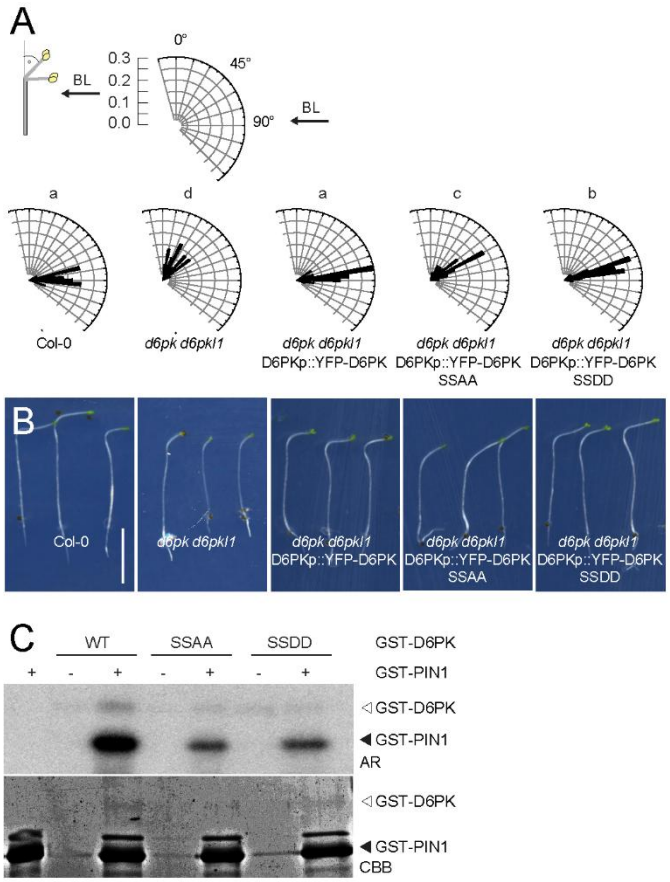

Figure 21. The S310/S311 phosphorylation site is required for proper D6PK function. A. Rose diagrams with frequency distribution in 5° intervals of hypocotyl bending angles of three-days-old dark grown seedlings of the genetic backgrounds as specified after four hours exposure to unilateral blue light (BL). The arrow indicates the direction of the blue light exposure. The statistically significant difference between groups was validated using a One-way ANOVA ($F(4, 295) = 178.7$, $p < 0.001$) and means were compared using a Tukey's test **B**. Photographs of three representative seedlings from the experiment analyzed in (A). Scale bar = 0.5 cm. **C.** Autoradiography (AR) and Coomassie Brilliant Blue-stained gel (CBB) from *in vitro* kinase assay experiment with recombinantly expressed and purified wildtype GST-D6PK or mutant variants as specified and the hydrophilic loop fragment of PIN1 (GST-PIN1) as phosphorylation substrate.

To evaluate the significance of S310/311 phosphorylation for YFP-D6PK function, I examined the ability of YFP-D6PK_SSAA and YFP-D6PK_SSDD to complement the phototropism defect of the *d6pk d6pkl1* mutant when expressed under a *D6PK* promoter fragment. Neither YFP-D6PK_SSAA nor YFP-D6PK_SSDD were sufficient to complement the phototropism defect compared to wildtype YFP-D6PK but they showed some phototropic bending in comparison to *d6pk d6pkl1* (Figure 21 A and B). GST-D6PK_SSAA and GST-D6PK_SSDD less efficiently phosphorylated GST-PIN1 *in vitro* compared to GST-D6PK (Figure 21 C). Consequently, I could not conclude whether the failure to complement the phototropism defect directly resulted from the reduced polarity and the decreased membrane localization or was an effect of the decreased catalytic activity exhibited by GST-D6PK_SSAA and GST-D6PK_SSDD when compared to wildtype GST-D6PK.

3.3.3 YFP-D6PK S310/S311 phosphorylation is required for proper auxin transport in the hypocotyl and apical hook formation

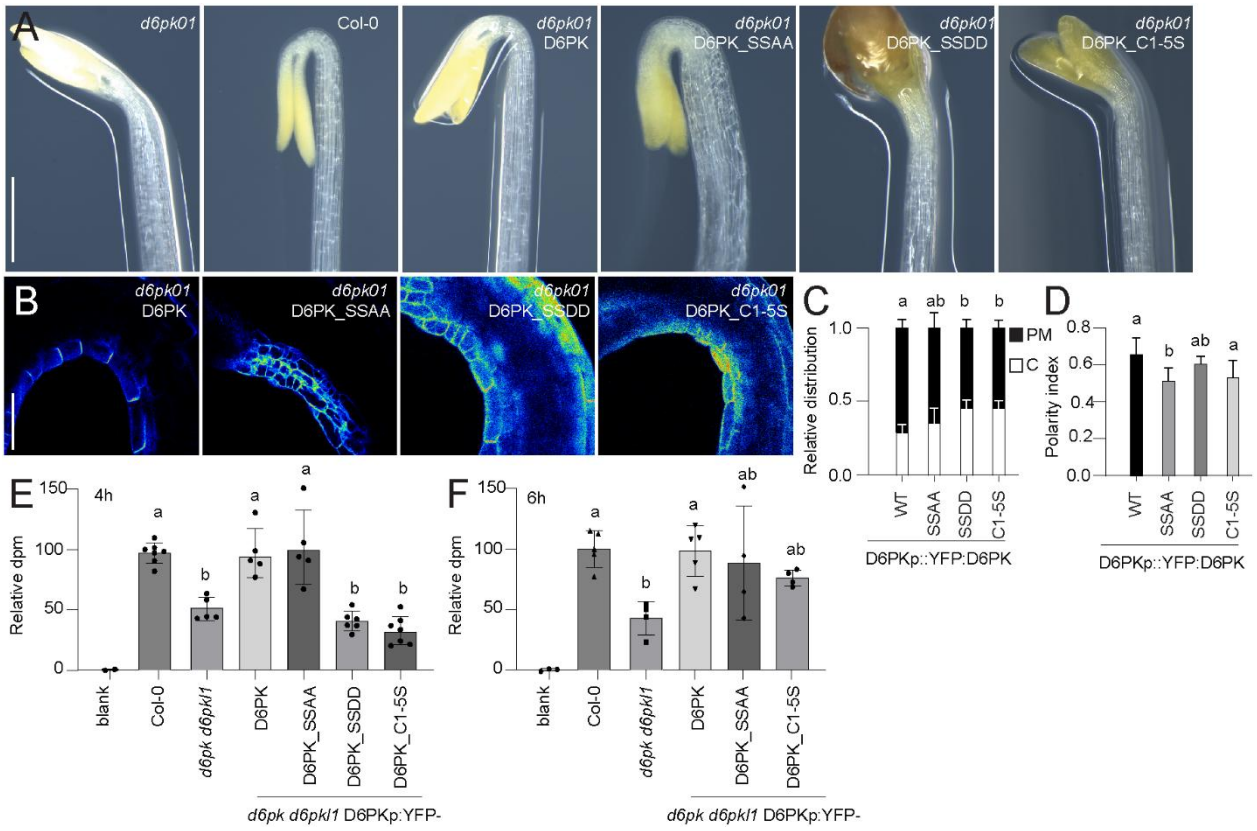

Figure 22. D6PK plasma membrane localization and polarity control are required for apical hook development. A. Representative images of apical hook formation of three-days-old dark grown seedlings showing the *d6pk d6pkl1* double mutant (*d6pk01*), the Columbia wildtype (Col-0), and YFP-D6PK and mutant variants as indicated expressed as YFP-tagged proteins under the *D6PK* promoter in the *d6pk d6pkl1* background. Scale bar = 0.5 mm. **B.** Representative images of the localization of YFP-D6PK and mutant variants in the apical hook region three-days-old dark grown seedlings as shown in (A). Scale bar = 50 µm. **C.** and **D.** Quantifications of cytosolic (C) to plasma membrane (PM) fraction (C) and polarity index (D) of n ≥ 15 cells from confocal microscope images as shown in (D). **E.** and **F.** Results from hypocotyl basipetal auxin transport assays with four-days-old dark grown seedlings measured after four hours (E) or six hours (F) of auxin transport. Quantifications were performed with n ≥ 4 replicates, consisting of 5 individual seedlings with the genotypes indicated. The statistically significant difference between groups in (B, C, E, F) was determined by One-way ANOVA and means were compared using a Tukey's test. Different letters indicate a statistically significant difference.

In addition to the inability of the *d6pk d6pkl1* mutants to bend towards of light source, we previously reported the impairment in apical hook formation in the *d6pk d6pkl1* background (Willige et al., 2013). A phenotype that is also associated with deficiencies in auxin transport (Willige et al., 2013; Vandenbussche et al., 2010; Žádníková et al., 2010). I analyzed the localization and ability to complement the apical hook formation defect for the generated D6PK variants in comparison to wildtype D6PK to provide a clear link between D6PK localization and biological function. Interestingly, the YFP-D6PK variants

YFP-D6PK_SSDD and YFP-D6PK_C1-5S which were more internalized and less present at the plasma membrane than wildtype YFP-D6PK, failed to complement the defect in apical hook formation when expressed from a *D6PK* promoter fragment. The mutant variant YFP-D6PK_SSAA, which localized apolarly to the plasma membrane demonstrated apical hook formation in some cases (Figure 22 A). However, it still exhibited growth defects as seen by deformed cells, particularly around the apical hook region (Figure 22 A and B).

I analyzed the localization of wildtype YFP-D6PK, YFP-D6PK_SSAA, YFP-D6PK_SSDD and YFP-D6PK_C1-5S in the apical hook region. Wildtype YFP-D6PK exhibited a polarized distribution in the bending cells and mostly plasma membrane associated protein. YFP-D6PK_SSAA showed a marginally more cytosolic localization, and a diminished polarity was observed for YFP-D6PK_SSAA (Figure 22 B-D). YFP-D6PK_SSDD still showed a polar distribution at the basal plasma membrane, but an increase of cytosolic signal was observed when compared to wildtype YFP-D6PK. YFP-D6PK_C1-5S also showed more intracellular accumulation when compared to the wildtype protein and a reduced polarity at the basal plasma membrane. The observed localization in the hypocotyl for YFP-D6PK, YFP-D6PK_SSAA, YFP-D6PK_SSDD and YFP-D6PK_C1-5S was therefore in line with the cell biological behavior previously observed in the root for the different YFP-D6PK variants.

To directly correlate how the localization in epidermal cells of the hypocotyl with auxin transport in the hypocotyl, I conducted *in planta* auxin transport experiments with the complementation line expressing YFP-D6PK as well as its variants YFP-D6PK_SSAA, YFP-D6PK_SSDD and YFP-D6PK_C1-5S from a *D6PK* promoter fragment. The *d6pk d6pkl1* mutant as well as the wildtype Col-0 were included as controls. When auxin transport was measured after four hours, I observed reduced auxin transport in YFP-D6PK_C1-5S and YFP-D6PK_SSDD compared to Col-0 and *d6pk d6pkl1* complemented with wildtype YFP-D6PK (Figure 22 E). When in another experiment auxin transport was measured after six hours, the transport rates of all the complementation lines resembled the wildtype Col-0 control, indicating that auxin transport is reduced but not completely abolished for all examined YFP-D6PK variants (Figure 22 F). All subsequent experiments were therefore conducted with four hours of auxin transport. I noted that the reduced capacity of the seedlings expressing YFP-D6PK_SSDD and YFP-D6PK_C1-5S to

transport auxin correlated well with the observed cell biological behavior of these proteins, which displayed a decreased abundance at the plasma membrane in favor of a more cytosolic distribution, and was therefore likely caused by decreased kinase activity and thus reduced PIN phosphorylation at the plasma membrane. This finding also correlated well with the identified impairment in apical hook formation. The apolarly localized YFP-D6PK_SSAA did not display significant differences in hypocotyl auxin transport in basipetal auxin transport assays when compared to wildtype YFP-D6PK. I speculated that this may be the case, because YFP-D6PK_SSAA remains localized at the plasma membrane and may, due to its longer residence time, activate auxin transport more efficiently than the more internalized YFP-D6PK_C1-5S and YFP-D6PK_SSDD.

3.3.4 PIN phosphorylation in lines expressing YFP-D6PK_SSAA

From the cell biological experiments with the phosphorylation-mutant YFP-D6PK_SSAA, I made two intriguing observations - YFP-D6PK_SSAA was less polarly localized in comparison to wildtype YFP-D6PK and less sensitive to the trafficking inhibitor BFA. The physiological experiments showed that YFP-D6PK_SSAA did not rescue the phototropism defect to wildtype level but was able to complement for basipetal auxin transport. I speculated that the failure of YFP-D6PK_SSAA to complement the phototropism defect may be caused by differences in PIN phosphorylation pattern. Therefore, I wanted to test whether PIN phosphorylation pattern was changed in seedlings expressing YFP-D6PK_SSAA in comparison to seedlings expressing wildtype YFP-D6PK. I conducted immunostainings with the previously established PIN1-S1p phosphospecific antibody that detects PIN1 phosphorylated in the S1-site of its cytosolic loop (Weller et al., 2017). In the mock treatments, I wanted to test whether the polarity of PIN phosphorylation is reduced in seedlings expressing YFP-D6PK_SSAA compared to seedlings expressing wildtype YFP-D6PK, due to the reduced polar localization observed for YFP-D6PK_SSAA. When I analyzed the immunostained seedlings using confocal microscopy, I did not observe a reduction of phosphorylated PIN1 in the lines expressing YFP-D6PK_SSAA compared to the ones expressing wildtype YFP-D6PK, indicating that PIN1-phosphorylation in the S1-site was not strongly affected by expression of the D6PK mutant variant YFP-D6PK_SSAA. I did not see a statistically significant change in polarity of PIN1-phosphorylation with YFP-D6PK_SSAA, when comparing signal intensity at the basal and lateral sides of stele cells (Figure 23 A – E). This suggested that even though YFP-

D6PK_SSAA localizes at the basal and lateral side of cells, PIN1 phosphorylation at the basal plasma membrane is maintained, which may explain why YFP-D6PK_SSAA can complement the basipetal auxin transport defect of *d6pk d6pkl1*.

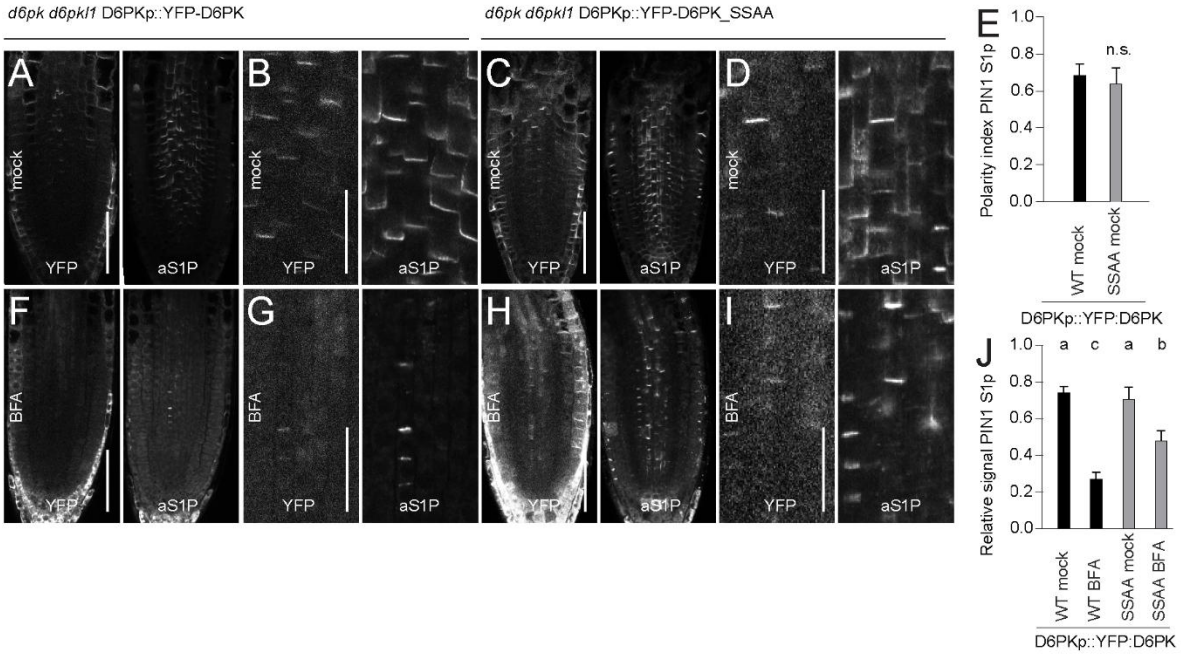

Figure 23. PIN1 S1-phosphorylation sensitivity to BFA is reduced in the YFP-D6PK_SSAA background. A. - D. and **F. – I.** Representative confocal microscopy images of immunostainings of four-days-old stably transformed *Arabidopsis thaliana* seedlings expressing wildtype YFP-D6PK (A,B,F,G) or the variant YFP-D6PK_SSAA (C,D,H,I) and treated with mock (A – D) or BFA (F – I) as indicated. Anti-S1p detects phosphorylated PIN1 in the S1-site. YFP is the residual signal found from YFP-tagged protein after immunostaining. Scale bar = 50 µm (A, C, F, H) and 20 µm (B, D, G, I). **E.** and **J.** Bar graphs with mean and standard deviation of polarity index (E) and relative plasma membrane intensity (J) of PIN1 S1p signal quantified in n > 15 cells from at least three seedlings from confocal microscopy images as shown in (A. -D. and F. – I.). The statistically significant difference between groups in (J) was determined by One-way ANOVA ($F(3, 56) = 25{,}64$; $p < 0.001$) and means were compared using a Tukey's test. Different letters indicate a statistically significant difference. In (E), polarity indices were compared to that of the mock-treated control using a Student's t-test: n.s., not significant.

I additionally aimed to observe whether PIN phosphorylation is less sensitive to BFA treatments in seedlings expressing YFP-D6PK_SSAA than in seedlings expressing wildtype YFP-D6PK, which would reflect the reduced sensitivity to BFA observed for YFP-D6PK_SSAA, and provide further evidence for its inefficient internalization. I performed immunostainings in seedlings expressing YFP-D6PK or YFP-D6PK_SSAA after a 30 min 50 µM BFA treatment. We demonstrated in the past that PIN1 phosphorylation, detected with the PIN1-S1p antibody, is efficiently removed after treatments with BFA which we explained with the fast removal of D6PK from the basal plasma membrane upon BFA treatment (Weller et al., 2017).

In line with the previous studies, PIN1-phosphorylation at the plasma membrane was clearly reduced after the BFA-treatment in my experiments. This was the case for seedlings expressing YFP-D6PK as well as for seedlings expressing YFP-D6PK_SSAA. I sometimes observed that PIN1 phosphorylation was retained after BFA-treatment in the YFP-D6PK_SSAA background which was not the case for the wildtype YFP-D6PK (Figure 23 F – J). I also observed that these results were not very uniform for YFP-D6PK_SSAA and the effect of the treatment was more severe in some cases than in others. Due to the technical limitations of the experiment, it was not clear whether this was due to differences in the effect of the treatment or differences in the quality of the immunostaining. To present a quantitative analysis, I measured the signal at the basal plasma membrane under mock conditions and after BFA-treatment and compared it to the signal found in the protophloem strand to calculate the intensity of plasma membrane signal compared to the signal in the protophloem strand (Figure 23 J). The signal found in the protophloem cells served as a control for a successful immunostaining, since I and other colleagues had observed the PIN phosphorylation in the protophloem to be less sensitive to BFA treatments than in other stele cells (Figure 23 F). In these analyses, I observed that more PIN1 phosphorylation signal was retained at the basal plasma membrane in seedlings expressing YFP-D6PK_SSAA compared to seedlings expressing wildtype YFP-D6PK after the BFA treatment. I concluded that, in line with the previously observed reduced sensitivity of YFP-D6PK_SSAA to BFA treatments, PIN1 phosphorylation is less responsive to BFA treatments in seedlings expressing YFP-D6PK_SSAA when compared to seedlings expressing wildtype YFP-D6PK, supporting my previous findings.

3.3.5 YFP-D6PK_SSAA and YFP-D6PK_SSDD are still sensitive to the S-acylation inhibitor 2-BP

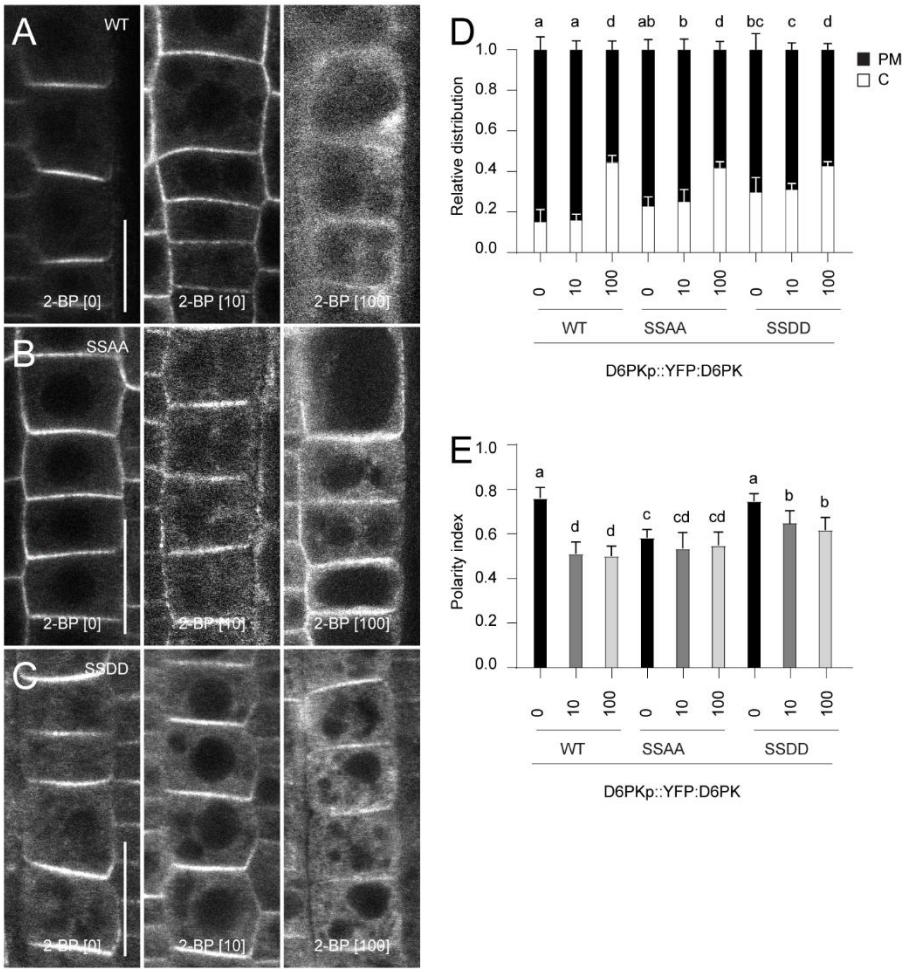

Figure 24. YFP-D6PK_SSAA and YFP-D6PK_SSDD are still sensitive to the S-acylation inhibitor 2-BP. A. – C. Representative confocal microscopy images of root epidermal cells from six-days-old stably transformed *Arabidopsis thaliana* seedlings expressing wildtype YFP-D6PK (A) or mutant variants YFP-D6PK_SSAA (B) or YFP-D6PK_SSDD (C) after 2 hour treatments with mock or 2-BP as specified. **D.** and **E.** Bar graphs with mean and standard deviation of cellular distribution (D) and polarity index (E) quantified in n > 15 cells from at least three seedlings from confocal microscopy images as shown in (A - C). The statistically significant difference between groups was determined by one-way ANOVA and means were compared using a Tukey's test (D, $F(8, 126) = 42.18$, $p < 0.001$; E, $F(8, 126) = 50.63$, $p < 0.001$). Different letters indicate a statistically significant difference.

In my experiments, I identified two posttranslational modifications taking place in the D6PK middle domain and affecting protein localization – cysteine S-acylations and serine phosphorylations. Since low concentrations of the S-acylation inhibitor and inhibition of phosphorylation both resulted in reduced polar localization of YFP-D6PK, I wanted to assess the potential interplay between S-acylations and phosphorylations (Figure 15 C - E, Figure 19 D - F). I treated six-days-old seedlings expressing wildtype YFP-D6PK as

well as seedlings expressing the phosphorylation-impaired variant YFP-D6PK_SSAA and the phosphorylation-mimicking variant YFP-D6PK_SSDD for two hours with concentrations of 0-100 µM 2-BP. YFP-D6PK_SSAA and YFP-D6PK_SSDD were still sensitive to high concentrations of 2-BP and showed increased intracellular protein accumulation comparable to the cytosolic signal observed for the wildtype YFP-D6PK after two hour treatment with 100 µM 2-BP (Figure 24 A - E). I concluded that S-acylation is required for plasma membrane association also in absence of phosphorylation-induced internalization of D6PK and that it occurs independently of middle domain phosphorylation status.

I showed before that the effect of 2-BP on D6PK cell biological behavior is dosage-dependent and that treatments with lower concentrations of 10 µM 2-BP led to a loss of polar localization at the plasma membrane for wildtype YFP-D6PK (Figure 15 C - E). Treating the serine-mutated variants YFP-D6PK_SSAA and YFP-D6PK_SSDD with 10 µM 2-BP revealed that the phosphorylation-mimicking YFP-D6PK_SSDD did not show a significant change of polarity when compared to the mock control and differed from the cell biological behavior of the wildtype YFP-D6PK in this regard, while at high concentrations of 2-BP they showed a similar response (Figure 24 A - E). This result may suggest that the observed reduction in polar localization for wildtype YFP-D6PK in the 10 µM 2-BP treatments could be caused by a reduction in phosphorylation and may suggest a potential influence of S-acylation on phosphorylation.

3.3.6 D6PK phosphorylation and S310/S311 site determine affinity to phosphoinositides *in vitro*

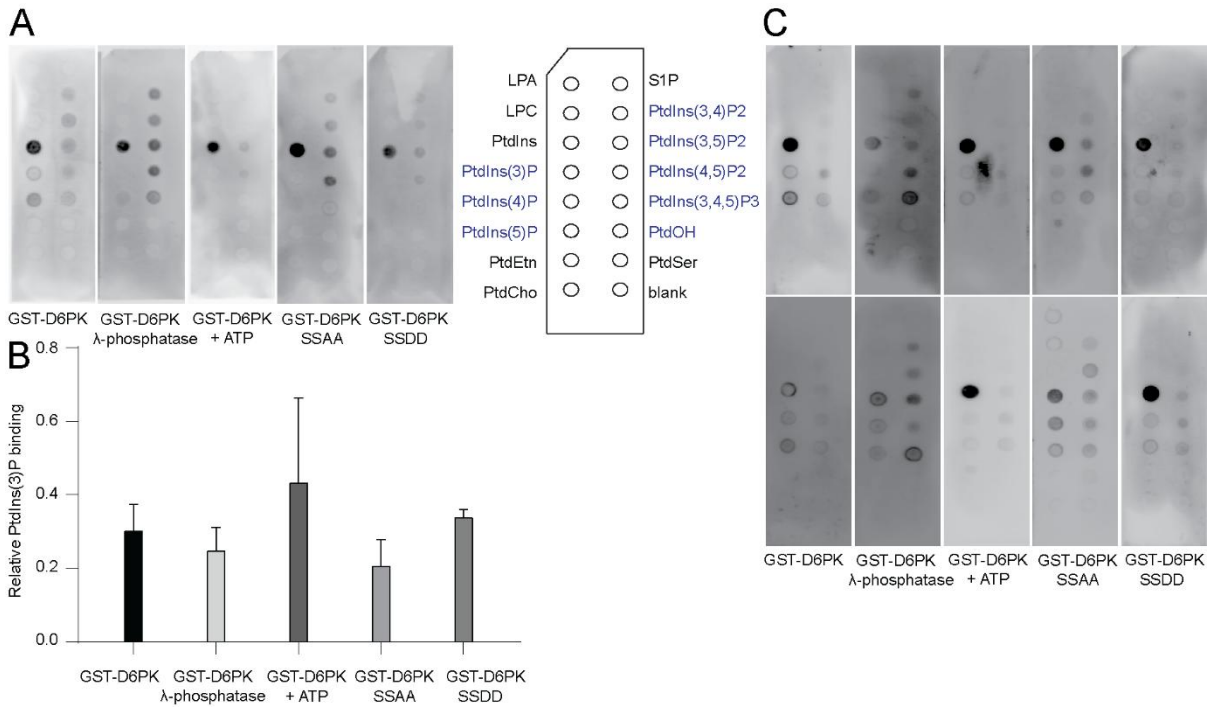

Figure 25. D6PK phosphorylation-status affects PIP-affinity in vitro. **A.** GST-D6PK treated with phosphatase or autophosphorylated with ATP and its mutant variants as specified incubated on PIP-strips loaded with lipids as shown and probed with anti-Glutathione S-Transferase (aGST) to detect the GST-tag. **B.** Quantification of PIP-binding profiles from three PIP-strips as shown in (A) and (C) from three independent protein purifications. **C.** Repetitions of PIP-strips serving as controls for the quantification in (B). Note that although qualitative differences in binding behavior were observed, these were not statistically significant when quantified and compared using one-way ANOVA ($F(4, 10) = 1.831$, $p=0.1996$).

In my experiments I observed and increased intracellular accumulation of YFP-D6PK_SSDD when compared to the wildtype YFP-D6P. However, I could not detect a substantial increase in solubility when performing subcellular fractionations of YFP-D6PK followed by immunoblotting. This indicated that YFP-D6PK_SSDD may associate with intracellular membranes. I examined whether the S310/S311 phosphorylation could influence the affinity of D6PK to different lipid compositions, hence altering its phosphoinositide-binding specificity. Our group previously showed that D6PK associates with membranes via interactions with phosphoinositides and that *in vitro* phosphoinositide-binding assays (PIP-strips) were suitable to demonstrate this interaction (Barbosa et al., 2016). I conducted lipid overlay assays on PIP-strips using GST-D6PK, GST-D6PK_SSAA, GST-D6PK_SSDD, and GST-D6PK treated with λ-phosphatase or auto-phosphorylated with ATP. GST-D6PK showed the strongest binding to PtdIns(3)P on the

PIP-strip (Figure 25 A – C). I also observed some GST-D6PK binding to PtdIns(5)P and to the double- and triple-phosphorylated phosphoinositides PtdIns(3,4)P_2, PtdIns(3,5)P_2, PtdIns(4,5)P_2 and PtdIns(3,4,5)P_2, as well as phosphatidic acid (PtdOH). GST-D6PK_SSAA and GST-D6PK, when treated with λ-phosphatase, preferably bound to PtdIns(3)P. However, I noticed stronger binding to PtdIns(4,5)P_2 and PtdIns(3,4,5)P_2 in comparison to wildtype GST-D6PK. Conversely, YFP-D6PK_SSDD and GST-D6PK autophosphorylated with excess ATP, demonstrated a strong specificity for PtdIns(3)P and both exhibited less binding to other PIPs apart from PI(3)P compared to wildtype GST-D6PK. Since the S310/S311 phosphorylation status changed GST-D6PK distribution in lipid overlay assays on PIP-strips, I concluded that S310/S311 phosphorylation may affect affinity for specific phosphoinositides. This could affect the cellular distribution of D6PK *in vivo* and may explain an increased association with internal membranes of YFP-D6PK_SSDD.

3.3.7 Further phosphorylation sites may be involved in D6PK internalization

In my experiments, I identified two phosphorylated serines preceding the polybasic K/R-rich motif of D6PK that play a role for D6PK internalization. Intriguingly, the middle domains of all D6PKs are enriched in serines although the exact position of the serines is not conserved (Figure 26). I aimed to investigate if these serines could serve as additional phosphorylation sites and may promote D6PK internalization, like the previously characterized serines S310/S311. I conducted mass spectrometry experiments on recombinant GST-D6PK to identify further phosphorylation sites and investigated whether they were upregulated in an autoregulatory way by D6PK. I incubated purified GST-D6PK or kinase-dead GST-D6PK_KD with ATP or phosphorylated them with their activating kinase PDK1. I identified six phosphorylation sites in the middle domain among them the S311-site (Figure 26)(PRIDE ID PXD037885). Both GST-D6PK and GST-D6PK_KD were phosphorylated by PDK1 in the activation loop serine demonstrating that PDK1 was active in both samples and specifically activated D6PK through phosphorylation of the activation loop, and none of the other detected phosphorylation sites were directly phosphorylated by PDK1 (Figure 26).

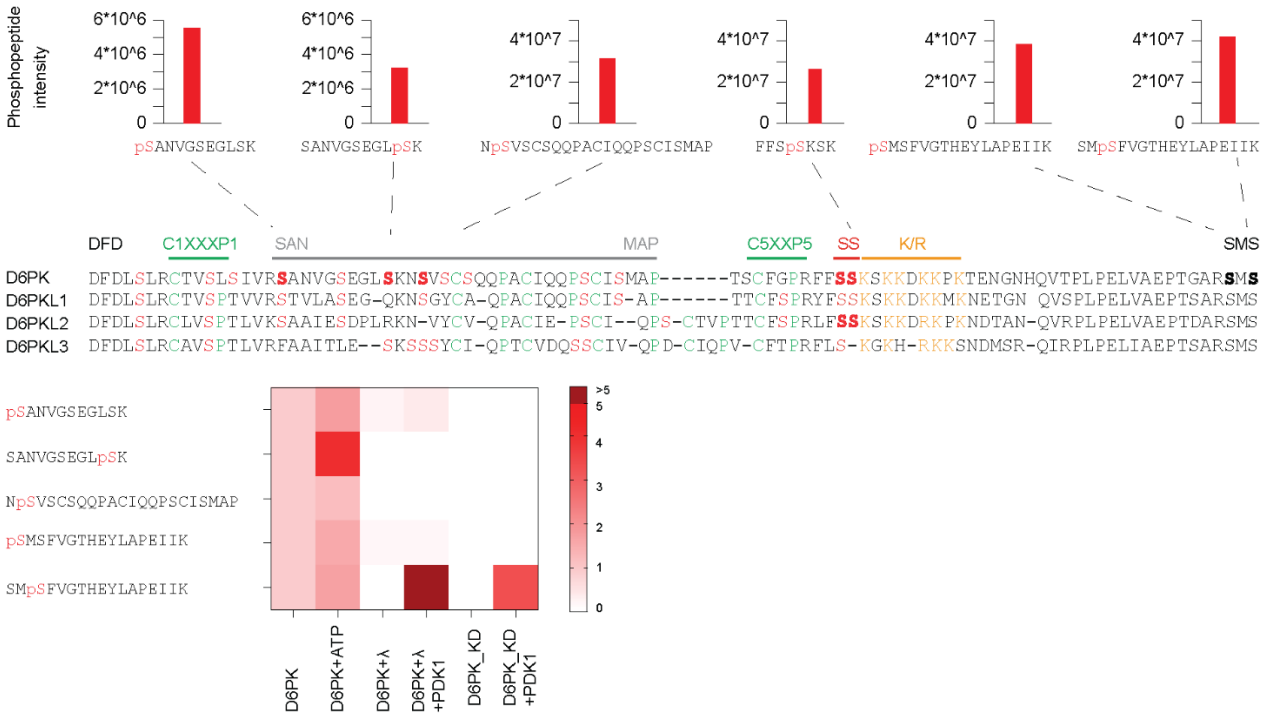

Figure 26. Mass spectrometric analysis of middle domain phosphorylation sites. Muscle alignment of D6PK and D6PKL1 – D6PKL3 middle domain sequences with the 31 amino acids deleted in YFP-D6PKΔSAN indicated and marked by a line. Serine residues in the middle region are highlighted in red, phosphorylated serines detected from mass spectrometry experiments are shown in bold letters together with the respective phosphopeptide intensity blots (upper panels) for the tryptic peptide fragments specified underneath. The heatmap shows the relative abundance of the normalized phosphorylated peptide in the different samples allowing to differentiate auto- and transphosphorylation events. The peptide corresponding to S310/S311, FFSSKSK, was recovered only in its phosphorylated form, not allowing to establish the corresponding correlations.

For structural studies, I had previously generated a YFP-D6PK variant with a 31 amino acid deletion in the middle domain, retaining the polybasic K/R-rich motif, CXX(X)P5 and the serines S310/S311, which are required for plasma membrane association and internalization, but lacking CXX(X)P2 – CXX(X)P4 as well as eight serines middle domain serines (Figure 27 A). When analyzing this deletion variant named YFP-D6PK_ΔSAN expressed in seedlings using confocal microscopy imaging, I detected a decreased polar distribution around the plasma membrane of root epidermis cells compared to the wildtype YFP-D6PK (Figure 27 A-C). Treatments with the exocytosis inhibitor BFA revealed a reduced internalization and accumulation inside BFA compartments in comparison to the wildtype YFP-D6PK (Figure 27 D – H). The reduced polarity and reduced sensitivity to BFA of YFP-D6PK_ΔSAN mirrored the behavior previously observed for YFP-D6PK_SSAA. I concluded that the deleted region was not required for plasma membrane association of YFP-D6PK but was required for maintaining D6PK polar distribution and BFA-sensitive trafficking, possibly because phosphorylation of additional middle domain

serines, identified as phosphorylation sites in my mass spectrometric analysis, may be required for proper internalization of D6PK.

YFP-D6PK_ΔSAN suppressed the phototropism defect of *d6pk d6pkl1* only to a minor extent, which was in agreement with the inability to rescue the basipetal auxin transport in the *d6pk d6pkl1* mutant (Figure 27 I - K). Due to the low signal intensity in confocal microscopy experiments of the lines expressing the YFP-D6PK_ΔSAN transgene, I could not extend my analysis to hypocotyl cells as I had previously done for other YFP-D6PK variants. In *in vitro* kinase assays GST-D6PK_ΔSAN was less active towards the PIN1 cytosolic loop than wildtype GST-D6PK. I could not conclude whether the observed failure to rescue the mutant phenotypes was due to a reduced activity *in vivo*. I concluded that in addition to S310/S311 the additional middle domain serine phosphorylation sites identified in mass spectrometric experiments with recombinant GST-D6PK may be required to maintain D6PK polarity.

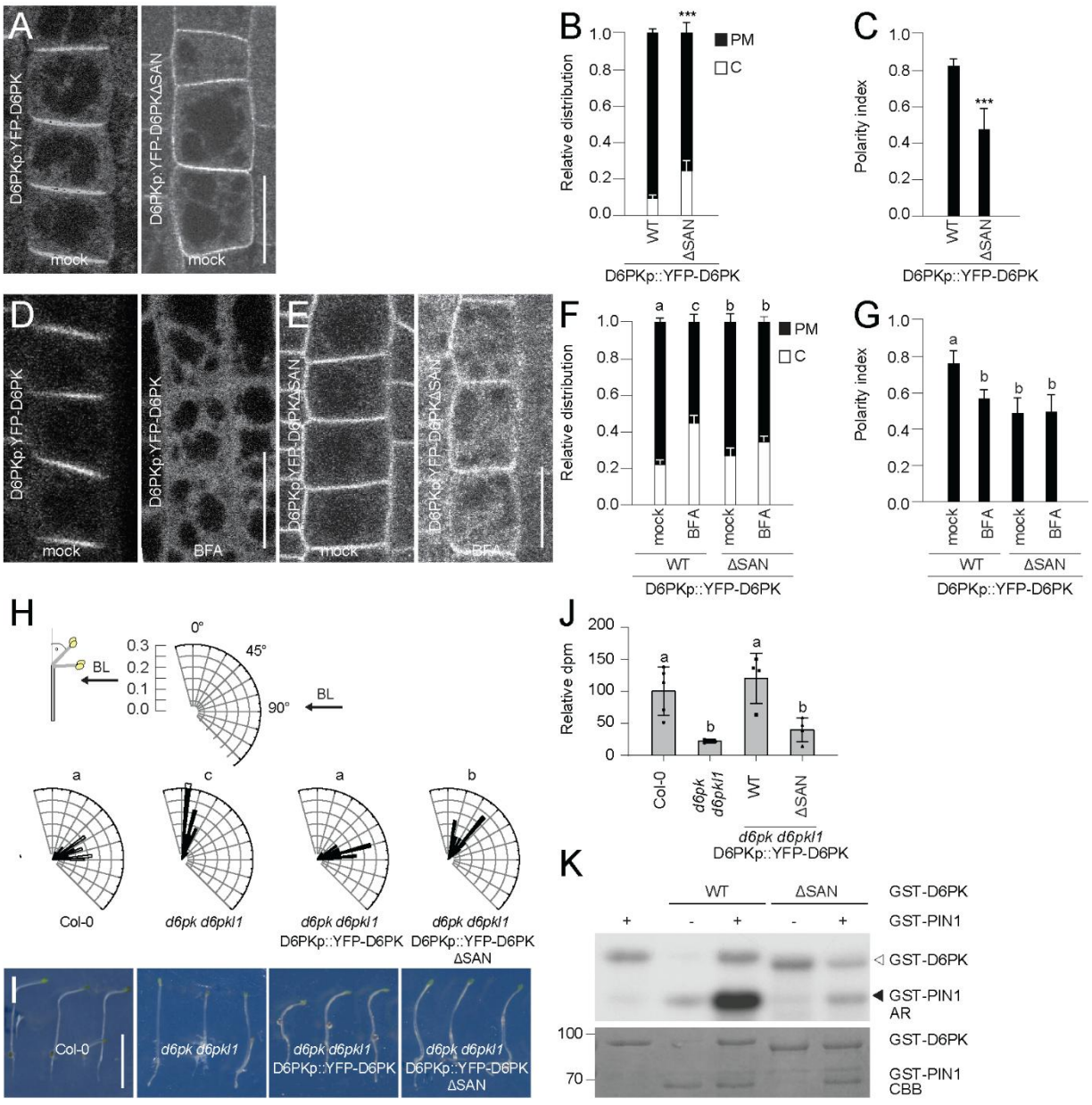

Figure 27. The D6PK deletion variant ΔSAN is apolar and insensitive to treatments with BFA. **A.** Representative confocal microscopy images of root epidermal cells from seedlings expressing wildtype YFP-D6PK or the deletion variant YFP-D6PKΔSAN. Scale bar = 20 µm. **B. - C.; F - G.** Bar graphs with mean and standard deviation of cellular cytosolic (C) to plasma membrane (PM) distribution (B, F) and polarity index (C, G) quantified in n > 15 cells from at least three seedlings from confocal microscopy images as shown in (A, D, E). **D.** and **E.** Representative confocal micoscopy images of root epidermal cells from six-days-old seedlings expressing wildtype YFP-D6PK (D) or the deletion variant YFP-D6PKΔSAN (E) after mock or 50 µM BFA treatment as specified. Scale bar = 20 µm. The statistically significant difference between groups was determined by **H.** Rose diagrams with frequency distribution in 5° intervals of hypocotyl bending angles of three-days-old dark grown seedlings of the genetic backgrounds as specified after four hours exposure to unilateral blue light (BL). The arrow indicates the direction of the blue light exposure. **I**. Photographs of three representative seedlings from the experiment analyzed in (H). Scale bar = 0.5 cm. **J.** Results from hypocotyl basipetal auxin transport assays with four-days-old dark grown seedlings measured after four hours. **K.** Autoradiography (AR) and Coomassie Brilliant Blue-stained gel (CBB) from *in vitro* kinase assay experiment with GST-D6PK or GST-D6PK_ΔSAN and the hydrophilic loop fragment of PIN1 (GST-PIN1) as phosphorylation substrate. The statistically significant difference between wildtype YFP-D6PK and YFP-D6PKΔSAN was determined using a Student's t-test (B,C): ***, $p < 0.001$ or one-way ANOVA (F, G, H, J) and means were compared

using a Tukey's test (F, F(3, 48) = 111.1, p < 0.0001; G, F(3,48) = 43.44, p < 0.0001, H, F(3, 117) = 176.8, p < 0.0001; J, F(3, 13) = 10.54, p = 0.0009). Different letters indicate a statistically significant difference.

3.3.8 D6PK phosphorylated at S310/S311 accumulates intracellularly

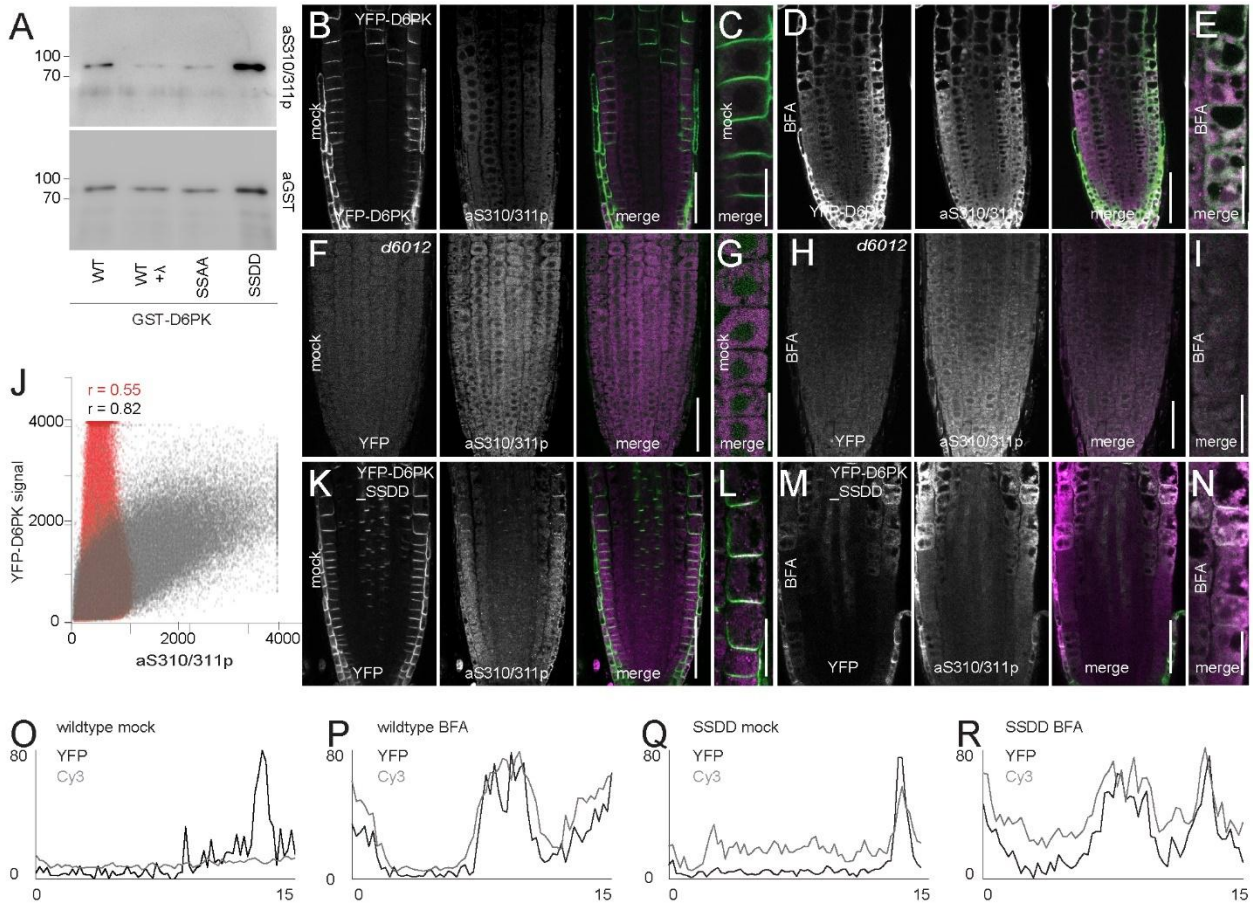

Figure 28. The phosphorylation-specific antibody aS310p/S311p detects D6PK phosphorylated at S310/S311 intracellularly. **A.** Immunoblot showing aS310/311p tested against GST-D6PK and variants as specified. Anti-S310p/S311p (aS310/311p) is specific to the phosphorylated site S310/S311; aGST detects the GST-tag and serves as a loading control. **B. – H.**; **K. – N.** Immunostainings of four-days-old stably transformed *Arabidopsis thaliana* seedlings expressing YFP-D6PK after mock (B, C) or 10 µM BFA treatment (F, G) and immunostaining of the d6pk d6pkl1 d6pkl2 triple mutant after mock (D, E) and 10 µM BFA treatment (H, I) as a negative control and seedlings expressing the phosphorylation-mimicking YFP-D6PK_SSDD as a positive control after mock (K,L) and 10 µM BFA-treatment (M, N). Scale bar = 50 µm (B, D, F, H, K, M) and 20 µm (C, E, G, I, L, N). **J.** Pearson's correlation coefficient of YFP-D6PK and aS310/311p-Cy3 signal after mock (red) and 10 µM BFA treatment (grey). **O. – R.** Profile plots to compare signal overlap of YFP and Cy3-signal from one cell of immunostained seedlings as shown in the images (B – I; K – N) expressing YFP-D6PK after mock (O) or 10 µM BFA-treatment (P) or expressing YFP-D6PK_SSDD after mock (Q) or 10 µM BFA-treatment (R).

I functionally described the role of phosphorylation of the serines S310/S311 for D6PK localization and trafficking, and their impact on its biological function. The physiological and cell biological experiments pointed towards the phosphorylation at S310/S311, and possibly phosphorylation of other serines in the D6PK middle domain, functioning as an electrostatic switch for D6PK trafficking and localization. However, due to technical

restrictions, I was unable to find evidence for this phosphorylation occuring *in planta*. I only found evidence for the S310/S311-phosphorylation using GST-D6PK recombinant protein or in D6PKL2 from the PhosPhAT 4.0 database (Figure 26)(Menz et al., 2016; Heazlewood et al., 2007). To test, whether the D6PK S310/S311-phosophorylation takes place *in planta*, we ordered an aS310p/S311p phosphorylation-specific antibody for use in immunostainings and immunoblots (Eurogentec, Seraing, Belgium). I tested the aS310p/S311p antibody against GST-D6PK expressed in *E.coli*. The aS310p/S311p antibody detected wildtype GST-D6PK, but not after dephosphorylation with λ-phosphatase, indicating that wildtype GST-D6PK was phosphorylated at the S310/S311-site in *E.coli* as I had previously observed in the mass spectrometric analysis. The phosphorylation-impaired variant GST-D6PK_SSAA was not detected unlike the phosphorylation-mimicking GST-D6PK_SSDD (Figure 28 A). I concluded that the antibody was specific to the S310/S311 phosphorylation and GST-D6PK_SSDD and thus suitable to study D6PK S310/S311 phosphorylation *in planta*.

In immunostainings, the aS310p/S311p antibody did not detect wildtype YFP-D6PK at the plasma membrane, although it showed the highest signal intensity there, visualized by its YFP-fluorescence. Contradictorily, the aS310p/S311p antibody merely generated cytosolic signal, which was hardly distinguishable from background signal (Figure 28 B and C). To enrich YFP-D6PK in BFA compartments and be able to differentiate intracellular specific aS310p/S311p-Cy3 signal from cytosolic background signal, I performed immunostainings on BFA-treated seedlings. I found that the antibody detected intracellular YFP-D6PK in BFA-compartments, demonstrating that S310/S311 phosphorylation occurred *in planta* and could be associated with D6PK internalization (Figure 28 F and G). I could verify the specificity of the cytosolic aS310p/S311p-Cy3 signal and specificity of the enrichment of signal in BFA-compartments in the *d6pk d6pkl1 d6pkl2* background, where I did not find increased aS310p/S311p-Cy3 signal in BFA compartments after treating the seedlings with BFA (Figure 28 D, E, H and I). I further analyzed the overlap of the aS310p/S311p-Cy3 signal and the YFP-D6PK signal by generating co-localization mappings and calculating the Pearson's correlation co-efficient of immunostained seedlings expressing YFP-D6PK after mock and 10 µM BFA-treatment (Figure 28 J). These graphs depicted a stronger signal overlap after BFA-treatments with a correlation coefficient of 0.82 after treatment with BFA compared to a correlation

coefficient of 0.55 before the treatment with BFA (Figure 28 J). I concluded that the antibody was specific for internalized YFP-D6PK and that YFP-D6PK phosphorylated in the S310/S311 site accumulates intracellularly.

When I tested the antibody in immunoblots with recombinantly expressed GST-D6PK, I observed that it strongly detected the phosphorylation-mimicking variant GST-D6PK_SSDD (Figure 28 A). I thus conducted immunostainings on seedlings expressing the phosphorylation-mimicking variant YFP-D6PK_SSDD as a positive control for the antibody function *in vivo*. YFP-D6PK_SSDD was more, but not completely, internalized when compared to wildtype YFP-D6PK, retaining substantial signal at the basal plasma membrane (Figure 20 A). As expected, I found aS310p/S311p-Cy3 signal at the plasma membrane in immunostainings of seedlings expressing YFP-D6PK_SSDD, while it still showed a strong intracellular accumulation (Figure 28 K and L). As before, co-localization was also observed after 10 µM BFA-treatments of seedlings expressing YFP-D6PK_SSDD (Figure 28 M and N). I further visualized the observations made in seedlings expressing the phosphorylation-mimicking variant YFP-D6PK_SSDD in comparison to those expressing the wildtype YFP-D6PK by generating profile plots of a cell each after mock and BFA-treatments as specified (Figure 28 O – R). These clearly showed the absence of aS310p/S311p-Cy3 signal peak at the plasma membrane of mock-treated cells expressing YFP-D6PK, where a maximum of YFP-D6PK signal was observed, and the overlap of aS310p/S311p-Cy3 and YFP-D6PK signal after BFA-treatment (Figure 28 O – P). In contrast, in mock-treated cells expressing YFP-D6PK_SSDD aS310p/S311p-Cy3 signal and YFP-D6PK signal clearly overlapped at the plasma membrane and an overlap of the two signals was also observed after BFA-treatment (Figure 28 Q - R). These results provided evidence that the S310/S311p antibody was specific for the S310/311 phosphorylation *in vivo*. I concluded that YFP-D6PK phosphorylated in S310/311 accumulates intracellularly, in line with the increased internalization of YFP-D6PK_SSDD and the reduced BFA sensitivity observed for YFP-D6PK_SSAA.

3.3.9 D6PK internalization and polarity do not depend on D6PK catalytic activity

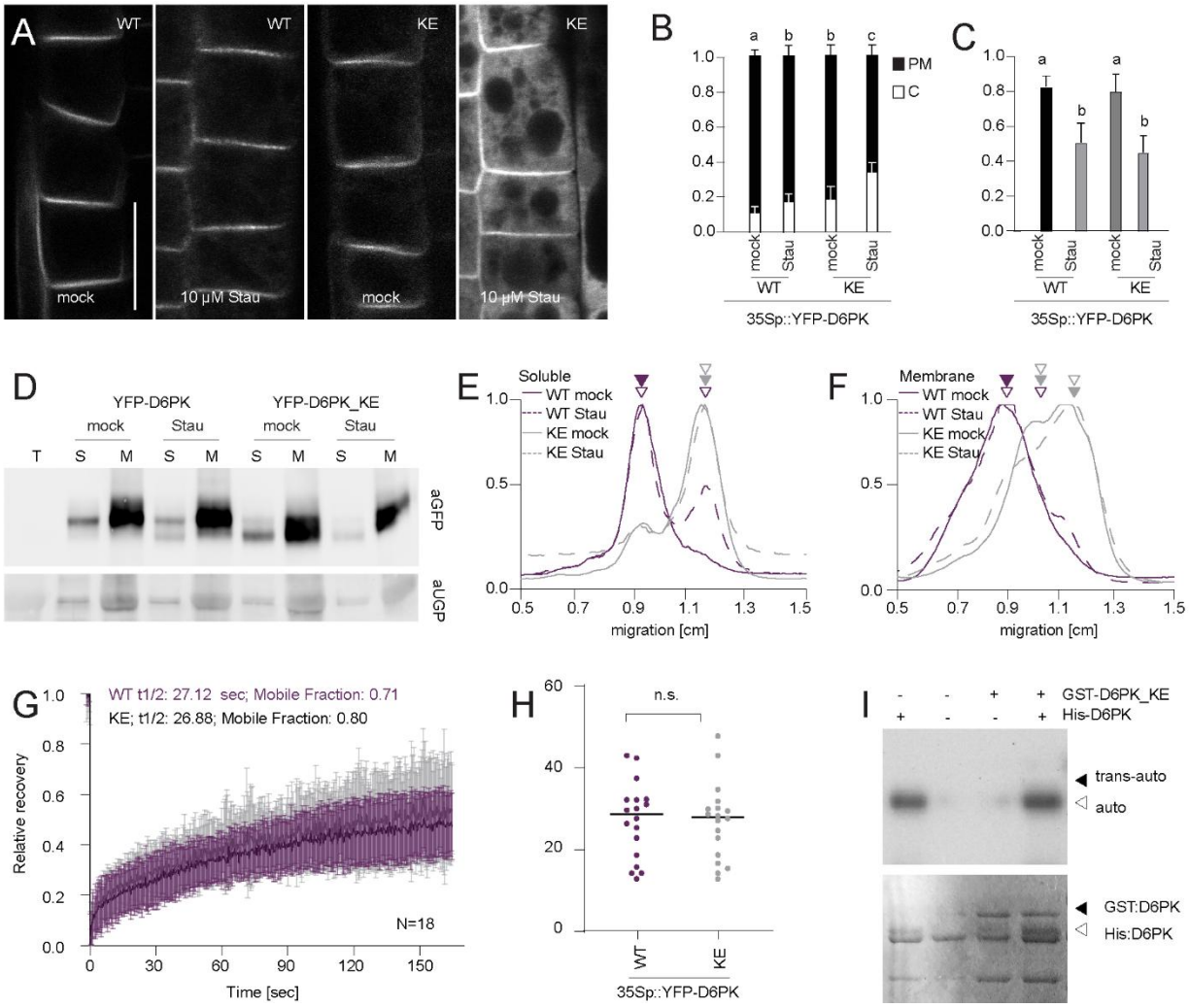

Figure 29. D6PK internalization and polarity do not require D6PK catalytic activity. **A.** Representative confocal microscopy images of root epidermal cells from six-days-old stably transformed *Arabidopsis thaliana* seedlings expressing wildtype YFP-D6PK (A) and the kinase-dead variant YFP-D6PK_KE (B). Scale bar = 20 µm. **B.** and **C.** Bar graphs with mean and standard deviation of cellular cytosolic (C) to plasma membrane (PM) distribution (B) and polarity index (C) quantified in n > 15 cells from at least three seedlings from confocal microscopy images as shown in (A). The statistically significant difference between groups in (B, C) was determined by one-way ANOVA (B, $F(3, 56) = 147.6$, $p < 0.001$; C, $F(3,56) = 69.3$, $p < 0.001$) and means were compared using a Tukey's test. Different letters indicate a statistically significant difference. **D.** Immunoblot of protein extracts from transgenic plants expressing wildtype YFP-D6PK or YFP-D6PK_KE after mock or 10 µM Staurosporine treatment and subcellular fractionation into soluble (S) and membrane (M) fraction. aGFP detects the YFP-tag; aUGP is a control for the soluble fraction. **E.** and **F.** Migration profiles of the soluble (E) and membrane (F) fractions from the immunoblot shown in (D). Arrow heads indicate signal peaks. **G.** and **H.** Results from FRAP experiments performed with epidermal cells of five-days-old seedlings expressing wildtype YFP-D6PK or YFP-D6PK_KE. Shown are normalized recovery curves (G) and mean and individual recovery times t1/2 (H) at the basal plasma membrane for wildtype YFP-D6PK and YFP-D6PK_KE. Recovery times were compared using a Student's t-test: n.s., not significant. **I.** Autoradiography and Coomassie Brilliant Blue-stained (CBB) gel from an *in vitro* kinase assay experiment with recombinantly expressed and purified wildtype His-SUMO-D6PK and the kinase-dead mutant variant GST-D6PK_KE as a substrate.

Following my demonstration that S310/S311 phosphorylation occurs *in planta*, using the aS310p/S311p antibody, I sought to identify which kinase could be responsible for regulating D6PK internalization. In multiple experiments, D6PK showed strong auto-phosphorylation activity *in vitro* (Figure 11 C, Figure 21 C). One hypothesis for the D6PK electrostatic switch mechanism could thus be that D6PK auto-phosphorylates S310/311, hence regulating its own internalization. Consequently, I investigated whether the kinase dead (KE) version of D6PK, where a lysine required for ATP-binding was substituted with glutamate, was impaired in polar localization and sensitive to treatments with the kinase inhibitor Staurosporine. I could confirm, as previously observed, that YFP-D6PK_KE was polarly localized at the basal plasma membrane like wildtype YFP-D6PK (Figure 29 A – C)(Barbosa et al., 2014). This basal polarity was reduced upon treatments with Staurosporine, consistent with the findings for wildtype YFP-D6PK (Figure 29 B – D). Notably, YFP-D6PK_KE showed increased cytosolic abundance compared to wildtype YFP-D6PK, which was further enhanced when roots were treated with Staurosporine (Figure 29 B and C). I concluded that D6PK internalization was most likely not promoted by auto-phosphorylation since YFP-D6PK_KE was polarly localized at the basal plasma membrane and its localization was still sensitive to the kinase inhibitor Staurosporine.

To elucidate the effect of Staurosporine on wildtype YFP-D6PK and YFP-D6PK_KE, I isolated protein from four-days-old seedlings, performed subcellular fractionations, and compared the migration behavior on an immunoblot. Immunoblot analysis revealed a faster migration and indicated a differential phosphorylation of YFP-D6PK_KE when compared to the wildtype YFP-D6PK in the soluble and in the membrane fraction (Figure 29 D - F). YFP-D6PK_KE migration in the soluble fraction resembled the wildtype after Staurosporine treatment. YFP-D6PK_KE also migrated faster in the membrane fraction compared to wildtype YFP-D6PK. Nonetheless, I could not conclude whether these differences in migration between wildtype YFP-D6PK and YFP-D6PK_KE were unequivocally due to differences in phosphorylation.

To further analyze YFP-D6PK_KE cellular dynamics, I performed FRAP experiments at the basal plasma membrane. The recovery time and mobile fraction of YFP-D6PK_KE resembled wildtype YFP-D6PK (Figure 29 G and H). I concluded that D6PK internalization was not, or not only, mediated by an autoregulatory mechanism, but that other kinases likely phosphorylated D6PK in the middle domain and promoted its release from the

plasma membrane. This hypothesis was further supported by *in vitro* kinase assays in which I found that His-SUMO-D6PK, although exhibiting strong auto-phosphorylation activity, could not directly trans-phosphorylate GST-D6PK_KE (Figure 29 I).

3.4.7 D6PK catalytic activity is neither required nor sufficient for D6PK polarity control

I demonstrated that YFP-D6PK_KE still showed comparable mobility to wildtype YFP-D6PK and that its localization was still sensitive to the kinase inhibitor Staurosporine (Figure 29 A - C). I concluded that D6PK kinase activity is not required for its own polarity maintenance. Nevertheless, I could not dismiss the possibility that D6PK catalytic activity may be sufficient to promote its own release from the plasma membrane, ensuring its polarity maintenance. To test whether D6PK catalytic can promote D6PK internalization in absence of other active AGC1 kinases, my colleague Lanassa Bassukas generated lines expressing wildtype YFP-D6PK and a constitutively activated variant YFP-D6PK_SMD in the *pdk1 pdk2* background. The AGC1 kinases D6PK and PAX are downstream targets of the AGC kinase PDK1 and require an activating phosphorylation in their activation loop by PDK1 (Tan et al., 2020; Xiao & Offringa, 2020). YFP-D6PK_SMD carries a mutation in its activation loop mimicking the PDK1 phosphorylation, hence complementing D6PK-dependent phenotypes in the *pdk1 pdk2* background (Tan et al., 2020). We conducted BFA treatments on YFP-D6PK and YFP-D6PK_SMD expressed in the *pdk1 pdk2* background to investigate their trafficking behavior. We quantified the effect of BFA on YFP-D6PK and YFP-D6PK_SMD in the *pdk1 pdk2* mutant background by measuring the signal found in the cytosol and at the plasma membrane and evaluated the results compared to the effect of BFA-treatments on YFP-D6PK in the *d6pk d6pkl1* background. YFP-D6PK exhibited reduced sensitivity to BFA-treatments when expressed in the *pdk1 pdk2* background compared to YFP-D6PK expressed in the *d6pk d6pkl1* background (Figure 30 A - D). Notably, YFP-D6PK_SMD expressed in the *pdk1 pdk2* background also demonstrated a reduced sensitivity to treatments with BFA, resembling wildtype YFP-D6PK (Figure 30 A - D). The behavior of the kinase-dead variant YFP-D6PK_KE was equivalent to that of wildtype YFP-D6PK. We concluded that D6PK trafficking, and consequently polarity maintenance, depends on PDK1 which directly or indirectly promotes D6PK phosphorylation and subsequent release from the plasma

membrane. Accordingly, D6PK catalytic activity is neither required nor sufficient for its trafficking and polarity maintenance.

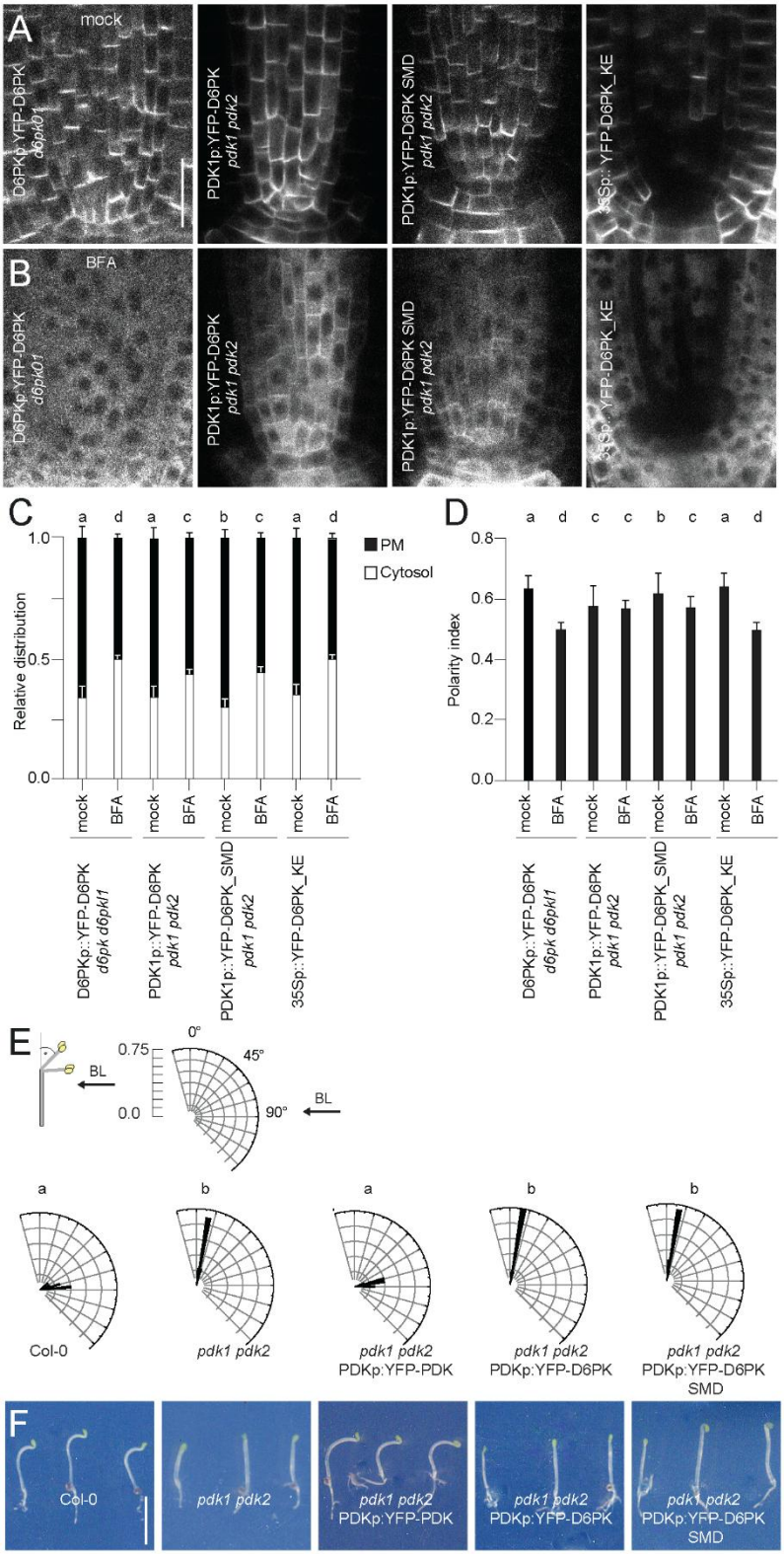

Figure 30. YFP-D6PK is not properly internalized and trafficked in the *pdk1 pdk2* mutant. A. and **B**. Representative confocal microscopy images of the stele of five-days-old *Arabidopsis thaliana* seedlings expressing YFP-D6PK, YFP-D6PK_SMD or YFP-D6PK_KE in the indicated genetic backgrounds under mock conditions (A) and after a 15 min 50 µM BFA treatment (B) (Experiment performed by Lanassa Bassukas). Scale bar = 20 µm. **C** and **D.** Bar chart with the mean and standard deviations of quantifications of YFP-D6PK cellular (C) and polar (D) distribution as determined from confocal microscopy images of 15 cells from at least three seedlings as shown in (A) and (B). The statistically significant difference was determined by One-way ANOVA and means were compared using a Tukey's test (C, $F(7, 112) = 90.88$, $p < 0.001$; D, $F(7, 112) = 51.70$, $p < 0.001$). Different letters indicate a statistically significant difference. **E.** Rose diagrams with the frequency distribution in 5° intervals of > 10 hypocotyl bending angles of three-days-old dark grown seedlings as specified after unilateral blue light (BL) exposure for four hours. The arrow indicates the direction of the BL exposure. **F.** Images of three representative seedlings from the experiment analyzed in (E). Scale bar = 0.5 cm. The statistically significant difference was determined by One-way ANOVA and means were compared using a Tukey's test ($F(4, 39) = 279.5$, $p < 0.001$). Different letters indicate a statistically significant difference.

Previous studies indicated that *pdk1 pdk2* mutant is impaired in phototropic bending, resembling *d6pk d6pkl1* (Tan et al., 2020). I could validate this phenotype in my phototropism assays. The phototropism defect in *pdk1 pdk2* was complemented by the introduction of YFP-PDK1 expressed under a *PDK1* promoter fragment (Figure 30 E-F). However, neither YFP-D6PK nor YFP-D6PK_SMD expressed under a *PDK1* promoter fragment in the *pdk1 pdk2* mutant background, rescued the phototropism defect of the *pdk1 pdk2* mutant, indicating that mimicking the activation loop phosphorylation was not sufficient to fully restore D6PK biological function which was in line with the observed trafficking defects.

To visualize D6PK phosphorylation in the *pdk1 pdk2* background, I performed immunostainings with the aS310p/S311p antibody on wildtype YFP-D6PK expressed in the *pdk1 pdk2* background in mock treated seedlings and after BFA treatment. I could not detect any accumulation of aS310p/S311p-Cy3 signal in BFA compartments when YFP-D6PK was expressed in the *pdk1 pdk2* background (Figure 31 C and D). In *pdk1 pdk2* complemented with YFP-PDK1 which was used as a control I detected aS310p/S311p-Cy3 signal in BFA compartments (Figure 31 A and B). These results were in line with the reduced sensitivity of YFP-D6PK to BFA when expressed in the *pdk1 pdk2* background, observed in the previous experiments.

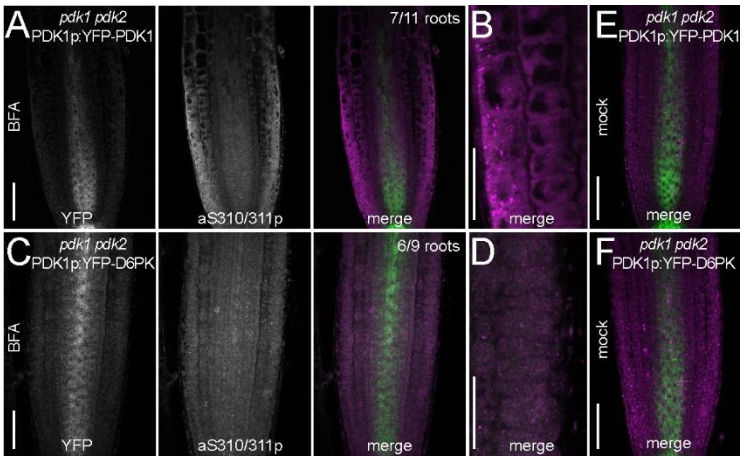

Figure 31. Immunostaining in *pdk1 pdk2* mutants reveals D6PK S310/S311 phosphorylation after BFA treatment. A - D. Representative images (A, C) and magnifications (B, D) of roots from four-days-old seedlings after immunostaining showing aS310p/S311p-Cy3 signal and YFP-PDK1 (A,B) or YFP-D6PK (C,D) after BFA treatment. **E.** and **F.** Roots from four-days-old seedlings after immunostaining with the aS310/S311 antibody and YFP fluorescence from YFP-PDK1 after mock treatment as a control. Scale bars = 50 µm (A, C, E, F) and 20 µm (B, D).

In addition to its failure to exhibit phototropic bending, *pdk1 pdk2* was found to be impaired in apical hook formation, therefore resembling *d6pk d6pkl1* (Tan et al., 2020; Willige et al., 2013). In disagreement with its failure to rescue the phototropism defect, the expression of YFP-D6PK_SMD under a *PDK1* promoter fragment in the *pdk1 pdk2* background

rescued the apical hook formation of *pdk1 pdk2*, indicating that the activation loop phosphorylation is sufficient to restore D6PK kinase activity in the *pdk1 pdk2* background, while seedlings expressing wildtype YFP-D6PK under a *PDK1* promoter fragment did not show formation of an apical hook (Figure 32 A). The auxin transport assays showed that auxin transport in *pdk1 pdk2* was significantly reduced when compared to the Col-0 wildtype. The introduction of YFP-PDK1 expressed under the *PDK1* promoter rescued the auxin transport defect of the *pdk1 pdk2* mutant to wildtype levels (Figure 32 B). YFP-D6PK_SMD could partially complement the *pdk1 pdk2* mutant, and I observed increased auxin transport when compared to *pdk1 pdk2 (*Figure 32 B*)*. Auxin transport was, however, reduced in comparison to the Col-0 wildtype and to seedlings complemented with YFP-PDK1. YFP-D6PK expressed from a *PDK1* promoter fragment did not rescue the reduced auxin transport observed in the *pdk1 pdk2* mutant (Figure 32 B). These findings were in line with the previously observed apical hook phenotypes. I concluded that YFP-D6PK_SMD was catalytically active in *pdk1 pdk2* and was, at least partially, able to activate polar auxin transport. Given that the phosphorylation-mimicking YFP-D6PK_SMD was impaired in trafficking in *pdk1 pdk2* and was deficient in phototropic bending, but partially rescued apical hook formation and auxin transport, we reasoned that PDK1 serves two distinct functions: activating D6PK to phosphorylate the PINs for auxin transport and regulating D6PK trafficking.

Figure 32. Apical hook formation and auxin transport is defective in *pdk1 pdk2* mutants and YFP-D6PK_SMD restores apical hook formation and partially auxin transport. A. *pdk1 pdk2* double mutants show defects in apical hook formation. Representative images of apical hook formation of three-days-old dark grown seedlings showing the Columbia wildtype (Col-0), the *pdk1 pdk2* double mutant and YFP-PDK1, YFP-D6PK and YFP-D6PK_SMD expressed as YFP-tagged proteins under a *PDK1* promoter fragment in the *pdk1 pdk2* double mutant background. Scale bar = 0.5 mm. **B.** Results from hypocotyl basipetal auxin transport assays with four-days-old dark grown seedlings after transported auxin for four hours. Each data point represents a measurement consisting of 5 individual seedlings with the genotypes indicated. The statistically significant difference between groups was determined by One-way ANOVA ($F(4, 17) = 9.344$, $p = 0.0003$) and means were compared using a Tukey's test. Different letters indicate a statistically significant difference.

In the third and last part of my thesis, I described the role of the serines S310/S311 preceding the polybasic K/R-rich motif for D6PK trafficking. I found that phosphorylation of the serines S310/S311, and potentially further phosphorylation sites, is required for D6PK release from the plasma membrane and that phosphorylated D6PK accumulates intracellularly. I discovered that this phosphorylation-dependent localization control directly or indirectly depends on the upstream kinase PDK1, suggesting a new role of PDK1 beyond catalytically activating D6PK and other AGC1 kinases.

4 Discussion

4.1 An expanded model for D6PK membrane association and polarity regulation

Auxin is involved in virtually all aspects of plant development. Its gradient formation with local and global maxima and minima plays a key role in polar growth processes. Hence, many efforts were invested by various research groups to understand all aspects of the underlying biology in more depth by studying auxin biosynthesis, signaling and transport. Many groups interested in understanding auxin transport on a molecular level focused on studying cell biology, activity and structure of the PINs as they transport auxin and show a peculiar polar localization in many cells, which is sufficient to explain auxin gradient formation in computer models (Grieneisen et al., 2007). However, it has become evident in the past years that kinases phosphorylating the PINs play crucial roles for their regulation (Dory et al., 2018; Marhava et al., 2018; Zourelidou et al., 2014; Dhonukshe et al., 2010; Zourelidou et al., 2009; Friml et al., 2004). Our group first characterized D6PK to be a polar protein kinase that strongly associates with the basal plasma membrane of cells where it phosphorylates PINs and promotes auxin efflux from the cell (Zourelidou et al., 2014; Zourelidou et al., 2009). Moreover, D6PK demonstrates fast and GNOM-dependent cycling to and from the plasma membrane. This observation makes it intriguing to believe that D6PK could be a molecular switch for polar auxin transport (Barbosa et al., 2014). We previously published a model in which D6PK membrane association is governed by electrostatic forces mediated by a polybasic K/R-rich motif, found in the middle domain of almost all AGC1 kinases (Barbosa et al., 2016). The questions that motivated my research were whether there are further motifs in the middle domain responsible for maintaining D6PK polar localization and how D6PK fast cycling to and from the plasma membrane can be reconciled with its strong plasma membrane association.

The first objective was to address these questions by resolving the crystal structure of D6PK to achieve a structural resolution of the middle domain and possibly enhance comprehension of the middle domain function *in vivo*. Much knowledge on regulation of mammalian kinases was derived from structural and *in vitro* data. Notably, the full

activation mechanism of the protein kinase Akt was, after decades of intensive research on this kinase, uncovered by combined use of protein semi-synthesis for crystallographic and cell biological analysis (Chu et al., 2018). The use of protein semi-synthesis allowed to generate site-specifically phosphorylated forms of Akt1 leading to the finding that C-terminal phosphorylations in Akt can operate independently of the N-lobe of the kinase domain to activate kinase activity (Chu et al., 2018). To this date structural data is lacking to perform such in-depth analyses on the regulation of *Arabidopsis thaliana* AGC1 kinases. Although the *Arabidopsis thaliana* AGCVIII kinases are highly comparable to the mammalian kinases in terms of kinase domains and activity regulation by the upstream kinase PDK1, most of the regulatory domains found in mammalian kinases are not present in the plant AGCVIII kinases (Bassukas et al., 2022; Rademacher & Offringa, 2012; Galván-Ampudia & Offringa, 2007). A better structural resolution of the *Arabidopsis thaliana* AGCVIII kinases could increase understanding of their regulation on the molecular level and help phrasing and testing new hypotheses. For this reason, I developed an optimized purification procedure allowing me to purify recombinant D6PK in higher quantities and to higher purity than before when expressed from *E. coli*. Although the crystallization of D6PK was ultimately not successful, these efforts were still insightful as the gel filtration chromatography helped to identify D6PK as mostly globular and monomeric when expressed and purified from *E. coli*. The established protocols could prove to be beneficial in the future for structural characterization of D6PK or other AGC1 kinases and to expand the knowledge on their regulation in the cell.

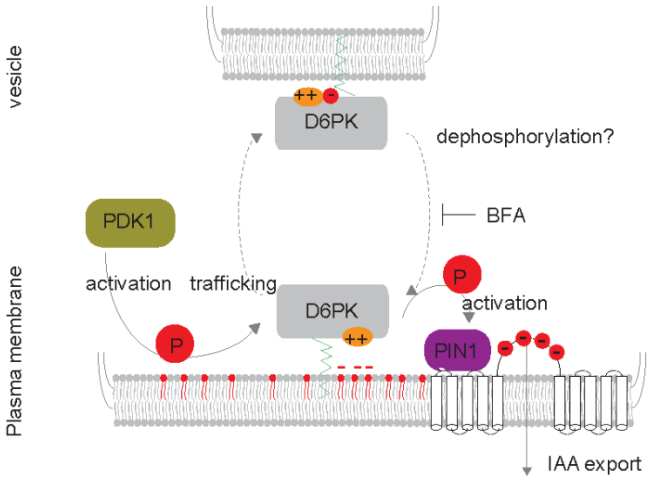

Figure 33. Model of D6PK membrane association and trafficking. The working model at the start of this thesis and presented in the Introduction was expanded by a strong anchoring of D6PK to the plasma membrane depending on S-acylations. D6PK dissociates from the plasma membrane driven by a PDK1-dependent phosphorylation at serines S310/S311 preceding the polybasic K/R-rich motif, leading to the release of D6PK from the basal plasma membrane and localization at internal membranes. At these internal membranes D6PK may be dephosphorylated and trafficked back to the basal plasma membrane.

Since the structural approach was not fruitful in bringing new mechanistic insights to the D6PK middle domain function, a functional approach ultimately enabled me to expand on

the previously established model of D6PK polar localization. I achieved this by examining S-acylations in the CXX(X)P-motifs and phosphorylation at the serines S310/S311, which precede the polybasic K/R-rich motif (Figure 33). The motifs for both modifications are located in the middle domain of D6PK and the responsible motifs were previously identified in sequence alignments of AGCVIII kinases (Bassukas et al., 2022; Day et al., 2000). I further refined these alignments and included AGCVIII kinases from other species in the alignments to help understand the origin and evolution of these motifs. To understand the role of the identified motifs, I analyzed D6PK carrying mutations in the respective motifs *in vitro* and *in vivo* using different physiological, cell biological and biochemical assays. I found out that plasma membrane association is established trough electrostatic interactions by the polybasic K/R-rich motif, whereas S-acylations contribute to anchor D6PK to the basal plasma membrane. PDK1-dependent phosphorylation at the serines S310/S311 is required for dissociation from the plasma membrane leading to localization with internal membranes and this electrostatic switch mechanism is required for maintenance of D6PK polar localization. At internal membranes, a dephosphorylation of D6PK likely takes place and D6PK is trafficked back to the basal plasma membrane GNOM-dependently (Figure 33). Taken together, the studied CXX(X)P motifs and phosphorylations in the middle domain provide a mechanism for basal plasma membrane association, membrane-anchoring and rapid D6PK internalization. My additions to the previously established model of D6PK plasma membrane association explain and reconcile the strong membrane association of D6PK with the fast trafficking to and from the basal plasma membrane. Moreover, the CXX(X)P motifs and the serines preceding the polybasic K/R-rich motif may be significant for comprehending the localization and trafficking of other AGCVIII kinases. I will elaborate on the contribution of the mentioned middle domain elements for D6PK localization throughout the subsequent sections.

4.2 The role of the composition of the polybasic K/R-rich motif

Inês Barbosa in our group characterized the role of the polybasic K/R-rich motif for D6PK localization. She demonstrated that membrane lipid composition and the polybasic K/R-rich motif determine plasma membrane localization of D6PK. She showed that the function of the polybasic K/R-rich motif is conserved in other *Arabidopsis thaliana* AGC1 kinases (Barbosa et al., 2016). Interestingly, I could see in my alignments that the

polybasic K/R-rich motif is present in the middle domains of AGCVIII subfamily kinases from other species. Thereby suggesting that its role may be conserved across species.

I provided one indication for a conserved role of the polybasic K/R-rich motif for membrane association in this thesis by testing the lipid binding properties of AGC1 kinase orthologues from Marchantia polymorpha – Mapoly0030s0017 (Mp17), Mapoly0008s0088 (Mp88) and Mapoly0060s0068 (Mp68) – using PIP-strips. Utilizing PIP-strips, I discovered that the resemblance of the lipid binding profile of the *Marchantia polymorpha* AGC1 orthologues compared to the lipid binding profile of D6PK correlates with the similarity of their middle domain composition. This supports the idea that the polybasic K/R-rich motifs play a key role for membrane lipid affinity depending on their electropositive potential. Therefore, their composition may account for differences in localization of different AGC1 kinases. These findings, along with prior research from our group, also indicated that a the neutralization of positive charges could be a plausible mechanism for membrane dissociation of D6PK by affecting the affinity to plasma membrane lipids (Bassukas et al., 2022; Barbosa et al., 2016).

Prior research has shown that that polybasic motifs are often required to mediate membrane association of peripheral membrane proteins via protein-lipid interactions, and that they can be sufficient for membrane association as well as for determining a protein's specificity for localization to specific membranes based on charge and composition (Li et al., 2014; Jaillais et al., 2011; Heo et al., 2006). This specific localization arises from the unique code of anionic phospholipids present in membranes, defining membrane and organelle identity. This distribution has been thoroughly characterized for mammals and plants (Platre et al., 2018; Bigay & Antonny, 2012). Notably, the low abundant phosphoinositides play a key role for the recruitment of peripheral membrane proteins, hence facilitating their polar localization (Barbosa et al., 2016; Balla, 2013). We therefore concluded in the past that the interaction between the polybasic K/R-rich motif and anionic lipids in the plasma membrane is required for the strong association of D6PK with the plasma membrane, and may also promote its polar localization (Barbosa et al., 2016). However, increasing evidence suggests that avidity generated by multivalent protein-lipid interactions is crucial for determining protein specificity for a particular membrane environment, rather than the affinity of a single component (Zhou et al., 2021; Meca et al., 2019; Zhou & Hancock, 2018). While polybasic motifs can efficiently promote membrane

association, peripheral membrane proteins frequently apply a combination of weak binding motifs to enable polar localization and spatio-temporal regulation of membrane association and dissociation (Zhou et al., 2021; Zhou & Hancock, 2018; Ahearn et al., 2012). The polybasic K/R-rich motif found in the middle domain of D6PK and many other AGC1 kinases likely serves to establish specificity of membrane localization based on the surface charge in an initial step, while the exact localization and strong anchoring is facilitated by the presence of S-acylations in the CXX(X)P motifs further refining the localization within the lipid environment.

4.3 S-acylations anchor D6PK to the plasma membrane

Polybasic motifs that drive association with membranes often occur in combination with covalent lipid modifications such as S-acylation or N-myristoylation, which can function as membrane anchors for peripheral membrane proteins by increasing hydrophobicity (Zhou et al., 2021; Zhou & Hancock, 2018; Resh, 2013; Ahearn et al., 2012; Farazi et al., 2001). S-acylation, among the identified protein lipid modifications, is recognized as a covalent reversible lipid modification due to the instability of the thioester bond, thus potentially providing a dynamic mechanism for regulating protein localization in a spatio-temporal manner (Won et al., 2018; Aicart-Ramos et al., 2011). Protein S-acylation, owing to its reversibility, has garnered significant interest as a protein modification, with numerous studies demonstrating its extensive effects on protein function through altering protein localization, trafficking, structure, stability or activity (Aicart-Ramos et al., 2011; Tulloch et al., 2011; Linder & Deschenes, 2007).

In my thesis I show that S-acylations in middle domain CXX(X)P motifs contribute to D6PK plasma membrane association, mediated by the polybasic K/R-rich motif. I excluded the possibility that the CXX(X)P motif cysteine residues are involved in disulfide bond formation or metal ion complexation and ultimately described D6PK to be S-acylated inside and outside of the middle domain *in vivo*. This conclusion is supported by biochemical assays and cell biological experiments. Mutation of the CXX(X)P motif cysteines residues, but not the proline residues, or acylation inhibition with 2-BP equally resulted in reduced plasma membrane localization and an increased abundance of cytosolic and soluble protein at the expense of plasma membrane localized D6PK. I could show that the GNOM-dependent trafficking was not affected in the CXX(X)P mutant

variant YFP-D6PK_C1-5S, indicating that S-acylation is required for membrane-anchoring rather than trafficking of D6PK. The importance of the CXX(X)P motifs for plasma membrane association and biological function was reinforced by physiological assays, where YFP-D6PK_C4S, YFP-D6PK_C5S and YFP-D6PK_C1-5S failed to complement the *d6pk d6pkl1* defect in phototropic hypocotyl bending. Due to their reduced plasma membrane localization, the cysteine mutants may phosphorylate their substrates, the PINs, less efficiently at the basal plasma membrane. This falls in line with our previous analysis of the polybasic K/R-rich motif, which we demonstrated to be required for D6PK plasma membrane localization and proper PIN phosphorylation (Barbosa et al., 2016). These results suggested that electrostatic interactions with the plasma membrane, mediated by the polybasic K/R-rich motif, and membrane-anchoring, mediated by the S-acylations, are both required for polar plasma membrane association and consequently kinase function. While this work was in progress, a recent proteomic screen disclosed the extent of S-acylation in *Arabidopsis thaliana* (Kumar et al., 2022). Some AGC1 kinases were also predicted to be S-acylated in that screen. Specifically, the D6PK middle domain CXX(X)P motifs were found to be S-acylated, supporting my findings presented in this thesis (Kumar et al., 2022).

S-acylations play an important role in the localization of peripheral and integral membrane proteins, and are particularly interesting due to the reversibility of the hydrophobic modification, enabling their involvement in dynamic processes, which is commonly observed in signaling proteins (Won et al., 2018; Ahearn et al., 2012; Aicart-Ramos et al., 2011). The process of S-acylation addition and removal can serve as a molecular mechanism for membrane-associated proteins to cycle to and from the plasma membrane and engage in trafficking processes. Probably the most notable example for a dynamic S-acylation mechanism are the guanosine triphosphate (GTP) binding proteins Hras and Nras (Aicart-Ramos et al., 2011; Ashery et al., 2006; Rocks et al., 2005). Differential S-acylations drive the compartmentalization of Hras and Nras at the Golgi apparatus and the plasma membrane, thereby preventing nonspecific binding to other endomembranes and maintaining proper signaling responses (Rocks et al., 2005). To this date, the understanding of plant S-acylation dynamics and mechanisms *in planta* lag after the progresses studying the role of this modification in the mammalian field and primarily relies on phenotypic, rather than mechanistic observations (Hemsley, 2020). However, proteins

that undergo cycles of S-acylation and de-S-acylation have been characterized *in planta*, exemplified by the lipid-anchored NAC transcription factor in *Medicago falcata* (MfNACsa). MfNACsa is translocated to the nucleus upon hydrolysis of the S-acylation by the thioesterase MfAPT1 under drought stress, providing evidence, that dynamic S-acylations can also contribute to signal transduction *in planta* (Duan et al., 2017). Notably, thioesterases promoting the hydrolysis of the thioester bond of the attached fatty acid remained uncharacterized in *Arabidopsis thaliana* for a long time, although evidence for dynamic S-acylation cycles existed. A family of ABAPT family proteins was recently characterized based on their de-S-acylation activity (Liu et al., 2021). Curiously, none of the characterized proteins demonstrating thioesterase activity, neither MfAPT1 nor the ABAPT family proteins, were found to be homologues or exhibit high sequence similarity to the mammalian APT1 and APT2, suggesting that the mechanisms for the hydrolysis of the thioester bond diverge between plant and mammalian cells (Liu et al., 2021; Hemsley, 2020). Given our observation of D6PK as a rapidly cycling protein and my interest in how its fast cycling could be reconciled with its strong membrane association, I investigated the hypothesis that reversible S-acylations promote D6PK membrane association and dissociation. I could not observe any difference between the S-acylation level in internalized D6PK after BFA-treatment and the untreated membrane-localized D6PK. Therefore, I conclude that the rapid cycling to and from the plasma membrane is not driven by dynamic S-acylation cycles. This conclusion is further supported by the observation that treatments with the S-acylation inhibitor 2-BP require relatively long treatment times of one to two hours to show an effect on D6PK cellular distribution and by the reduction in sensitivity of YFP-D6PK to 2-BP when co-treated with the protein biosynthesis inhibitor CHX. This indicates that primarily newly synthesized protein is S-acylated and thus affected by 2-BP treatments. S-acylations in D6PK are a stable modification and do not undergo fast dynamics that would be consistent with D6PK rapid trafficking to and from the plasma membrane. My data suggest that S-acylations are not involved in D6PK trafficking but serve as a plasma membrane anchor.

Not all S-acylated proteins undergo dynamic cycles of lipid modification. Besides its potential effects on protein trafficking, protein S-acylation can also have an impact on protein localization by promoting protein association with specific membrane microdomains (Noack et al., 2022; Turnbull & Hemsley, 2017; Levental et al., 2010). I did

not test in my thesis if D6PK S-acylation may influence its affinity for specific membrane environments or membrane microdomains, although I repeatedly observed a reduction in polar plasma membrane localization and an increased lateral localization for YFP-D6PK_C5S, and of wildtype YFP-D6PK when treated with low concentrations of 2-BP. Examples of proteins restricted to specific membrane environments based on their S-acylation status have also been described *in planta,* exemplified by the the Rho-related GTPase ROP6, the receptor-like cytosolic kinase SGN1, and EFR3-OF-PLANTS (EFOP) (Noack et al., 2022; Alassimone et al., 2016; Sorek et al., 2010; Lavy & Yalovsky, 2006). Interestingly, in EFOP, the S-acylation site is located closely to a polybasic motif, comparable to D6PK. EFOP localizes in stable nanodomains within a protein complex, responsible for recruitment of the phosphatidylinositol 4-kinase alpha (PI4Kα1) to these nanodomains (Noack et al., 2022). I found indications for D6PK localizing in detergent resistant membranes (DRMs) as analyzed by solubilization experiments with Triton-X-100. Additionally, I often observed D6PK in dot-like structures at the plasma membrane rather than a continuous signal at the plasma membrane which could be another indication. DRMs are commonly referred to as lipid rafts and are insensitive to mild detergents such as Triton-X-100 due to a tight packing with cholesterol and sphingolipids (Brown & London, 1998; Simons & Ikonen, 1997). However, I did not address this observation and its potential functional consequences in my thesis. The localization in membrane microdomains and potential effect on D6PK activity at the plasma membrane could be studied by microscopic techniques, for example using total internal reflection fluorescence (TIRF) microscopy.

A number of studies indicate that protein S-acylation can directly or indirectly affect protein conformation, resulting from the incorporation of a large hydrophobic moiety and its potential steric influences (Cassinelli et al., 2022; Abrami et al., 2008). In my experiments with D6PK expressed *in planta*, I observed significant variations in SDS-PAGE migration behavior among different D6PK variants, particularly in the CXX(X)P-mutants YFP-D6PK_C4S and YFP-D6PK_C5S compared to the wildtype YFP-D6PK and when YFP-D6PK was treated with 2-BP. Interestingly, the effect on D6PK SDS-PAGE migration of the introduced mutations in the CXX(X)P motifs seemed to be plant specific and was not found in protein recombinantly expressed in *E. coli.* These shifts could be caused by the difference in molecular weight due to the loss of the S-acylation or a different migration

behavior due to a structural change induced by the S-acylations. Therefore, the S-acylations in the CXX(X)P repeats could also play a structural role to mediate D6PK membrane association. The occurrence of proline, typically succeeding cysteine in the CXX(X)P repeats, renders this model appealing for D6PK, as prolines affect the backbone properties of proteins due to the pyrrolidine ring. I demonstrate in my thesis that the proline residue of the CXX(X)P5 motif in contrast to the cysteine residue is not required for D6PK membrane association in *Arabidopsis thaliana* protoplasts, making it unlikely that the proline residues play a direct role for the membrane anchoring. Unfortunately, I was not successful in achieving a structural resolution of D6PK, which would have given more insight into the structure of the middle domain. The structure of the middle domain associated with the plasma membrane and potential further roles of the S-acylations remain to be revealed.

The S-acylation-mediated membrane association may be conserved among the AGC1 kinases. I show in my alignments that the CXX(X)P repeats are present in all AGC1 kinases although the number of repeats differ. For the AGC1 kinases PAX and KIPK, I demonstrate that both kinases are S-acylated *in vivo*, and that the corresponding CXX(X)P4 and the CXX(X)P5 motif are required for plasma membrane association of PAX and KIPK in *Arabidopsis thaliana* protoplasts, indicating that the function of the CXX(X)P motif may be conserved among AGC1 kinases. Interestingly, I did not observe a strong plasma membrane association of KIPK in protoplasts, nevertheless mutagenesis of the corresponding cysteine in the CXX(X)P5 motif led to a complete abolishment of plasma membrane association. KIPK shows strong plasma membrane association *in planta*, in disagreement with the localization I observed in the protoplasts, and its cycling is largely GNOM-independent which may suggest that its localization and trafficking may follow a different mechanism than that of D6PK and other AGC1 kinases (Xiao et al., 2025). KIPK does not contain a strongly pronounced polybasic K/R-rich motif in its middle domain when compared to other AGC1 kinases, but still binds to anionic phospholipids *in vitro*, supporting that its mechanism for membrane association may differ from that of D6PK, but notably, at least in protoplast, still requires the CXX(X)P5 motif (Xiao et al., 2025). Interestingly, the CXX(X)P motifs are not found in the non-polar but plasma membrane localized AGC3 kinases PID which is largely insensitive to treatments with BFA (Figure 3)(Kleine-Vehn et al., 2009). It would be interesting to investigate whether the presence

of the CXX(X)P motifs in the middle domain could explain differences in localization or trafficking between PID and D6PK.

4.4 D6PK trafficking and polar localization require middle domain phosphorylations

The identified S-acylation of D6PK may explain its strong plasma membrane association by serving as a membrane anchor, but not its rapid trafficking between the cytosol and the plasma membrane. Consequently, I continued to investigate the hypothesis that phosphorylation at the serines S310/311 preceding the polybasic K/R-rich motif may serve as electrostatic switch mechanism which releases D6PK from the plasma membrane. We postulated in the past that D6PK may function as a molecular switch for polar auxin transport, requiring a mechanism that regulates its fast internalization. The described PDK1-dependent phosphorylation facilitates rapid internalization, presumably by neutralizing the positive charges of the polybasic K/R-rich motif with the negative charges from the phosphorylations.

In my thesis I demonstrate that D6PK localization *in planta* is dependent on phosphorylation. Inhibiting phosphorylations with drug treatments and mutation of the serine residues S310/S311 equally lead to a reduction in polar localization at the plasma membrane and an increased lateral signal. On the other hand, mimicking the phosphorylation results in increased cytosolic signal, supporting a role of the serines S310/S311 for D6PK localization and polarity maintenance. In line with these findings, I show that D6PK S310/S311 phosphorylation is primarily detected on internalized D6PK accumulated in BFA compartments when inhibiting GNOM-dependent trafficking, suggesting that phosphorylation leads to dissociation from the plasma membrane. Moreover, in absence of the phosphorylation D6PK is less sensitive to treatments with BFA and shows reduced accumulation in BFA compartments, indicating that phosphorylation at the serines S310/S311 is required for D6PK internalization. The phosphorylation-dependent internalization of D6PK fits the previously observed fast dissociation rate of D6PK from the plasma membrane (Barbosa et al., 2014). I validated S311 as a phosphorylation site by mass spectrometry experiments, using GST-D6PK extracted from *E.coli* and identified additional phosphorylation sites in the middle domain. These phosphorylation sites may also be required for D6PK trafficking, as evidenced by

a reduction in polar localization and reduced BFA-sensitivity of the variant YFP-D6PK_ΔSAN, which lacks these phosphorylation sites and shows comparable cell biology to the phosphorylation-mutant YFP-D6PK_SSAA. The hypothesis that additional phosphorylation sites are required for proper internalization of D6PK may also explain that YFP-D6PK repeatedly showed stronger internalization when treated with the phosphorylation inhibitor Calyculin A with around 42% of cytosolic signal than the phosphorylation-mimicking YFP-D6PK_SSDD with around 29% of cytosolic signal. The identification of the respective phosphorylation sites *in planta* using mass spectrometry is constrained by the peculiar localization of the interesting phosphorylation-sites close to the polybasic K/R-rich motif, complicating the extraction, the choice of appropriate proteases and proteomic analysis of the middle domain phosphorylation sites. However, phosphorylation at the equivalent S392/S393 was detected in D6PKL2 extracted from plants in an independent proteomic study (Menz et al., 2016).

The decrease of polar membrane localization in the phosphorylation-mutant YFP-D6PK_SSAA and the increased internalization in the phosphorylation-mimicking YFP-D6PK_SSDD support a phosphorylation-dependent internalization of D6PK. The loss of polar distribution in absence of S310/S311 phosphorylation may result from an enhanced lateral diffusion in the plasma membrane due to a reduced turnover. The FRAP experiments, that I established to investigate D6PK dynamics at the plasma membrane, revealed that YFP-D6PK_SSAA recovers more slowly at the basal plasma membrane in comparison to wildtype YFP-D6PK, hence indicating a reduced turnover of YFP-D6PK_SSAA at the basal plasma membrane. The additional use of a photoconvertible fluorophore such as Eos would have enhanced our understanding of D6PK dynamics at the plasma membrane by enabling differentiation between diffusion within the plasma membrane and trafficking. However, the low fluorescent signal and consequently high photobleaching did not allow for reliable results with this fluorophore in my experiments.

The importance of the S310/S311 phosphorylation for D6PK localization and biological function was reinforced by physiological assays. Both the phosphorylation-mutant YFP-D6PK_SSAA and the phosphorylation-mimicking YFP-D6PK_SSDD failed to complement the *d6pk d6pkl1* defect in phototropic hypocotyl bending. Nonetheless, the expression of YFP-D6PK_SSAA in the *d6pk d6pkl1* background restored auxin transport capacity and apical hook formation in these seedlings, whereas the expression of YFP-D6PK_SSDD

failed to restore basipetal auxin transport and apical hook formation. It is important to note that the apical hook cells of seedlings expressing YFP-D6PK_SSAA were altered in their shape and structure compared to seedlings expressing YFP-D6PK, indicating that YFP-D6PK_SSAA cannot fully restore normal apical hook formation relative to the wildtype. The disparity in the ability to rescue *d6pk d6pkl1* phenotypes between YFP-D6PK_SSAA and YFP-D6PK_SSDD may be attributed to a prolonged residence time of YFP-D6PK_SSAA at the plasma membrane, where D6PK phosphorylates and activates the PINs, in contrast to the more internalized YFP-D6PK_SSDD. The defect in photrotropic hypocotyl bending may be a more direct readout of the quantity of auxin available in the hypocotyl than apical hook formation and maintenance. We previously explained the defect in phototropic bending exhibited by the *d6pk d6pkl1* mutants with a reduced amount of auxin overall available in the hypocotyl and thus a less efficient establishment of asymmetric auxin distribution resulting in reduced gradient strength (Willige et al., 2013). According to this hypothesis, I would expect a good correlation of the ability to rescue the phototropism defect with the conducted auxin transport assays. This was true for all studied YFP-D6PK mutant variants except YFP-D6PK_SSAA. This observation may suggest a more complex picture than previously postulated, in which D6PK not only affects the available amount of auxin in the hypocotyl but also plays a direct role for the directionality of auxin transport in the hypocotyl, as it could be required for phototropic bending.

Phosphorylation-dependent electrostatic switches present an intriguing mechanism for protein localization, since they are essential for internalization and maintenance of polarity in various peripheral membrane proteins (Clarke, 2023; Almagor et al., 2019; Gerganova et al., 2019; Hachet et al., 2011; Maures et al., 2011; McLaughlin & Aderem, 1995). Although mechanistic descriptions of phosphorylation-dependent electrostatic switches in plants are limited, the molecular mechanisms of electrostatic switches are thoroughly elucidated in polar developmental processes requiring fine-tuning of protein gradients in mammals and yeast (Gerganova et al., 2019; Hong, 2018; Martin & Berthelot-Grosjean, 2009). Phosphorylation-dependent electrostatic switch mechanisms facilitate quick responses to signaling cues and are therefore dynamic and in some cases autoregulatory. The protein kinase Pom1 functions as a dose-dependent inhibitor of the entry into mitosis, establishing a protein gradient depending on the degree of its autophosphorylation. This

gradient is achieved by co-localization with the protein phosphatase Dis2 which enhances membrane binding and lateral diffusion, whereas Pom1 autophosphorylation weakens the membrane association (Hachet et al., 2011; Martin & Berthelot-Grosjean, 2009; Moseley et al., 2009). Intriguingly, Pom1 membrane association is mediated by a polybasic motif while dissociation is mediated by phosphorylation in five sites, leading to an additive membrane detachment through the increased negative charge of the phosphorylations – a similar mechanism to the one I suggest for D6PK (Gerganova et al., 2019; Hachet et al., 2011). The phosphorylation-dependent membrane dissociation makes the gradient formation autoregulatory and extremely robust towards changes in protein amount. Additionally, phosphorylation-dependent maintenance of plasma membrane localization and polarity has been described for various proteins downstream of PKC, in conjunction with membrane localization via a polybasic motif (Hong, 2018; Bailey & Prehoda, 2015; Dong et al., 2015; Smith et al., 2007). The aPKC substrates Lgl, Numb and Mir possess essential phosphorylation sites that are located inside their polybasic motifs, resulting in charge neutralization and subsequent loss of plasma membrane association upon phosphorylation (Bailey & Prehoda, 2015; Dong et al., 2015; Smith et al., 2007). These studies show that phosphorylations often act together with polybasic motifs to modulate the plasma membrane localization of proteins. Combinations of electrostatic switch mechanisms and S-acylations have also been evidenced (Charych et al., 2010; Tian et al., 2008). Most notably in BK potassium channels, S-acylation is required for membrane targeting of the C-terminus, while a phosphorylation upstream of the S-acylation site introduces a negative charge in an otherwise basic region resulting in dissociation from the plasma membrane, resembling the mechanism I propose here for D6PK (Tian et al., 2008).

A crosstalk between phosphorylation and S-acylation has been observed for several proteins, where S-acylation may have inhibitory or promoting effects on protein phosphorylation, possibly due to steric effects (Hayashi et al., 2009; Lin et al., 2009). Consistent with a possible crosstalk between D6PK S-acylation and phosphorylation, I observed a reduction of YFP-D6PK polar localization at the plasma membrane when treated with low concentrations of 2-BP, resembling the localization observed for YFP-D6PK_SSAA and YFP-D6PK_ΔSAN. I could not determine unequivocally if this observation resulted from a decrease in phosphorylation or whether it was a secondary

effect of the inhibitor treatment. This observation led me to investigate the hypothetical influence of phosphorylation on D6PK S-acylation. I discovered that YFP-D6PK_SSAA and YFP-D6PK_SSDD remain susceptible to the S-acylation inhibitor 2-BP, suggesting that the phosphorylation in S310/S311 does not influence S-acylation of D6PK. However, I observed that YFP-D6PK_SSDD does not show a reduction in polar localization at the basal plasma membrane when treated with 10 µM 2-BP in contrast to wildtype YFP-D6PK, suggesting that S-acylation may have a promoting effect on middle domain phosphorylation. This observation makes it highly unlikely that the phosphorylation status of D6PK influences its S-acylation. However, S-acylation may promote phosphorylation in the middle domain, possibly by making the serines sterically more accessible, which may account for the diminished polar localization of YFP-D6PK when treated with low concentrations of 2-BP.

Electrostatic switches can lead to internalization or re-localization of proteins within the cell by different mechanisms. One potential outcome is that due to the neutralization of charge or a change in conformation caused by the phosphorylation, the protein is rendered more cytosolic and soluble. Another possibility is that the protein affinity for the plasma membrane decreases due to a reduction in positive charge, which reduces its residence time at the plasma membrane, and it may associate with less electronegative internal membranes. This is possible due to the unique lipid code of many membranes (Clarke, 2023; Platre et al., 2018). Our group showed in the past that D6PK polar localization with the plasma membrane strongly depends on the phospholipid composition of the plasma membrane, making it likely that a change in affinity may affect its localization (Barbosa et al., 2016). I showed that the phosphorylation-mimicking YFP-D6PK_SSDD does not show increased protein abundance in the soluble fraction when performing subcellular fractionations, indicating that YFP-D6PK_SSDD remains associated with internal membranes. Additionally, I still observed YFP-D6PK_SSDD largely associated with the plasma membrane of cells, although it was more cytosolic than wildtype YFP-D6PK. These observations contrast with the observations from the analysis of YFP-D6PK_C1-5S which is deficient in membrane-anchoring and is more cytosolic and more soluble compared to wildtype GST-D6PK. This suggests that YFP-D6PK_SSDD, in contrast to YFP-D6PK_C1-5S, remains attached with internal membranes. Previous experiments demonstrated that mutagenesis of the polybasic K/R-rich motif results in a

complete abolishment of D6PK binding to phosphoinositides (Barbosa et al., 2016). In contrast, the recombinantly expressed phosphorylation-mimicking GST-D6PK_SSDD bound to phosphoinositides in my PIP-strip assays, suggesting that it may also associate with membranes *in vivo*. The protein binding profile on the PIP-strip indicated a different lipid preference of YFP-D6PK_SSDD when compared to the wildtype GST-D6PK, which may be in line with an altered affinity for membrane lipids. These findings support a potential role of S310/S311 phosphorylation for shifting D6PK subcellular localization to endomembranes like vesicles, rather than enhancing its solubility and cytosolic localization.

I never detected phosphorylated D6PK at the plasma membrane with the aS310p/S311p antibody, although YFP-D6PK localizes mainly there, indicating that an active dephosphorylation at endomembranes could be required to initiate D6PK trafficking back to the plasma membrane. The proposed dephosphorylation of D6PK at endomembranes would likely be facilitated by protein phosphatases co-localizing with D6PK. 150 protein phosphatases have been identified in *Arabidopsis thaliana* and are classified depending on their substrate specificity (Bheri et al., 2021). In mammalian cells Calyculin A was shown to be a potent inhibitor of protein phosphatase 1 (PP1) and protein phosphatase 2 A (PP2A) (Bheri et al., 2021; Wang et al., 2007). Analysis of D6PK localization in knockout mutants of these phosphatases could elucidate putative functional interactions. Interestingly, PP2A has been implicated to play a role in auxin transport by regulating PIN trafficking antagonistically to the phosphorylation activity of PID, and could thus be an interesting candidate to study in the context of D6PK polar localization (Michniewicz et al., 2007).

An interesting question is whether phosphorylation-dependent trafficking to and from the plasma membrane is conserved among other AGC1 kinases. Intriguingly, in the tomato AGCVIII kinase AvrPto-DEPENDENT Pto-INTERACTING PROTEIN 3 (ADI3), PDK1-dependent phosphorylation in the activation segment is required to recruit ADI3 to the nucleus upon pathogen attack, suggesting that phosphorylation-dependent internalization may be a conserved mechanism in plant AGC kinases (Ek-Ramos et al., 2010). Within the *Arabidopsis thaliana* AGCVIII subfamily, the serines preceding the polybasic K/R-rich motif can only be found in the AGC1 clade and PID2. It would be interesting to understand whether the phosphorylation-dependent internalization is conserved in these kinases. I

did not test whether other AGC1 kinases are internalized in a phosphorylation-dependent way. When analyzing the middle domains of AGC1 kinases from other species, I noted that the enrichment in serines in the middle domain sequence is conserved among them, but not the exact positioning. Interestingly, I noted that the length of the polybasic K/R-rich motif correlated with an increased number of serines surrounding the polybasic K/R-rich motif, which could be indicative of a conserved electrostatic switch mechanism. It would be interesting to investigate whether electrostatic switch mechanisms are conserved in plant AGC1 kinases and whether their presence may explain differences in trafficking and localization between different kinases.

4.5 D6PK catalytic activity is neither required nor sufficient for its PDK1-dependent release from the plasma membrane

The electrostatic switch mechanism, based on the phosphorylation at the serines S310/311, could be driven by D6PK auto-phosphorylation or trans-phosphorylation by another kinase. Prior studies showed that D6PK catalytic activity is not required for its polar localization at the basal plasma membrane of cells and its GNOM-dependent recycling (Barbosa et al., 2014). I could confirm these findings in my thesis. In FRAP experiments with the inactive YFP-D6PK_KE in root epidermis cells, I demonstrated that YFP-D6PK_KE still shows comparable dynamics at the basal plasma membrane to the wildtype YFP-D6PK. Additionally, its localization remains sensitive to the kinase inhibitor Staurosporine, leading to the conclusion that D6PK kinase activity is not required for D6PK localization and cycling. Based on these experiments, I could however not dismiss the possibility that D6PK kinase activity is sufficient to promote its own internalization via autophosphorylation in absence of other functional AGC kinases.

To assess whether D6PK can promote its own internalization, me and my colleague Lanassa Bassukas examined D6PK internalization in the *pdk1 pdk2* mutant where D6PK cannot be activated by its upstream regulator PDK1, and presumably other AGC kinases activated by PDK1-dependent phosphorylation are also inactive in this mutant. YFP-D6PK exhibits a slower internalization upon BFA treatment in the *pdk1 pdk2* mutant, resembling the phosphorylation-deficient YFP-D6PK_SSAA and YFP-D6PK_ΔSAN. The introduction of the phosphorylation-mimicking mutation in the activation segment, which was previously shown to render D6PK active, was not sufficient to restore normal GNOM-

dependent trafficking for YFP-D6PK_SMD (Tan et al., 2020). Here we demonstrate that D6PK activity is not sufficient to promote its own internalization and that PDK1 or kinases requiring PDK1-dependent activation are required for D6PK internalization. Our results are partially contradictory to previously published findings. D6PK was previously reported to maintain polarity in the *pdk1 pdk2* mutant (Tan et al., 2020). It is important to emphasize however, that this analysis was conducted in epidermis cells where PDK1 is not strongly expressed, while we confined our analysis to the PDK1 expression domain, specifically looking at stele cells. It was also described, that the *pdk1 pdk2* mutants used in that analysis are leaky and a CRISPR-generated mutant shows stronger phenotypes (Xiao & Offringa, 2020). The utilization of the CRISPR-generated *pdk1 pdk2* mutant in our analysis may therefore provide another explanation for the conflicting results.

The *pdk1 pdk2* mutant does not show phototropic hypocotyl bending towards a light source (Tan et al., 2020). I found that this phenotype could be complemented by introducing YFP-PDK1 expressed under a *PDK1* promoter fragment, but not when introducing wildtype YFP-D6PK or YFP-D6PK_SMD expressed under a *PDK1* promoter fragment. Remarkably, YFP-D6PK_SMD could rescue the apical hook phenotype, suggesting that it is catalytically active in the *pdk1 pdk2* background and the observed effects can be contributed to improper cycling and polarity regulation rather than an absence of D6PK catalytic activity. In line with these findings, YFP-D6PK_SMD partially complemented basipetal auxin transport in the *pdk1 pdk2* mutant. Intriguingly, the inability of YFP-D6PK_SMD to rescue the defect in phototropic hypocotyl bending of the *pdk1 pdk2* mutant but partially complementing basipetal auxin transport and apical hook formation, resembled the observations I made for YFP-D6PK_SSAA. This implies that both are catalytically active and plasma membrane localized, but, due to their defects in trafficking and polar localization, this may not be sufficient to complement all associated physiological defects. The results from the analysis of the *pdk1 pdk2* mutants allowed us to extend the proposed model of D6PK localization to include a PDK1-dependent internalization of D6PK. In my mass spectrometric analysis of D6PK phosphorylation, I could not find any direct PDK1 phosphorylation targets apart from the activation segment, indicating that instead of direct phosphorylation and internalization by PDK1, a downstream target of PDK1 may be directly involved in D6PK trafficking. It is particularly intriguing that both D6PK activation and polarity control depend on PDK1 activity.

Previously, no link between PDK1 activity and D6PK trafficking could be established, marking our results as the first indication that PDK1 function *in planta* extends beyond promoting the catalytic activity of D6PK and other AGC kinases, and that activation and polarity control may be coupled.

4.6 Further scope of D6PK polar plasma membrane localization – scaffold proteins and other interactors of AGCVIII kinases

In addition to PDK1, other known interactors of plant AGC kinases include scaffold proteins such as the BRX family. BRX was shown to be an inhibitor of PIN-dependent auxin transport, and can be recruited and regulated by the AGC1 kinase PAX (Marhava et al., 2018). In a collaboration with Christian Hardtke at the University of Lausanne, our group could show that PAX recruits BRX and that its activity is required to release BRX from the plasma membrane in the protophloem to allow for auxin transport to take place in this highly specified tissue (Marhava et al., 2018). We could further show that phosphorylation of BRX by PAX and D6PK mainly takes place in the linker region between the BRX domains and specifically which BRX phosphorylation-sites are mainly targeted by these AGC1 kinases (Figure 34)(Koh et al., 2021). Interestingly, engineering these phosphorylation-sites into the auxin-insensitive BRXL2 led to rendering this protein auxin sensitive and increased its activity in the root protophloem (Koh et al., 2021). These findings implied a role of AGC1 kinases in finetuning polar auxin transport beyond merely phosphorylating and activating the PINs and suggested that a tight control and finetuning of their activity is required in these processes and can be achieved through the presence of additional molecular regulators such as scaffold proteins.

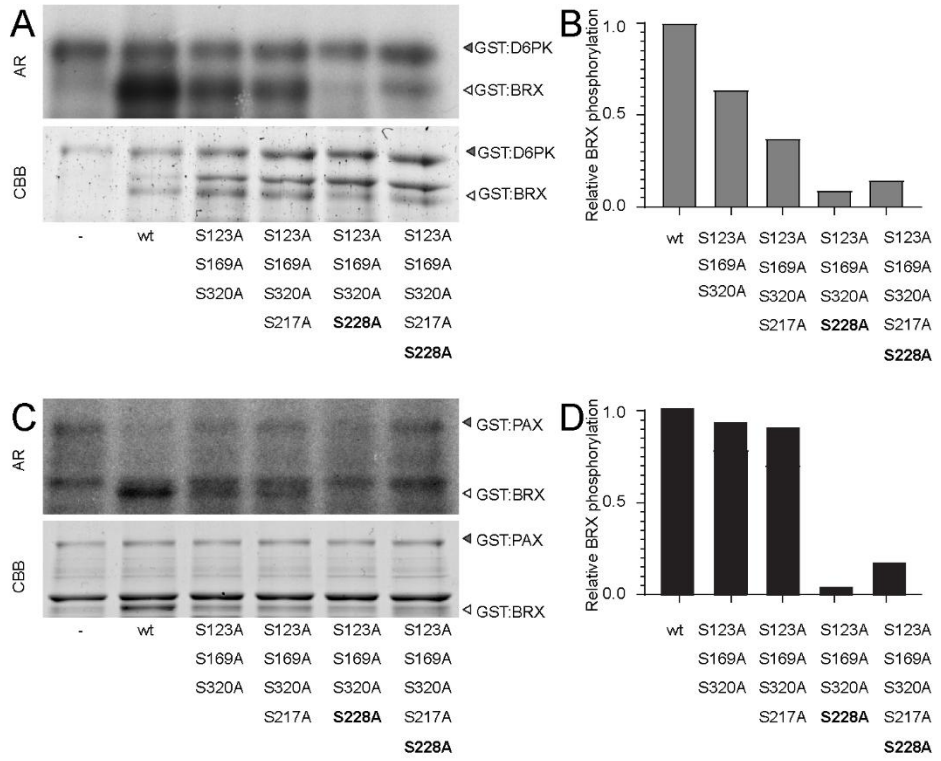

Figure 34. D6PK and PAX phosphorylate the scaffold protein BRX in its linker region. A. and C. Kinase assays of GST-D6PK (A) and GST-PAX (C) using GST-BRX as a substrate and introducing mutations in the BRX phosphorylation sites as published in (Koh et al., 2021). Autoradiography (AR) shows the phosphorylation signal while the Coomassie Brilliant Blue (CBB) stained gel serves as a loading control. B. and D. Quantification of the relative phosphorylation intensity normalized to the intensity in the CBB-stained gel shows that in the case of GST-D6PK (B) and GST-PAX (D) mutation of the S228-site localized in the BRX linker region leads to a strong reduction in trans-phosphorylation activity on GST-BRX.

The biological relevance of the interaction of AGCVIII kinase family members and scaffold proteins was additionally demonstrated in another study revealing how PAX and BRX act together to establish polarity in protophloem differentiation. Together, they recruit phosphatidylinositol-4-phosphate 5 kinases (PIP5Ks) (Marhava et al., 2020). PIP5Ks mediate the production of $PI(4,5)P_2$ from PI4P. $PI(4,5)P_2$ is crucial for many processes taking place at the plasma membrane of *Arabidopsis thaliana*, including the polar plasma membrane association of AGC1 kinases and clathrin-mediated trafficking (Barbosa et al., 2016; Heilmann & Heilmann, 2015; Stanislas et al., 2015; Ischebeck et al., 2013). The recruitment and interaction with PIP5Ks hypothetically reinforce PAX polarity through the phosphoinositide turnover catalyzed by the PIP5Ks. The interaction of PAX, BRX and PIP5K1 and PIP5K2 was detected *in vivo* in immunoprecipitations of BRX-CITRINE or CITRINE-PAX and supported by their co-localization observed *in planta*. In line with these findings, *pipk5k1 pip5k2* mutants show defects in protophloem differentiation that phenotypically reflect the defects found in *brx* and *pax* mutants (Marhava et al., 2020).

We could show in the past that D6PK shows significantly reduced plasma membrane abundance in the *pip5k1 pip5k2* mutant background and inhibitor treatments indicated a strong dependence of D6PK polar plasma membrane association on the membrane phosphoinositide composition (Barbosa et al., 2016). Therefore, PAX activity may additionally have indirect effects for D6PK polar localization – an intriguing indication for a crosstalk between these closely related AGC1 kinases. The example of PAX and PIP5K interaction further shows that studies on the polarity formation and maintenance of the AGCVIII kinases can add further understanding to cellular differentiation and signaling events that require polarity established by phosphoinositide composition and trafficking events and these events may not be directly linked to PIN-dependent polar auxin transport. Thus, further investigations into this interaction may expand our understanding of the AGCVIII kinase family beyond their role in auxin transport.

4.7 Concluding Remarks

The objective of my thesis was to elucidate how the polar plasma membrane association of D6PK is mediated and to investigate the role of the middle domain in this process. During my work for this thesis, I changed my approach from a structural characterization of D6PK to a functional characterization to comprehend the function of the D6PK middle domain for its polar localization. The functional characterization of CXX(X)P motifs and serine phosphorylations in the middle domain allowed me to draft an updated model on D6PK membrane association and polarity control which I presented in this thesis. Using physiological assays, I showed how these mechanisms affect kinase functionality *in planta*. The proposed model for D6PK plasma membrane association mediated by the polybasic K/R-rich motif and the CXX(X)P motifs with D6PK polarity maintained by PDK1-dependent phosphorylation requires a high level of molecular finetuning. Notably, many of the described motifs described here are found in other AGCVIII kinases. The polybasic K/R-rich motif and the CXX(X)P motif are prevalent in most AGC1 kinases, while intriguingly, the CXX(X)P motifs are not found in the AGC3 kinases PID, WAG1 and WAG2. These kinases differ from D6PK in their cell biological behavior, exhibiting a non-polar distribution at the plasma membrane and remaining largely insensitive to BFA treatments (Bassukas et al., 2022; Kleine-Vehn et al., 2009). The difference in cell biological behavior of PID, WAG1 and WAG2 compared to D6PK could thus also be a consequence of differences in the middle domain composition. It would be interesting to

reveal in the future whether the observed cell biological differences between D6PK and the AGC3 kinases PID, WAG1 and WAG2 may be attributed to differences in middle domain composition.

In future research, it would be interesting to elucidate the structure of D6PK, potentially revealing molecular details of its interaction with its substrates the PINs at the plasma membrane, as well as interactions with other proteins such as scaffold proteins like BRX. I established constructs and strategies for improved recombinant expression and purification of D6PK in this thesis, potentially serving as a foundation for subsequent structural and biochemical investigations. A better molecular understanding of the different players in polar auxin transport, as I sought to achieve in my research, will help to elucidate how one signaling molecule can regulate such a vast number of developmental processes.

Acknowledgements

I want to express my appreciation to all those who helped and encouraged me throughout the journey of my PhD. Science is teamwork and it would be impossible to name all the scientists individually who contributed with inspiring ideas and fruitful discussions to this thesis, but I hope to point out the most central ones.

First, I would like to thank my supervisor Claus Schwechheimer for giving me an engaging project and the opportunity to conduct my research in his lab. I appreciate that I was always allowed to explore my interests and try many different techniques and approaches during the project. I am grateful for all the ideas and discussions helping me to improve my research. Thank you for the opportunities to collaborate with different research groups and visit many conferences. All these opportunities shaped me as a scientist.

I would like to thank Prof. Kay Schneitz and Prof. Chris Carolin Schön for kindly volunteering to be my second examiner and chair for my thesis defense. Many thanks to Luz Irina A. Calderón Villalobos at the Leibniz Institut in Halle and Ulrich Krauß at the Forschungszentrum Jülich, whose labs I visited during my PhD time and who taught me new techniques and provided me with fresh ideas. Thanks to Brenda Schulman, my graduate school mentor, who gave me excellent input at the start of this project. I would like to extend my thanks to Uli and Philipp for discussions during progress reports and in the corridor which resulted in great advice for my research.

I want to thank my colleagues Yao and Pawan with whom I was lucky enough to share a lab and ideas. Many thanks to Inês Barbosa for introducing me to D6PK and teaching me many techniques. Big thanks to Franzi for helping me with D6PK purifications and for never giving up even in the most difficult circumstances. Special thanks to Lana, with whom I could always discuss science, politics and philosophical questions and who never complained about the chaos on my bench. Many thanks to Peter, Jan and Dario for becoming dear friends and doing all kinds of crazy stuff together from the Friday lunches to tough hikes. Without all of you, my time in the lab would have been much less fun and memorable. I am grateful for all the students to whom I hope I was a good teacher but who also taught me many things by asking great questions, leading interesting discussions and ultimately not always following what I told them to do. Thank you to all

members of the Chair of Plant Systems Biology for the great work environment. Many thanks to Petra and Dani for all your help throughout the years. You rock!

I would like to express my gratitude to Carlos for all his patience and advice privately and scientifically. Having to suffer with me, being torn between politics, going climbing and writing this thesis, was definitely a challenge. Thank you for keeping up with my crap. I am looking forward to the journey ahead.

Last but not least, I want to thank my family Kirstin, Peter and Lisanne. They may not have contributed on a scientific level but contributed to me having the curiosity, confidence, patience and positive attitude one needs to go on this journey. Thank you for always providing a warm basecamp to come home to from all my adventures.

Literature

Abrami, L., Audagnotto, M., Ho, S., Marcaida, M. J., Mesquita, F. S., Anwar, M. U., Sandoz, P. A., Fonti, G., Pojer, F., Dal Peraro, M., & van der Goot, F. G. (2021). Palmitoylated acyl protein thioesterase APT2 deforms membranes to extract substrate acyl chains [OriginalPaper]. *Nature Chemical Biology*, *17*(4), 438-447.

Abrami, L., Kunz, B., Iacovache, I., & van der Goot, F. G. (2008). Palmitoylation and ubiquitination regulate exit of the Wnt signaling protein LRP6 from the endoplasmic reticulum. *Proceedings of the National Academy of Sciences*, *105*(14), 5384-5389.

Ahearn, I. M., Haigis, K., Bar-Sagi, D., & Philips, M. R. (2012). Regulating the regulator: post-translational modification of RAS. *Nature Reviews Molecular Cell Biology*, *13*(1), 39-51.

Aicart-Ramos, C., Valero, R., & Rodriguez-Crespo, I. (2011). Protein palmitoylation and subcellular trafficking. *Biochimica et biophysica acta*, *1808*(12).

Alassimone, J., Fujita, S., Doblas, V., van Dop, M., Barberon, M., Kalmbach, L., Vermeer, J., Rojas-Murcia, N., Santuari, L., Hardtke, C., & Geldner, N. (2016). Polarly localized kinase SGN1 is required for Casparian strip integrity and positioning. *Nature Plants*, *2*.

Almagor, L., Ufimtsev, I. S., Ayer, A., Li, J., & Weis, W. I. (2019). Structural insights into the aPKC regulatory switch mechanism of the human cell polarity protein lethal giant larvae 2. *Proceedings of the National Academy of Sciences*, *116*(22), 10804-10812.

Ashery, U., Yizhar, O., Rotblat, B., & Kloog, Y. (2006). Nonconventional Trafficking of Ras Associated with Ras Signal Organization. *Traffic*, *7*(9), 1119-1126.

Bailey, M. J., & Prehoda, K. E. (2015). Establishment of Par-Polarized Cortical Domains via Phosphoregulated Membrane Motifs. *Dev Cell*, *35*(2), 199-210.

Balla, T. (2013). Phosphoinositides: Tiny Lipids With Giant Impact on Cell Regulation. *Physiological Reviews*, *93*(3), 1019-1137.

Barbosa, I., Zourelidou, M., Willige, B., Weller, B., & Schwechheimer, C. (2014). D6 PROTEIN KINASE Activates Auxin Transport-Dependent Growth and PIN-FORMED Phosphorylation at the Plasma Membrane. *Developmental Cell*, *29*(6), 674-685.

Barbosa, I. C. R. (2015). Trafficking and polarity control of the D6 PROTEIN KINASE from Arabidopsis thaliana.

Barbosa, I. C. R., Shikata, H., Zourelidou, M., Heilmann, M., Heilmann, I., & Schwechheimer, C. (2016). Phospholipid composition and a polybasic motif determine D6 PROTEIN KINASE polar association with the plasma membrane and tropic responses. *Development*, *143*(24), 4687-4700.

Bassukas, A. E. L., Xiao, Y., & Schwechheimer, C. (2022). Phosphorylation control of PIN auxin transporters. *Curr Opin Plant Biol*, *65*, 102146.

Benková, E., Michniewicz, M., Sauer, M., Teichmann, T., Seifertová, D., Jürgens, G., & Friml, J. (2003). Local, Efflux-Dependent Auxin Gradients as a Common Module for Plant Organ Formation. *Cell*, *115*(5), 591-602.

Bennett, S. R. M., Alvarez, J., Bossinger, G., & Smyth, D. R. (1995). Morphogenesis in pinoid mutants of Arabidopsis thaliana. *The Plant Journal*, *8*(4), 505-520.

Bheri, M., Mahiwal, S., Sanyal, S. K., & Pandey, G. K. (2021). Plant protein phosphatases: What do we know about their mechanism of action? *The FEBS Journal*, *288*(3), 756-785.

Bi, Y. M., Zhang, Y., Signorelli, T., Zhao, R., Zhu, T., & Rothstein, S. (2005). Genetic analysis of Arabidopsis GATA transcription factor gene family reveals a nitrate-inducible member important for chlorophyll synthesis and glucose sensitivity. *Plant J*, *44*(4), 680-692.

Bigay, J., & Antonny, B. (2012). Curvature, Lipid Packing, and Electrostatics of Membrane Organelles: Defining Cellular Territories in Determining Specificity. *Developmental Cell*, *23*(5), 886-895.

Biondi, R. M., Cheung, P. C. F., Casamayor, A., Deak, M., Currie, R. A., & Alessi, D. R. (2000). Identification of a pocket in the PDK1 kinase domain that interacts with PIF and the C-terminal residues of PKA. *The EMBO Journal*, *19*(5), 979-988-988.

Blilou, I., Xu, J., Wildwater, M., Willemsen, V., Paponov, I., Friml, J., Heidstra, R., Aida, M., Palme, K., & Scheres, B. (2005). The PIN auxin efflux facilitator network controls growth and patterning in Arabidopsis roots [OriginalPaper]. *Nature*, *433*(7021), 39-44.

Bögre, L., Okrész, L., Henriques, R., & Anthony, R. G. (2003). Growth signalling pathways in Arabidopsis and the AGC protein kinases. *Trends Plant Sci*, *8*(9), 424-431.

Boivin, S., Kozak, S., & Meijers, R. (2013). Optimization of protein purification and characterization using Thermofluor screens. *Protein Expression and Purification*, *91*(2), 192-206.

Brown, D., & London, E. (1998). Structure and origin of ordered lipid domains in biological membranes. *The Journal of membrane biology*, *164*, 103-114.

Brunoud, G., Wells, D. M., Oliva, M., Larrieu, A., Mirabet, V., Burrow, A. H., Beeckman, T., Kepinski, S., Traas, J., Bennett, M. J., & Vernoux, T. (2012). A novel sensor to map auxin response and distribution at high spatio-temporal resolution. *Nature*, *482*(7383), 103-106.

Brzeska, H., Guag, J., Remmert, K., Chacko, S., & Korn, E. D. (2010). An experimentally based computer search identifies unstructured membrane-binding sites in proteins: application to class I myosins, PAKS, and CARMIL. *J Biol Chem*, *285*(8), 5738-5747.

Cassinelli, S., Viñola-Renart, C., Benavente-Garcia, A., Navarro-Pérez, M., Capera, J., & Felipe, A. (2022). Palmitoylation of Voltage-Gated Ion Channels. *Int J Mol Sci*, *23*(16).

Charych, E. I., Jiang, L.-X., Lo, F., Sullivan, K., & Brandon, N. J. (2010). Interplay of Palmitoylation and Phosphorylation in the Trafficking and Localization of Phosphodiesterase 10A: Implications for the Treatment of Schizophrenia. *The Journal of Neuroscience*, *30*(27), 9027-9037.

Chen, R., Hilson, P., Sedbrook, J., Rosen, E., Caspar, T., & Masson, P. H. (1998). The Arabidopsis thaliana AGRAVITROPIC 1 gene encodes a component of the polar-auxin-transport efflux carrier. *Proceedings of the National Academy of Sciences*, *95*(25), 15112-15117.

Cholodny, N. (1927). Wuchshormone und Tropismen bei den Pflanzen. *Biologisches Zentralblatt*(47), 604-626.

Cholodny, N. (1928). Beiträge zur hormaonalen Theorie von Tropismen. *Planta*(6), 118-134.

Christensen, S. K., Dagenais, N., Chory, J., & Weigel, D. (2000). Regulation of Auxin Response by the Protein Kinase PINOID. *Cell*, *100*(4), 469-478.

Chu, N., Salguero, A. L., Liu, A. Z., Chen, Z., Dempsey, D. R., Ficarro, S. B., Alexander, W. M., Marto, J. A., Li, Y., Amzel, L. M., Gabelli, S. B., & Cole, P. A. (2018). Akt Kinase Activation Mechanisms Revealed Using Protein Semisynthesis. *Cell*, *174*(4), 897-907.e814.

Clarke, R. J. (2023). Electrostatic switch mechanisms of membrane protein trafficking and regulation. *Biophysical Reviews*, *15*(6), 1967-1985.

Clough, S. J., & Bent, A. F. (1998). Floral dip: a simplified method forAgrobacterium-mediated transformation ofArabidopsis thaliana. *The Plant Journal*, *16*(6), 735-743.

Darwin, C. (1880). The Power of Movement in Plants. Cambridge University Press. DOI: 10.1017/CBO9780511693670 (1880)

Day, I. S., Miller, C., Golovkin, M., & Reddy, A. S. N. (2000). Interaction of a Kinesin-like Calmodulin-binding Protein with a Protein Kinase*. *Journal of Biological Chemistry*, *275*(18), 13737-13745.

Dharmasiri, N., Dharmasiri, S., & Estelle, M. (2005). The F-box protein TIR1 is an auxin receptor. *Nature*, *435*(7041), 441-445.

Dhonukshe, P., Huang, F., Galvan-Ampudia, C. S., Mähönen, A. P., Kleine-Vehn, J., Xu, J., Quint, A., Prasad, K., Friml, J., Scheres, B., & Offringa, R. (2010). Plasma membrane-bound AGC3 kinases phosphorylate PIN auxin carriers at TPRXS(N/S) motifs to direct apical PIN recycling. *Development*, *137*(19), 3245-3255.

Ding, Z., Galván-Ampudia, C. S., Demarsy, E., Łangowski, Ł., Kleine-Vehn, J., Fan, Y., Morita, M. T., Tasaka, M., Fankhauser, C., Offringa, R., & Friml, J. (2011). Light-mediated polarization of the PIN3 auxin transporter for the phototropic response in Arabidopsis. *Nature Cell Biology*, *13*(4), 447-452.

Dong, W., Zhang, X., Liu, W., Chen, Y. J., Huang, J., Austin, E., Celotto, A. M., Jiang, W. Z., Palladino, M. J., Jiang, Y., Hammond, G. R., & Hong, Y. (2015). A conserved polybasic domain mediates plasma membrane targeting of Lgl and its regulation by hypoxia. *J Cell Biol*, *211*(2), 273-286.

Dory, M., Hatzimasoura, E., Kállai, B. M., Nagy, S. K., Jäger, K., Darula, Z., Nádai, T. V., Mészáros, T., López-Juez, E., Barnabás, B., Palme, K., Bögre, L., Ditengou, F. A., & Dóczi, R. (2018). Coevolving MAPK and PID phosphosites indicate an ancient environmental control of PIN auxin transporters in land plants. *FEBS Letters*, *592*(1), 89-102.

Drisdel, R. C., & Green, W. N. (2004). Labeling and quantifying sites of protein palmitoylation. *Biotechniques*, *36*(2), 276-285.

Duan, M., Zhang, R., Zhu, F., Zhang, Z., Gou, L., Wen, J., Dong, J., & Wang, T. (2017). A Lipid-Anchored NAC Transcription Factor Is Translocated into the Nucleus and Activates Glyoxalase I Expression during Drought Stress. *The Plant Cell*, *29*(7), 1748-1772.

Dunphy, J. T., & Linder, M. E. (1998). Signalling functions of protein palmitoylation. *Biochimica et Biophysica Acta (BBA)-Molecular and Cell Biology of Lipids*, *1436*(1-2), 245-261.

Ek-Ramos, M. J., Avila, J., Cheng, C., Martin, G. B., & Devarenne, T. P. (2010). The T-loop Extension of the Tomato Protein Kinase AvrPto-dependent Pto-interacting Protein 3 (Adi3) Directs Nuclear Localization for Suppression of Plant Cell Death. *Journal of Biological Chemistry*, *285*(23), 17584-17594.

Facchinetti, V., Ouyang, W., Wei, H., Soto, N., Lazorchak, A., Gould, C., Lowry, C., Newton, A. C., Mao, Y., Miao, R. Q., Sessa, W. C., Qin, J., Zhang, P., Su, B., & Jacinto, E. (2008). The mammalian target of rapamycin complex 2 controls folding and stability of Akt and protein kinase C. *Embo j*, *27*(14), 1932-1943.

Farazi, T. A., Waksman, G., & Gordon, J. I. (2001). The biology and enzymology of protein N-myristoylation. *J Biol Chem*, *276*(43), 39501-39504.

Fastner, A., Absmanner, B., & Hammes, U. Z. (2017). Use of Xenopus laevis Oocytes to Study Auxin Transport. In *Methods in Molecular Biology* (pp. 259-270). Springer New York.

Forrester, M. T., Hess, D. T., Thompson, J. W., Hultman, R., Moseley, M. A., Stamler, J. S., & Casey, P. J. (2011). Site-specific analysis of protein S-acylation by resin-assisted capture. *J Lipid Res*, *52*(2), 393-398.

Friml, J., Benková, E., Blilou, I., Wisniewska, J., Hamann, T., Ljung, K., Scheres, B., & Palme, K. (2002a). AtPIN4 Mediates Sink-Driven Auxin Gradients and Root Patterning in Arabidopsis. *Cell*, *108*(5), 661-673.

Friml, J., Benková, E., Mayer, U., Palme, K., & Muster, G. (2003a). Automated whole mount localisation techniques for plant seedlings. *The Plant Journal*, *34*(1), 115-124.

Friml, J., Gallei, M., Gelová, Z., Johnson, A., Mazur, E., Monzer, A., Rodriguez, L., Roosjen, M., Verstraeten, I., Živanović, B. D., Zou, M., Fiedler, L., Giannini, C., Grones, P., Hrtyan, M., Kaufmann, W. A., Kuhn, A., Narasimhan, M., Randuch, M., . . . Rakusová, H. (2022). ABP1–TMK auxin perception for global phosphorylation and auxin canalization. *Nature*, *609*(7927), 575-581.

Friml, J., Vieten, A., Sauer, M., Weijers, D., Schwarz, H., Hamann, T., Offringa, R., & Jürgens, G. (2003b). Efflux-dependent auxin gradients establish the apical–basal axis of Arabidopsis. *Nature*, *426*(6963), 147-153.

Friml, J., Wiśniewska, J., Benková, E., Mendgen, K., & Palme, K. (2002b). Lateral relocation of auxin efflux regulator PIN3 mediates tropism in Arabidopsis. *Nature*, *415*(6873), 806-809.

Friml, J., Yang, X., Michniewicz, M., Weijers, D., Quint, A., Tietz, O., Benjamins, R., Ouwerkerk, P. B., Ljung, K., Sandberg, G., Hooykaas, P. J., Palme, K., & Offringa, R. (2004). A PINOID-dependent binary switch in apical-basal PIN polar targeting directs auxin efflux. *Science*, *306*(5697), 862-865.

Fujiki, Y., Hubbard, A. L., Fowler, S., & Lazarow, P. B. (1982). Isolation of intracellular membranes by means of sodium carbonate treatment: application to endoplasmic reticulum. *Journal of Cell Biology*, *93*(1), 97-102.

Galván-Ampudia, C. S., & Offringa, R. (2007). Plant evolution: AGC kinases tell the auxin tale. *Trends in plant science*, *12*(12), 541-547.

Gälweiler, L., Guan, C., Müller, A., Wisman, E., Mendgen, K., Yephremov, A., & Palme, K. (1998). Regulation of Polar Auxin Transport by AtPIN1 in Arabidopsis Vascular Tissue. *Science*, *282*(5397), 2226-2230.

Garbers, C., Delong, A., Deruére, J., Bernasconi, P., & Söll, D. (1996). A mutation in protein phosphatase 2A regulatory subunit A affects auxin transport in Arabidopsis. *The EMBO Journal*, *15*(9), 2115-2124.

Geiger, D., Maierhofer, T., Al-Rasheid, K., Scherzer, S., Mumm, P., Liese, A., Ache, P., Wellmann, C., Marten, I., Grill, E., Romeis, T., & Hedrich, R. (2011). Stomatal closure by fast abscisic acid signaling is mediated by the guard cell anion channel SLAH3 and the receptor RCAR1. *Science signaling*, *4*(173).

Geldner, N., Anders, N., Wolters, H., Keicher, J., Kornberger, W., Muller, P., Delbarre, A., Ueda, T., Nakano, A., & Jürgens, G. (2003). The Arabidopsis GNOM ARF-GEF Mediates Endosomal Recycling, Auxin Transport, and Auxin-Dependent Plant Growth. *Cell*, *112*(2), 219-230.

Gerganova, V., Floderer, C., Archetti, A., Michon, L., Carlini, L., Reichler, T., Manley, S., & Martin, S. G. (2019). Multi-phosphorylation reaction and clustering tune Pom1 gradient mid-cell levels according to cell size.

Giles, N. M., Watts, A. B., Giles, G. I., Fry, F. H., Littlechild, J. A., & Jacob, C. (2003). Metal and redox modulation of cysteine protein function. *Chem Biol*, *10*(8), 677-693.

Goehring, N. W., Chowdhury, D., Hyman, A. A., & Grill, S. W. (2010). FRAP Analysis of Membrane-Associated Proteins: Lateral Diffusion and Membrane-Cytoplasmic Exchange. *Biophysical Journal*, *99*(8), 2443-2452.

Grieneisen, V. A., Xu, J., Marée, A. F., Hogeweg, P., & Scheres, B. (2007). Auxin transport is sufficient to generate a maximum and gradient guiding root growth. *Nature*, *449*(7165), 1008-1013.

Hachet, O., Berthelot-Grosjean, M., Kokkoris, K., Vincenzetti, V., Moosbrugger, J., & Martin, G., Sophie. (2011). A Phosphorylation Cycle Shapes Gradients of the DYRK Family Kinase Pom1 at the Plasma Membrane. *Cell*, *145*(7), 1116-1128.

Hager, A., Menzel, H., & Krauss, A. (1971). [Experiments and hypothesis concerning the primary action of auxin in elongation growth]. *Planta*, *100*(1), 47-75. (Versuche und Hypothese zur Primärwirkung des Auxins beim Streckungswachstum.)

Hanks, S., & Hunter, T. (1995). Protein kinases 6. The eukaryotic protein kinase superfamily: kinase (catalytic) domain structure and classification. *FASEB journal : official publication of the Federation of American Societies for Experimental Biology*, *9*(8).

Hayashi, T., Thomas, G. M., & Huganir, R. L. (2009). Dual Palmitoylation of NR2 Subunits Regulates NMDA Receptor Trafficking. *Neuron*, *64*(2), 213-226.

Heazlewood, J. L., Durek, P., Hummel, J., Selbig, J., Weckwerth, W., Walther, D., & Schulze, W. X. (2007). PhosPhAt: a database of phosphorylation sites in Arabidopsis thaliana and a plant-specific phosphorylation site predictor. *Nucleic Acids Research*, *36*(Database), D1015-D1021.

Heilmann, M., & Heilmann, I. (2015). Plant phosphoinositides—complex networks controlling growth and adaptation. *Biochimica et Biophysica Acta (BBA) - Molecular and Cell Biology of Lipids*, *1851*(6), 759-769.

Hemsley, P. A. (2013). Assaying protein S-acylation in plants. *Methods Mol Biol*, *1043*, 141-146.

Hemsley, P. A. (2020). S-acylation in plants: an expanding field. *Biochemical Society Transactions*, *48*(2), 529-536.

Hemsley, P. A., Taylor, L., & Grierson, C. S. (2008). Assaying protein palmitoylation in plants. *Plant Methods*, *4*, 2.

Heo, W. D., Inoue, T., Park, W. S., Kim, M. L., Park, B. O., Wandless, T. J., & Meyer, T. (2006). PI(3,4,5)P and PI(4,5)P2 Lipids Target Proteins with Polybasic Clusters to the Plasma Membrane. *Science*, *314*(5804), 1458-1461.

Holland, J. J., Roberts, D., & Liscum, E. (2009). Understanding phototropism: from Darwin to today. *Journal of Experimental Botany*, *60*(7), 1969-1978.

Hong, Y. (2018). aPKC: the Kinase that Phosphorylates Cell Polarity. *F1000Research*, *7*, 903.

House, C., & Kemp, B. (1987). Protein kinase C contains a pseudosubstrate prototope in its regulatory domain. *Science (New York, N.Y.)*, *238*(4834).

Ikenoue, T., Inoki, K., Yang, Q., Zhou, X., & Guan, K. L. (2008). Essential function of TORC2 in PKC and Akt turn motif phosphorylation, maturation and signalling. *Embo j*, *27*(14), 1919-1931.

Ischebeck, T., Werner, S., Krishnamoorthy, P., Lerche, J., Meijón, M., Stenzel, I., Löfke, C., Wiessner, T., Im, Y. J., Perera, I. Y., Iven, T., Feussner, I., Busch, W., Boss, W. F., Teichmann, T., Hause, B., Persson, S., & Heilmann, I. (2013). Phosphatidylinositol 4,5-Bisphosphate Influences PIN Polarization by Controlling Clathrin-Mediated Membrane Trafficking in Arabidopsis *The Plant Cell*, *25*(12), 4894-4911.

Jaillais, Y., Hothorn, M., Belkhadir, Y., Dabi, T., Nimchuk, Z. L., Meyerowitz, E. M., & Chory, J. (2011). Tyrosine phosphorylation controls brassinosteroid receptor activation by triggering membrane release of its kinase inhibitor. *Genes & Development*, *25*(3), 232-237.

Janacek, D. P., Kolb, M., Schulz, L., Mergner, J., Kuster, B., Glanc, M., Friml, J., ten Tusscher, K., Schwechheimer, C., & Hammes, U. Z. (2024). Transport properties of canonical PIN-FORMED proteins and the role of the loop domain in auxin transport. *bioRxiv*, 2024.2002.2015.580428.

Ji, Y., Leymarie, N., Haeussler, D. J., Bachschmid, M. M., Costello, C. E., & Lin, C. (2013). Direct Detection of S-Palmitoylation by Mass Spectrometry. *Analytical Chemistry*, *85*(24), 11952-11959.

Joberty, G., Petersen, C., Gao, L., & Macara, I. G. (2000). The cell-polarity protein Par6 links Par3 and atypical protein kinase C to Cdc42. *Nature Cell Biology*, *2*(8), 531-539.

Katsiarimpa, A., Anzenberger, F., Schlager, N., Neubert, S., Hauser, M.-T., Schwechheimer, C., & Isono, E. (2011). The Arabidopsis Deubiquitinating Enzyme AMSH3 Interacts with ESCRT-III Subunits and Regulates Their Localization. *The Plant Cell*, *23*(8), 3026-3040.

Kepinski, S., & Leyser, O. (2005). The Arabidopsis F-box protein TIR1 is an auxin receptor. *Nature*, *435*(7041), 446-451.

Kleine-Vehn, J. r., Huang, F., Naramoto, S., Zhang, J., Michniewicz, M., Offringa, R., & Friml, J. i. (2009). PIN Auxin Efflux Carrier Polarity Is Regulated by PINOID Kinase-Mediated Recruitment into GNOM-Independent Trafficking in Arabidopsis. *The Plant Cell*, *21*(12), 3839-3849.

Kogl, F. H.-S., AJ. (1931). I. Mitteilung uber pflanzliche wachstumsstoffe. Uber die vhemie des euchsstoffs. *Proceedings Koninklijke Nederlandse Akademie van Wetenschappen*(34), 1411-1416.

Koh, S. W. H., Marhava, P., Rana, S., Graf, A., Moret, B., Bassukas, A. E. L., Zourelidou, M., Kolb, M., Hammes, U. Z., Schwechheimer, C., & Hardtke, C. S. (2021). Mapping and engineering of auxin-induced plasma membrane dissociation in BRX family proteins. *The Plant Cell*, *33*(6), 1945-1960.

Komander, D., Kular, G., Deak, M., Alessi, D. R., & Van Aalten, D. M. F. (2005). Role of T-loop Phosphorylation in PDK1 Activation, Stability, and Substrate Binding. *Journal of Biological Chemistry*, *280*(19), 18797-18802.

Koulouras, G., Panagopoulos, A., Rapsomaniki, M. A., Giakoumakis, N. N., Taraviras, S., & Lygerou, Z. (2018). EasyFRAP-web: a web-based tool for the analysis of fluorescence recovery after photobleaching data. *Nucleic Acids Research*, *46*(W1).

Kumar, M., Carr, P., & Turner, S. R. (2022). An atlas of Arabidopsis protein S-acylation reveals its widespread role in plant cell organization and function [OriginalPaper]. *Nature Plants*, *8*(6), 670-681.

Lavy, M., & Yalovsky, S. (2006). Association of Arabidopsis type-II ROPs with the plasma membrane requires a conserved C-terminal sequence motif and a proximal polybasic domain. *The Plant Journal*, *46*(6), 934-947.

Le Good, J. A., Ziegler, W. H., Parekh, D. B., Alessi, D. R., Cohen, P., & Parker, P. J. (1998). Protein kinase C isotypes controlled by phosphoinositide 3-kinase through the protein kinase PDK1. *Science*, *281*(5385), 2042-2045.

Levental, I., Lingwood, D., Grzybek, M., Coskun, U., & Simons, K. (2010). Palmitoylation regulates raft affinity for the majority of integral raft proteins. *Proc Natl Acad Sci U S A*, *107*(51), 22050-22054.

Li, L., Shi, X., Guo, X., Li, H., & Xu, C. (2014). Ionic protein–lipid interaction at the plasma membrane: what can the charge do?: Trends in Biochemical Sciences.

Li, L., Verstraeten, I., Roosjen, M., Takahashi, K., Rodriguez, L., Merrin, J., Chen, J., Shabala, L., Smet, W., Ren, H., Vanneste, S., Shabala, S., De Rybel, B., Weijers, D., Kinoshita, T., Gray, W. M., & Friml, J. (2021). Cell surface and intracellular auxin signalling for H+ fluxes in root growth. *Nature*, *599*(7884), 273-277.

Lin, D.-T., Makino, Y., Sharma, K., Hayashi, T., Neve, R., Takamiya, K., & Huganir, R. L. (2009). Regulation of AMPA receptor extrasynaptic insertion by 4.1N, phosphorylation and palmitoylation. *Nature Neuroscience*, *12*(7), 879-887.

Linder, M. E., & Deschenes, R. J. (2007). Palmitoylation: policing protein stability and traffic. *Nature Reviews Molecular Cell Biology*, *8*(1), 74-84.

Liu, X., Li, M., Li, Y., Zhuge, C., Ouyang, Y., Zhao, Y., Xie, Q., Yang, C., & Lai, J. (2021). An ABHD17-like hydrolase screening system to identify de-S-acylation enzymes of protein substrates in plant cells. *The Plant Cell*, *33*(10), 3235-3249.

Ljung, K., Bhalerao, R. P., & Sandberg, G. (2002). Sites and homeostatic control of auxin biosynthesis in Arabidopsis during vegetative growth. *The Plant Journal*, *28*(4), 465-474.

Ljung, K., Hull, A., Celenza, J., Yamada, M., Estelle, M., Normanly, J., & Sandberg, G. (2005). Sites and regulation of auxin biosynthesis in Arabidopsis roots. *The Plant Cell*, *17*(4).

Luschnig, C., Gaxiola, R. A., Grisafi, P., & Fink, G. R. (1998). EIR1, a root-specific protein involved in auxin transport, is required for gravitropism in Arabidopsis thaliana. *Genes & Development*, *12*(14), 2175-2187.

Marhava, P., Aliaga Fandino, A. C., Koh, S. W. H., Jelínková, A., Kolb, M., Janacek, D. P., Breda, A. S., Cattaneo, P., Hammes, U. Z., Petrášek, J., & Hardtke, C. S. (2020). Plasma Membrane Domain Patterning and Self-Reinforcing Polarity in Arabidopsis. *Developmental Cell*, *52*(2), 223-235.e225.

Marhava, P., Bassukas, A. E. L., Zourelidou, M., Kolb, M., Moret, B., Fastner, A., Schulze, W. X., Cattaneo, P., Hammes, U. Z., Schwechheimer, C., & Hardtke, C. S. (2018). A molecular rheostat adjusts auxin flux to promote root protophloem differentiation. *Nature*, *558*(7709), 297-300.

Marino, S. M., & Gladyshev, V. N. (2010). Cysteine Function Governs Its Conservation and Degeneration and Restricts Its Utilization on Protein Surfaces. *Journal of Molecular Biology*, *404*(5), 902-916.

Martin, S., & Berthelot-Grosjean, M. (2009). Polar gradients of the DYRK-family kinase Pom1 couple cell length with the cell cycle. *Nature*, *459*(7248).

Maures, T. J., Su, H.-W., Argetsinger, L. S., Grinstein, S., & Carter-Su, C. (2011). Phosphorylation controls a dual-function polybasic nuclear localization sequence in the adapter protein SH2B1β to regulate its cellular function and distribution. *Journal of Cell Science*, *124*(9), 1542-1552.

McLaughlin, S., & Aderem, A. (1995). The myristoyl-electrostatic switch: a modulator of reversible protein-membrane interactions. *Trends Biochem Sci*, *20*(7), 272-276.

Meca, J., Massoni-Laporte, A., Martinez, D., Sartorel, E., Loquet, A., Habenstein, B., & McCusker, D. (2019). Avidity-driven polarity establishment via multivalent lipid-GTPase module interactions. *The EMBO Journal*, *38*(3), e99652.

Menz, J., Li, Z., Schulze, W. X., & Ludewig, U. (2016). Early nitrogen-deprivation responses in Arabidopsis roots reveal distinct differences on transcriptome and (phospho-) proteome levels between nitrate and ammonium nutrition. *Plant J*, *88*(5), 717-734.

Michniewicz, M., Zago, M. K., Abas, L., Weijers, D., Schweighofer, A., Meskiene, I., Heisler, M. G., Ohno, C., Zhang, J., Huang, F., Schwab, R., Weigel, D., Meyerowitz, E. M., Luschnig, C., Offringa, R., & Friml, J. (2007). Antagonistic Regulation of PIN Phosphorylation by PP2A and PINOID Directs Auxin Flux. *Cell*, *130*(6), 1044-1056.

Mockaitis, K., & Estelle, M. (2008). Auxin Receptors and Plant Development: A New Signaling Paradigm. *Annual Review of Cell and Developmental Biology*, *24*(1), 55-80.

Moloney, M. M., Elliott, M. C., & Cleland, R. E. (1981). Acid growth effects in maize roots: Evidence for a link between auxin-economy and proton extrusion in the control of root growth. *Planta*, *152*(4), 285-291.

Moseley, J., Mayeux, A., Paoletti, A., & Nurse, P. (2009). A spatial gradient coordinates cell size and mitotic entry in fission yeast. *Nature*, *459*(7248).

Müller, A., Guan, C., Gälweiler, L., Tänzler, P., Huijser, P., Marchant, A., Parry, G., Bennett, M., Wisman, E., & Palme, K. (1998). AtPIN2 defines a locus of Arabidopsis for root gravitropism control. *The EMBO Journal*, *17*(23), 6903-6911.

Noack, L., Bayle, V., Armengot, L., Rozier, F., Mamode-Cassim, A., Stevens, F., Caillaud, M., Munnik, T., Mongrand, S., Pleskot, R., & Jaillais, Y. (2022). A nanodomain-anchored scaffolding complex is required for the function and localization of phosphatidylinositol 4-kinase alpha in plants. *The Plant Cell*, *34*(1).

Normanly, J. (2010). Approaching Cellular and Molecular Resolution of Auxin Biosynthesis and Metabolism. *Cold Spring Harbor perspectives in biology*, *2*(1), a001594-a001594.

Okushima, Y., Overvoorde, P. J., Arima, K., Alonso, J. M., Chan, A., Chang, C., Ecker, J. R., Hughes, B., Lui, A., Nguyen, D., Onodera, C., Quach, H., Smith, A., Yu, G., & Theologis, A. (2005). Functional genomic analysis of the AUXIN RESPONSE FACTOR gene family members in Arabidopsis thaliana: unique and overlapping functions of ARF7 and ARF19. *Plant Cell*, *17*(2), 444-463.

Paige, L. A., Nadler, M. J., Harrison, M. L., Cassady, J. M., & Geahlen, R. L. (1993). Reversible palmitoylation of the protein-tyrosine kinase p56lck. *Journal of Biological Chemistry*, *268*(12), 8669-8674.

Papayannopoulos, V., Co, C., Prehoda, K. E., Snapper, S., Taunton, J., & Lim, W. A. (2005). A Polybasic Motif Allows N-WASP to Act as a Sensor of PIP2 Density. *Molecular Cell*, *17*(2), 181-191.

Pearce, L. R., Komander, D., & Alessi, D. R. (2010). The nuts and bolts of AGC protein kinases. *Nature Reviews Molecular Cell Biology*, *11*(1), 9-22.

Pérez, V. I., Pierce, A., de Waal, E. M., Ward, W. F., Bokov, A., Chaudhuri, A., & Richardson, A. (2010). Chapter 8 - Detection and Quantification of Protein Disulfides in Biological Tissues: A Fluorescence-Based Proteomic Approach. In E. Cadenas & L. Packer (Eds.), *Methods in Enzymology* (Vol. 473, pp. 161-177). Academic Press.

Petersson, S., Johansson, A., Kowalczyk, M., Makoveychuk, A., Wang, J., Moritz, T., Grebe, M., Benfey, P., Sandberg, G., & Ljung, K. (2009). An auxin gradient and maximum in the Arabidopsis root apex shown by high-resolution cell-specific analysis of IAA distribution and synthesis. *The Plant Cell*, *21*(6).

Phillips, K., & De La Peña, A. H. (2011). The Combined Use of the Thermofluor Assay and ThermoQ Analytical Software for the Determination of Protein Stability and Buffer Optimization as an Aid in Protein Crystallization. *Current Protocols in Molecular Biology*, *94*(1).

Platre, M. P., Noack, L. C., Doumane, M., Bayle, V., Simon, M. L. A., Maneta-Peyret, L., Fouillen, L., Stanislas, T., Armengot, L., Pejchar, P., Caillaud, M.-C., Potocký, M., Čopič, A., Moreau, P., & Jaillais, Y. (2018). A Combinatorial Lipid Code Shapes the Electrostatic Landscape of Plant Endomembranes. *Developmental Cell*, *45*(4), 465-480.e411.

Rademacher, E. H., & Offringa, R. (2012). Evolutionary Adaptations of Plant AGC Kinases: From Light Signaling to Cell Polarity Regulation. *Frontiers in Plant Science*, *3*.

Rashotte, A. M., DeLong, A., & Muday, G. K. (2001). Genetic and chemical reductions in protein phosphatase activity alter auxin transport, gravity response, and lateral root growth. *Plant Cell*, *13*(7), 1683-1697.

Rayle, D. L., & Cleland, R. (1970). Enhancement of wall loosening and elongation by Acid solutions. *Plant Physiol*, *46*(2), 250-253.

Resh, M. D. (2013). Covalent lipid modifications of proteins. *Curr Biol*, *23*(10), R431-435.

Richter, R., Behringer, C., Müller, I. K., & Schwechheimer, C. (2010). The GATA-type transcription factors GNC and GNL/CGA1 repress gibberellin signaling downstream from DELLA proteins and PHYTOCHROME-INTERACTING FACTORS. *Genes & Development*, *24*(18), 2093-2104.

Rocks, O., Peyker, A., Kahms, M., Verveer, P., Koerner, C., Lumbierres, M., Kuhlmann, J., Waldmann, H., Wittinghofer, A., & Bastiaens, P. (2005). An acylation cycle regulates localization and activity of palmitoylated Ras isoforms. *Science (New York, N.Y.)*, *307*(5716).

Ruschhaupt, M., Mergner, J., Mucha, S., Papacek, M., Doch, I., Tischer, S. V., Hemmler, D., Chiasson, D., Edel, K. H., Kudla, J., Schmitt-Kopplin, P., Kuster, B., & Grill, E. (2019). Rebuilding core abscisic acid signaling pathways of Arabidopsis in yeast. *The EMBO Journal*, *38*(17), e101859.

Sauer, M., Balla, J., Luschnig, C., Wisniewska, J., Reinöhl, V., Friml, J., & Benková, E. (2006). Canalization of auxin flow by Aux/IAA-ARF-dependent feedback regulation of PIN polarity. *Genes Dev*, *20*(20), 2902-2911.

Sawano, A., & Miyawaki, A. (2000). Directed evolution of green fluorescent protein by a new versatile PCR strategy for site-directed and semi-random mutagenesis. *Nucleic Acids Res*, *28*(16), E78.

Schindelin, J., Arganda-Carreras, I., Frise, E., Kaynig, V., Longair, M., Pietzsch, T., Preibisch, S., Rueden, C., Saalfeld, S., Schmid, B., Tinevez, J.-Y., White, D. J., Hartenstein, V., Eliceiri, K., Tomancak, P., & Cardona, A. (2012). Fiji: an open-source platform for biological-image analysis. *Nature Methods*, *9*(7), 676-682.

Shevchenko, A., Tomas, H., Havlis, J., Olsen, J. V., & Mann, M. (2006). In-gel digestion for mass spectrometric characterization of proteins and proteomes. *Nat Protoc*, *1*(6), 2856-2860.

Simon, M. L. A., Platre, M. P., Marquès-Bueno, M. M., Armengot, L., Stanislas, T., Bayle, V., Caillaud, M.-C., & Jaillais, Y. (2016). A PtdIns(4)P-driven electrostatic field controls cell membrane identity and signalling in plants. *Nature Plants*, *2*(7), 16089.

Simons, K., & Ikonen, E. (1997). Functional rafts in cell membranes. *Nature*, *387*(6633), 569-572.

Smith, C. A., Lau, K. M., Rahmani, Z., Dho, S. E., Brothers, G., She, Y. M., Berry, D. M., Bonneil, E., Thibault, P., Schweisguth, F., Le Borgne, R., & McGlade, C. J. (2007). aPKC-mediated phosphorylation regulates asymmetric membrane localization of the cell fate determinant Numb. *Embo j*, *26*(2), 468-480.

Sorek, N., Segev, O., Gutman, O., Bar, E., Richter, S., Poraty, L., Hirsch, J. A., Henis, Y. I., Lewinsohn, E., Jürgens, G., & Yalovsky, S. (2010). An S-Acylation Switch of Conserved G Domain Cysteines Is Required for Polarity Signaling by ROP GTPases. *Current Biology*, *20*(10), 914-920.

Stanislas, T., Hüser, A., Barbosa, I. C. R., Kiefer, C. S., Brackmann, K., Pietra, S., Gustavsson, A., Zourelidou, M., Schwechheimer, C., & Grebe, M. (2015). Arabidopsis D6PK is a lipid domain-dependent mediator of root epidermal planar polarity. *Nature Plants*, *1*(11), 15162.

Sticht, H., & Rösch, P. (1998). The structure of iron–sulfur proteins. *Progress in Biophysics and Molecular Biology*, *70*(2), 95-136.

Su, N., Zhu, A., Tao, X., Ding, Z. J., Chang, S., Ye, F., Zhang, Y., Zhao, C., Chen, Q., Wang, J., Zhou, C. Y., Guo, Y., Jiao, S., Zhang, S., Wen, H., Ma, L., Ye, S., Zheng, S. J., Yang, F., . . . Guo, J. (2022). Structures and mechanisms of the Arabidopsis auxin transporter PIN3. *Nature*, *609*(7927), 616-621.

Swarup, R., Friml, J., Marchant, A., Ljung, K., Sandberg, G., Palme, K., & Bennett, M. (2001). Localization of the auxin permease AUX1 suggests two functionally distinct hormone transport pathways operate in the Arabidopsis root apex. *Genes Dev*, *15*(20), 2648-2653.

Takahashi, K., Hayashi, K.-i., & Kinoshita, T. (2012). Auxin Activates the Plasma Membrane H+-ATPase by Phosphorylation during Hypocotyl Elongation in Arabidopsis *Plant Physiology*, *159*(2), 632-641.

Tan, S., Zhang, X., Kong, W., Yang, X.-L., Molnár, G., Vondráková, Z., Filepová, R., Petrášek, J., Friml, J., & Xue, H.-W. (2020). The lipid code-dependent phosphoswitch PDK1–D6PK activates PIN-mediated auxin efflux in Arabidopsis. *Nature Plants*, *6*(5), 556-569.

Taylor, S. S., Buechler, J. A., & Yonemoto, W. (1990). cAMP-dependent protein kinase: framework for a diverse family of regulatory enzymes. *Annu Rev Biochem*, *59*, 971-1005.

Tewari, R., West, S. J., Shayahati, B., & Akimzhanov, A. M. (2020). Detection of Protein S-Acylation using Acyl-Resin Assisted Capture. *J Vis Exp*(158).

Tian, L., Jeffries, O., McClafferty, H., Molyvdas, A., Rowe, I. C. M., Saleem, F., Chen, L., Greaves, J., Chamberlain, L. H., Knaus, H.-G., Ruth, P., & Shipston, M. J. (2008). Palmitoylation gates phosphorylation-dependent regulation of BK potassium channels. *Proceedings of the National Academy of Sciences*, *105*(52), 21006-21011.

Tian, Q., Uhlir, N. J., & Reed, J. W. (2002). Arabidopsis SHY2/IAA3 inhibits auxin-regulated gene expression. *Plant Cell*, *14*(2), 301-319.

Tulloch, L. B., Howie, J., Wypijewski, K. J., Wilson, C. R., Bernard, W. G., Shattock, M. J., & Fuller, W. (2011). The Inhibitory Effect of Phospholemman on the Sodium Pump Requires Its Palmitoylation *. *Journal of Biological Chemistry*, *286*(41), 36020-36031.

Turnbull, D., & Hemsley, P. (2017). Fats and function: protein lipid modifications in plant cell signalling. *Current opinion in plant biology*, *40*.

Ulmasov, T., Murfett, J., Hagen, G., & Guilfoyle, T. J. (1997). Aux/IAA proteins repress expression of reporter genes containing natural and highly active synthetic auxin response elements. *The Plant Cell*, *9*(11), 1963-1971.

Ung, K. L., Winkler, M., Schulz, L., Kolb, M., Janacek, D. P., Dedic, E., Stokes, D. L., Hammes, U. Z., & Pedersen, B. P. (2022). Structures and mechanism of the plant PIN-FORMED auxin transporter. *Nature*, *609*(7927), 605-610.

Van Berkel, K., De Boer, R. J., Scheres, B., & Ten Tusscher, K. (2013). Polar auxin transport: models and mechanisms. *Development*, *140*(11), 2253-2268.

Vandenbussche, F., Petrášek, J., Žádníková, P., Hoyerová, K., Pešek, B., Raz, V., Swarup, R., Bennett, M., Zažímalová, E., Benková, E., & Van Der Straeten, D. (2010). The auxin influx carriers AUX1 and LAX3 are involved in auxin-ethylene interactions during apical hook development in Arabidopsis thaliana seedlings. *Development*, *137*(4), 597-606.

Wang, H., Chevalier, D., Larue, C., Cho, S. K., & Walker, J. (2007). The Protein Phosphatases and Protein Kinases of Arabidopsis thaliana. *The Arabidopsis Book*.

Weller, B., Zourelidou, M., Frank, L., Barbosa, I. C. R., Fastner, A., Richter, S., Jürgens, G., Hammes, U. Z., & Schwechheimer, C. (2017). Dynamic PIN-FORMED auxin efflux carrier phosphorylation at the plasma membrane controls auxin efflux-dependent growth. *Proceedings of the National Academy of Sciences*, *114*(5), E887-E896.

Went, F. (1926). On growth accelerating substances in the coleoptile of Avena sativa. *Proceedings Koninklijke Nederlandse Akademie van Wetenschappen*(30), 10-19.

Williamson, M. P. (1994). The structure and function of proline-rich regions in proteins. *Biochem J*, *297 (Pt 2)*(Pt 2), 249-260.

Willige, B. C., Ahlers, S., Zourelidou, M., Barbosa, I. C. R., Demarsy, E., Trevisan, M., Davis, P. A., Roelfsema, M. R. G., Hangarter, R., Fankhauser, C., & Schwechheimer, C. (2013). D6PK AGCVIII Kinases Are Required for Auxin Transport and Phototropic Hypocotyl Bending in Arabidopsis. *The Plant Cell*, *25*(5), 1674-1688.

Wisniewska, J., Xu, J., Seifertová, D., Brewer, P. B., Ruzicka, K., Blilou, I., Rouquié, D., Benková, E., Scheres, B., & Friml, J. (2006). Polar PIN localization directs auxin flow in plants. *Science*, *312*(5775), 883.

Won, S. J., Cheung See Kit, M., & Martin, B. R. (2018). Protein depalmitoylases. *Crit Rev Biochem Mol Biol*, *53*(1), 83-98.

Wong, W., & Scott, J. D. (2004). AKAP signalling complexes: focal points in space and time. *Nature Reviews Molecular Cell Biology*, *5*(12), 959-970.

Xiao, Y., & Offringa, R. (2020). PDK1 regulates auxin transport and Arabidopsis vascular development through AGC1 kinase PAX. *Nature Plants*, *6*(5), 544-555.

Xiao, Y., Zourelidou, M., Bassukas, A. E. L., Weller, B., Janacek, D. P., Šimura, J., Ljung, K., Hammes, U. Z., Li, J., & Schwechheimer, C. (2025). The protein kinases KIPK and KIPK-LIKE1 suppress overbending during negative hypocotyl gravitropic growth in Arabidopsis. *The Plant Cell*, *37*(4).

Yang, J., Cron, P., Thompson, V., Good, V. M., Hess, D., Hemmings, B. A., & Barford, D. (2002). Molecular Mechanism for the Regulation of Protein Kinase B/Akt by Hydrophobic Motif Phosphorylation. *Molecular Cell*, *9*(6), 1227-1240.

Yang, Z., Xia, J., Hong, J., Zhang, C., Wei, H., Ying, W., Sun, C., Sun, L., Mao, Y., Gao, Y., Tan, S., Friml, J., Li, D., Liu, X., & Sun, L. (2022). Structural insights into auxin recognition and efflux by Arabidopsis PIN1. *Nature*, *609*(7927), 611-615.

Zaccolo, M., & Pozzan, T. (2002). Discrete Microdomains with High Concentration of cAMP in Stimulated Rat Neonatal Cardiac Myocytes. *Science*, *295*(5560), 1711-1715.

Žádníková, P., Petrášek, J., Marhavý, P., Raz, V., Vandenbussche, F., Ding, Z., Schwarzerová, K., Morita, M. T., Tasaka, M., Hejátko, J., Van Der Straeten, D., Friml, J., & Benková, E. (2010). Role of PIN-mediated auxin efflux in apical hook development of Arabidopsis thaliana. *Development*, *137*(4), 607-617.

Zegzouti, H., Anthony, R. G., Jahchan, N., Bögre, L., & Christensen, S. K. (2006a). Phosphorylation and activation of PINOID by the phospholipid signaling kinase 3-phosphoinositide-dependent protein kinase 1 (PDK1) in Arabidopsis. *Proceedings of the National Academy of Sciences*, *103*(16), 6404-6409.

Zegzouti, H., Li, W., Lorenz, T. C., Xie, M., Payne, C. T., Smith, K., Glenny, S., Payne, G. S., & Christensen, S. K. (2006b). Structural and Functional Insights into the Regulation of Arabidopsis AGC VIIIa Kinases*. *Journal of Biological Chemistry*, *281*(46), 35520-35530.

Zhao, Y. (2010). Auxin biosynthesis and its role in plant development. *Annu Rev Plant Biol*, *61*, 49-64.

Zhou, Y., & Hancock, J. F. (2018). A novel prenyl-polybasic domain code determines lipid-binding specificity of the K-Ras membrane anchor. *Small GTPases*, 1-5.

Zhou, Y., Prakash, P. S., Liang, H., Gorfe, A. A., & Hancock, J. F. (2021). The KRAS and other prenylated polybasic domain membrane anchors recognize phosphatidylserine acyl chain structure. *Proceedings of the National Academy of Sciences*, *118*(6), e2014605118.

Zourelidou, M., Absmanner, B., Weller, B., Barbosa, I. C., Willige, B. C., Fastner, A., Streit, V., Port, S. A., Colcombet, J., De La Fuente Van Bentem, S., Hirt, H., Kuster, B., Schulze, W. X., Hammes, U. Z., & Schwechheimer, C. (2014). Auxin efflux by PIN-FORMED proteins is activated by two different protein kinases, D6 PROTEIN KINASE and PINOID. *eLife*, *3*.

Zourelidou, M., Müller, I., Willige, B. r. C., Nill, C., Jikumaru, Y., Li, H., & Schwechheimer, C. (2009). The polarly localized D6 PROTEIN KINASE is required for efficient auxin transport in Arabidopsis thaliana. *Development*, *136*(4), 627-636.